Fluorinated zinc and erbium complexes based on benzothiazole derived ligands for optoelectronic devices

Zhe Li

School of Biological and Chemical Sciences

School of Physics and Astronomy

Queen Mary, University of London

Submitted for the degree of Doctor of Philosophy

Declaration

I herewith certify that any material in this thesis that is not my own work has been properly acknowledged.

Zhe Li

Acknowledgement

First I would like to express my sincere gratitude to my supervisor Dr. Peter Wyatt for his great guidance throughout my PhD. I really appreciate him for his outstanding expertise, precise and hands-on training of me in chemistry, and especially his great patience and tolerance of my stupid mistakes and different opinions. This thesis would not have been complete without his great deal of attention and inexhaustible reviewing. My special thankfulness also goes to my co-supervisor Prof. William Gillin. I am grateful for his invaluable direction during my PhD. He has shaped me with a brain of open mind, and the ability of logical and critical thinking. My interdisciplinary research would not have been possible without his guidance in knowledge and practical skills.

I would like to thank and acknowledge Dr. Ignacio Hernandez for introducing me many of the spectroscopic techniques and useful discussions of this area. A special thank goes to the X-ray experimental officer Majid Motevalli who has run all the XRD measurements and refining the data. I also appreciate Dr. Roger Nix for running the DFT calculations of the molecules we synthesised. Acknowledgements also go to technicians in both departments, Jalal, Geoff and Ken for helping me to run experiments smoothly.

Many thanks to my colleagues and friends, Yu, Huangqing, Hannah, Niranjeni, Pengfei, Ahmed, Graziano, Song, Sijie, Nicola, Pratik, Sai, for all your help and the precious time we spent. Especially, I would like to thank my colleague and previous flat mate Jingyao Song for his helps in both accommodation and researching at the beginning of my PhD.

My deep gratefulness is always with my parents and other family members, who have been caring my life and research thousands of miles away trying their best to understand what I have been doing. I am also thankful to the China Scholarship Council (CSC) for funding my PhD studentship.

My most special thank you goes to Hui-Jiuan Chen, her love, caring and optimism has been carrying me through. There are no words, but the supporting in every plain minute can be the way we understand and cherish each other.

Abstract

Three families of fluorinated ligands based on benzothiazole derivatives, including 2-(2-hydroxyphenyl)benzothiazoles, bis(benzothiazolyl)amines and *N*-benzothiazol-2-yl-methanesulfonamides, have been synthesised with different locations and extents of fluorination. Zinc complexes of the fluorinated 2-(2-hydroxyphenyl)benzothiazoles and bis(benzothiazolyl)amines have been successfully prepared. Crystallographic characterisations of these zinc complexes have revealed various molecular packing behaviours in their crystals in terms of π_H-π_H, π_H-π_F and π_F-π_F stacking under the influence of partial and complete fluorination. DFT calculations and photophysical studies of these complexes have demonstrated that fluorination of these molecules decreases their HOMO and LUMO levels simultaneously by about the same amount, roughly 0.1 eV per substitution of hydrogen by a fluorine atom. An inverse correlation has been found between the dihedral angles of conjugating aromatic rings and the photoluminescence full width at half maximum (FWHM), which could be one of the reasons for the broadening of photoluminescence spectra upon fluorination. The applications of the zinc complex of 2-(2-hydroxy-3,4,5,6-tetrafluorophenyl)-4,5,6,7-tetrafluorobenzothizole ($Zn(F\text{-}BTZ)_2$) in organic light emitting diode (OLEDs) have been investigated. The electroluminescence of $Zn(F\text{-}BTZ)_2$ has shown remarkable phosphorescence in the red region, indicating enhanced spin mixing and intersystem crossing introduced by the substitution of the hydrogen atoms by the higher atomic number fluorine atoms. This ability of providing a large population of triplets, together with the lack of CH or OH oscillators of this perfluorinated $Zn(F\text{-}BTZ)_2$ molecule, allowed its use as an efficient chromophore to sensitise the erbium ions in a long-lifetime erbium complex, erbium (III) tris (pentafluorophenyl)imidodiphosphinate ($Er(FTPIP)_3$). By doping $Er(FTPIP)_3$ into $Zn(F\text{-}BTZ)_2$ in the OLED, we achieved significant and long-lifetime emission from erbium at the important telecommunication wavelength of 1.5 μm.

Table of contents

List of abbreviations

APCI: atmospheric-pressure chemical ionization
Alq_3: tris(8-hydroxyquinolinato)aluminium
ATR: attenuated total reflectance
BCP: bathocuproine (2,9-dimethyl-4,7-diphenyl-1,10-phenanthroline)
BTZ : 2-(2-hydroxyphenyl)benzothiazole anion
CT: charge transfer
EDWA: erbium-doped waveguide amplifier
EDX: energy-dispersive X-ray spectroscopy
EL: electroluminescence
EML: emissive layer
ETL: electron transport layer
F-BTZ: 2-(2-hydroxy-3,4,5,6-tetrafluorophenyl)-4,5,6,7-tetrafluorobenzothiazole
FTPIP: fluorinated tris(perfluorophenyl)imidodiphosphinate ligand anion
H-BTZ: 2-(2-hydroxyphenyl)benzothiazole
H-HFA: 1,1,1,5,5,5-hexafluoro-2,4-pentanedione
HFA: 1,1,1,5,5,5-hexafluoro-2,4-pentanedione anion
HMTPD: *N*,*N*,*N*',*N*'-tetrakis(3-methylphenyl)-3,3'-dimethylbenzidine
HRMS: high-resolution mass spectroscopy
HTL: hole transport layer
ISC: intersystem crossing
ITO: indium tin oxide
NMP: *N*-Methyl-2-pyrrolidone
OLEDs: organic light emitting diodes
RC: resistor–capacitor
TPD: *N*,*N*'-bis(3-methylphenyl)-*N*,*N*'-diphenylbenzidine

Chapter 1 - Introduction

1.1 Motivation

Organic conjugated molecules have been extensively studied as promising materials for optoelectronic applications, such as lighting emitting diodes, photovoltaic cells and transistors. An attractive advantage of organic materials is the unlimited tunability of their physical properties through engineering the molecular structures.

Among the molecular engineering tools kit, fluorination has been regarded as a powerful method to modify the electronic structure and solid state property, such as in some planar polycyclic hydrocarbons or heterocyclic systems.[1] The effects of fluorination on these planar molecules were discovered to stabilise both the highest occupied molecular orbital (HOMO) and the lowest unoccupied molecular orbital (LUMO) energy levels, and change the molecular packing from typical edge-to-face/herringbone mode in nonfluorinated systems to columnar π-stacking mode in fluorinated systems which lead to significant difference in the solid state property.[2-4] However, the impact of fluorination on non-planar metal chelate systems is much less studied, and deserves more investigations in aspects of structures and optoelectronic properties, especially luminescence. A particular desire of this project is to develop a completely fluorinated metal complex chromophore, which can absorb energy at the visible-spectrum range and sensitise the erbium ion to give emission at the important telecommunication wavelength of 1.5 μm.

This thesis will present the systematic studies on several highly fluorinated metal complexes across different chapters including synthesis, structural and photophysical studies, and applications in optoelectronic devices.

1.2 Organic semiconductors

The breakthrough of electrically conducting organic materials was attributed to the discovery of a highly conductive polymer by Shirakawa *et al.* in 1977,[5] although organic semiconducting behaviours were found much earlier in a polyaniline-type material by Henry Letheby in 1862,[6] and in some polycyclic aromatic complexes in the 1950s.[7]

These materials, either polymers or small molecules, all contain large backbones of conjugated π obitals, which are composed of many adjacent parallel p orbitals of trigonal C atoms or heteroatoms such as N. The electrons on these π obitals are delocalized and can therefore move freely over the conjugated backbone.

Although the wavefunctions of the molecular π orbitals are spread over many atoms, the bulk organic material is still composed of discrete molecules or polymer chains, between which there are no orbitals for electrons to move as freely as they do intramolecularly. Therefore, the charge carriers in the organic semiconductors are transported quite differently from the movement of carriers through the continuous bands in inorganic semiconductors. However, similarities can be drawn from the highest occupied molecular orbitals (HOMOs) and the lowest unoccupied molecular orbitals (LUMO) in organic semiconductors to the valence band and conducting band in inorganic semiconductors, respectively. Therefore, the excited electrons can be transported by hopping through the discrete LUMOs while the holes hopping through the discrete HOMOs under a driving electric field (Figure 1.1).

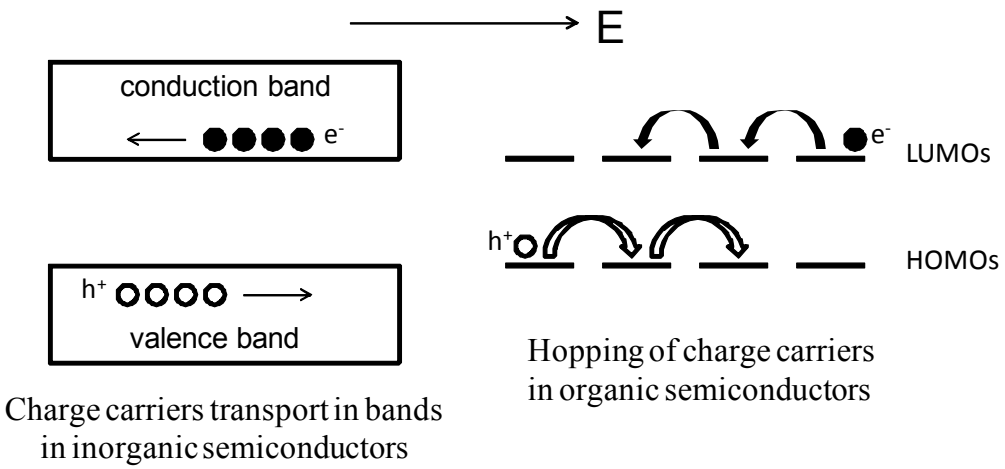

Figure 1.1: Illustration of charge transport in organic semiconductors compared with that in inorganic semiconductors

Apart from electric conductivity, organic semiconductors are also attractive because of their optical properties that arise from their typical HOMO–LUMO energy gaps of 1.5~3.5 eV, which corresponds to photon energy covering a wide range of the electromagnetic spectrum including the whole visible part (1.65~3.1 eV). When an excited electron decays radiatively from the LUMO to combine with a hole on the HOMO, a photon will be emitted at the wavelength decided by the specific energy gap of that molecule. The emission process is called photoluminescence (PL) if the electron is photoexcited from the HOMO to the LUMO, or electroluminescence (EL) if the electron is electrically injected into the LUMO. Since the first organic light emitting diode (OLED) was reported by Tang and VanSlyke in 1987,[8] the luminescent organic semiconductors are still being intensively studied because of their advantages, such as high energy efficiency, light weight, and ease of processing. Recently, the reverse process of photoluminescence – the photovoltaic effect, has been another research focus of organic semiconductors because of its solar energy harvesting application. When a photon is absorbed by the material, an electron in the HOMO can be excited to the LUMO and an electron-hole bound state, an exciton, is generated. This bound state needs to be broken to produce free electrons and holes to give the photocurrent. A great advantage of organic photovoltaic materials, besides light weight and large area processing, is that the molar absorption coefficient of organic materials is usually higher

compared with crystalline or polycrystalline silicon (<10^4 cm^{-1} when above 500 nm for silicon).

1.3 Organic light emitting diodes (OLEDs)

1.3.1 Excited states in OLEDs

In order to generate photoemission, electrons and holes need to be injected into the organic material(s). The two type of charge carriers are transported towards each other and combine to form the excitons, excited states of electron-hole pairs, which could decay radiatively to give emission, or nonradiatively to generate heat.

The excitons can be categorized into two types depending on the combination of electron and hole spin: singlets and triplets. The possibilities of forming singlets and triplets from injected carriers are different because of statistics. The statistical ratio of forming singlets and triplets is 1:3, which has also been proved by experimental results.[9]

The photophysical transitions from the excited states can be illustrated by a simplified Jablonski diagram, adapted from literature (Figure 1.2).[10] According to the selection rules for electronic spectroscopy, only transitions between states with the same total spin quantum number are allowed. Therefore, the transition from the excited singlet state S_1 to the ground singlet state S_0 is allowed and this process is termed as fluorescence; while the transition form the triplet state T_1 to the ground singlet state S_0 is forbidden. Because of this transition rule, coupled with the fact that only one quarter of the excitons formed from injected carriers are singlets, the maximum quantum efficiency (photon/electron) for a fluorescent material that can be achieved is 25%. However, the selection rules are not absolute and can be relaxed. One route for the relaxation is through the spin-orbit coupling induced by some heavy atoms, which brings a certain mixing of the wavefunctions of the singlet state and the triplet state. This mixing therefore allows a finite probability for the transition from the triplet state T_1 to the ground state S_0, and this radiative process is termed as phosphorescence. By

utilising phosphorescence as well as fluorescence, 100% quantum efficiency can be theoretically achieved.

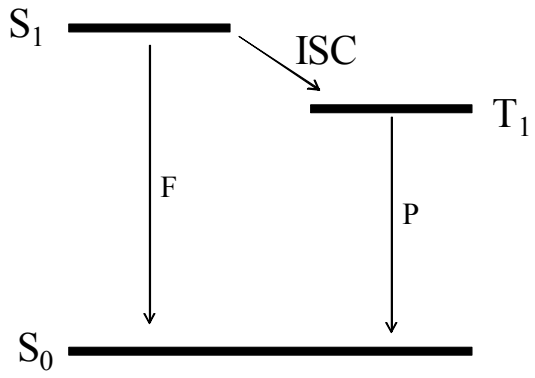

Figure 1.2: Photophysical transitions of excited states. S_0: singlet ground state, S_1: first excited singlet state, T_1: first excited triplet state, F: fluorescence, P: phosphorescence

Recently a lot of heavy metal complexes have been developed as phosphorescent materials. These metal elements include Ir, Pt, Os and Ru.[11-12] Besides these expensive heavy metal elements, enhanced spin-orbit coupling has also been observed in fluorinated graphene,[13] and in fluorinated zinc phthalocyanine.[14] However, until now there is no report on non-heavy-metal fluorinated phosphorescent materials.

1.3.2 Structure of OLEDs

The first reported OLED fabricated by Tang and VanSlyke has a two-layer structure,[8] a metal chelate complex tris(8-hydroxyquinolinato)aluminium (Alq_3) and a diamine were used as the electron transport layer (ETL) and the hole transport layer (HTL) respectively (Figure 1.3). Due to a larger barrier for electrons than for holes, the excitons were formed at the Alq_3 side of the interface. So the device gave a green emission which came from the Alq_3 layer.

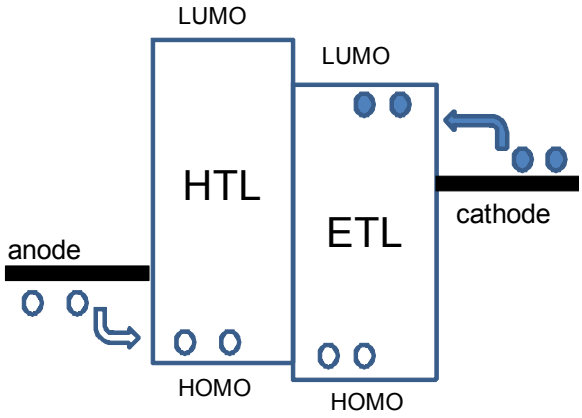

Figure 1.3: Structure of a two-layer OLED

Some of the emissive materials may not have very good carrier injection or transport properties. In this case a multilayer (three layers or more) structure is needed and each layer has a specific function (Figure 1.4), and the emissive material is only used as the emissive layer (EML) where electrons and holes are injected from other materials. Sometimes a hole (or electron) blocking layer is also needed between the EML and ETL (or HTL) to confine the excitons to the EML.

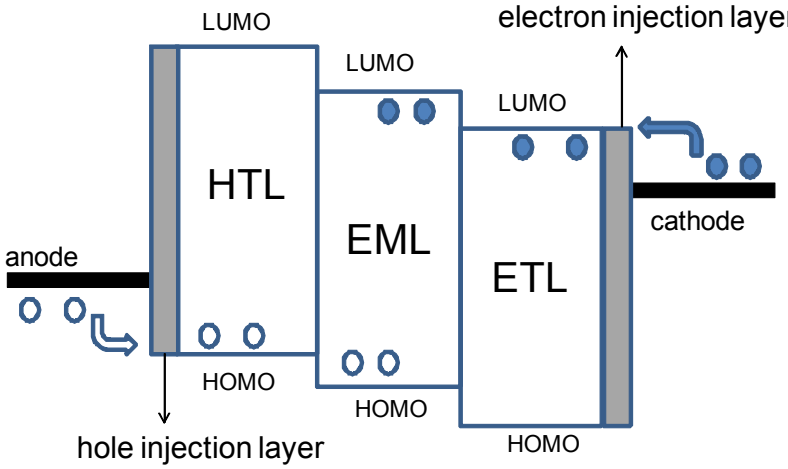

Figure 1.4: Structure of a multilayer OLED

The energy levels of the HOMO and LUMO are important because the values of these will affect the injection/transport of carriers into the neighbouring layers. Meanwhile the mobility of carriers in a material is dependent on how well the conjugated molecules

are aligned in the amorphous film. Therefore the methods used to modify molecular energy levels and to organise the molecular packing will be essential for improving the properties of organic semiconductors. Fluorination is an effective tool to engineer both aspects.

1.4 Impact of fluorination on the properties of organic optoelectronic materials

1.4.1 Fluorination effect on molecular electronic properties

Due to them having the largest electronegativity (Pauling electronegativity = 4) in the periodic table, fluorine atoms can lower the molecular orbital energy levels when they are covalently bonded to other atoms. The fluorination strategy has been used in many organic semiconductor materials to decrease both their LUMO and HOMO energy levels.[15] However, attention needs to be paid when making fluorination on aromatic rings that both the negative inductive effect (electron withdrawing) and the positive mesomeric effect (electron releasing) have to be considered. Taking the well known fluorescent molecule Alq_3 for example, when F substitution is made at the C-5 position which is far from the large electron density at O atom, the positive mesomeric effect is dominating and thus results in an increased HOMO compared to the parent Alq_3. When F substitution is made at the C-7 position which is ortho to the O atom, both negative inductive effect and positive mesomeric effect are contributing to the electron density so the HOMO does not change substantially.[16]

Besides the affect on energy levels of electronic states, fluorination has also been found to enhance the spin-orbit coupling and increase the singlet-triplet mixing,[13] which would benefit processes that involve triplet state, such as phosphorescence and sensitisation of long-lived excited states in lanthanide ions.

1.4.2 Fluorination effect on intermolecular interactions

Fluorination has not only a great impact on the properties of a molecule itself, but also a

strong influence on intermolecular interactions and hence solid state properties. For a comprehensive knowledge of fluorine interactions, one can refer to the review "Fluorine in crystal engineering — the little atom that could".[17] Due to its strongest electron negativity among all elements, several different types of intermolecular forces can be produced by fluorine.

1. π-π_F interaction

π-π_F interaction is recognised as the strongest stabilising force among all types of fluorine interactions. A 1:1 mixture of liquid benzene and liquid hexafluorobenzene gives a solid crystal at room temperature as reported by Patrick and Prosser in 1960.[18] In the past the π-π_F interaction was only regarded as electrostatic, as a perfluorinated aromatic shows an inverted electron density distribution and an opposite sign of quadrupole moment compared with the nonfluorinated aromatic. However, recent calculations by the PIXEL method indicate that dispersion plays a more important role than the electrostatic interactions as explained by Gavezzotti *et al*.[19] This dispersion interaction between a perfluorinated and a nonfluorinated aromatic ring features a stabilizing energy of about 20–25 $kJ \cdot mol^{-1}$, just smaller than the hydrogen bonds in carboxylic acids or amides among all the recognition forces in supramolecular chemistry.

2. C–F···H interaction

Although F^- is one of the best hydrogen bond acceptors, C–F···H only forms weak interactions compared to typical hydrogen bonds with O or N as acceptor atoms. According to the acidity of the hydrogen, C–F···H interactions can be classified into two types: the strong donor type C–F···H–X with X being electronegative O or N and the weak donor type C–F···H–C.[20] Strong hydrogen bonds always feature strong directionality and small distance, less than the sum of the van der Waals radii of fluorine and hydrogen which is about 2.67 Å. But C–F···H–C interactions show a very diverse angles range from 70° to 180°, suggesting small directionality and weak interactions. If C–F is one part of an aromatic ring, the fluorine lone pair will participate

in the conjugation with π electrons, thus reducing its ability as a hydrogen bond acceptor.

3. F···F interaction

The existence of F···F interaction is still in debate both theoretically and experimentally. The nature of F···F interaction should be a dispersion force. But fluorine is sitting at the upper-right corner of the periodic table, regarded as a 'hard' element with low polarisability. So the attractive dispersion force should be very low. In the CSD data base, only very few structures exhibit short F···F distance less than the sum of their van der Waals radii 2.94 Å. And even in these cases it is not clear whether the close contact of F···F is due to its stabilising effect, or just a consequence of close packing.[21]

4. C–F···π_F interactions

In a perfluorinated aromatic system, the electron density distribution is reversed compared to the nonfluorinated version, so the electropositive centre of a perfluorinated ring tends to have an electrostatic attraction with electronegative fluorine atoms. The evidence of this interaction is found in several compounds, such as hexafluorobenzene, fluorinated benzophenones, fluorinated N-phenylmaleimides and phthalimides.[21]

5. C–F···metal interactions

The interactions between organic fluorine and metal cations, especially alkali and alkaline earth metal ions, are extensively studied by Plenio and Takemura*et al*.[22-24] This C–F···M^{n+} interaction can be considered as a dipole interaction between the C–F bond and those "hard" metal cations. Existence of C–F···M^{n+} interactions can be probed by the chemical shift and coupling constant between C and F using NMR, and by short F···M^{n+} distances and prolonged C-F bond lengths in X-ray structures. Advantages of this C–F···M^{n+} interaction can be exploited in the area of C–F activation. But disadvantages also exist when fluorinated metal complexes need to be deposited by sublimation, because the F···M^{n+} attractions will weaken the C–F bonds while the metal cation can bridge between surrounding fluorine atoms, thus generating metal fluorides

as byproducts.

1.4.3 Fluorinated electronic and optoelectronic materials

Due to the impact of fluorination on molecular and solid state properties, fluorination has been widely used in a wide range of electronic and optoelectronic materials to achieve better performance.

(1) Fluorinated poly(phenylenevinylene)s (PPVs)

Poly(phenylenevinylene) and its derivatives have been used as emissive layers in LEDs. There are two major drawbacks of materials of this kind. The first is its susceptibility to photo oxidation of the double bonds, leading to reduced device lifetime. The second is its high LUMO which makes electron injection difficult. As fluorination can decrease both HOMO and LUMO, it is expected that both problems can be solved by fluorination and lots of effort has been made to synthesise fluorinated PPVs and incorporate these novel materials into LEDs.

Mono-fluorinated PPV at the 2-position of phenyl ring was reported by Shim and co-workers (Figure 1.5, left).[25] They observed red shifted EL spectra in an ITO/PPV/Al OLED and ascribed it to the shallow trap states. The operating voltage of the fluorinated device was higher than that of nonfluorinated device because of higher energy barrier between ITO and decreased HOMO in fluorinated PPV. However, EL quantum efficiency of fluorinated device was 10 times higher because the injection of electrons as minor carrier was facilitated. 2,5-Difluorinated PPV was reported by Lathi, Karasz and co-workers and has even more red-shifted PL and EL spectra (Figure 1.5, Middle).[26] Homopolymer with completely fluorinated phenyl units was firstly reported by Babudri, Naso and co-workers (Figure 1.5, right).[27] The product is not soluble in common organic solvents and has to be sublimed to make devices. The single layer device ITO/polymer/Al did not give any emission because of unmatched energy levels between the work function of ITO and the HOMO of polymer. The two layer device ITO/TPD/polymer/Al gave green emission with turn-on voltage of 6.5 V.

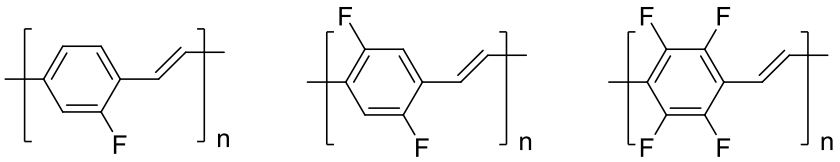

Figure 1.5 Left: PPVs with fluorination at 2-position; Middle: 2,5-difluorinated PPV; Right: PPV with perfluorinated phenyl ring

(2) Fluorinated thiophenes

Oligothiophenes are promising materials for field effect transistors (FETs) due to their high charge carrier mobility. But unsubstituted oligothiophenes are mainly p-type semiconductors and only holes can be transported. To obtain n-type semiconductors, various fluorination techniques have been used.

Marks and co-workers prepared fluoroalkyl chain substituted thiophenes at different parts of the molecule frame.[28-29] Those fluorinated oligothiophenes indeed show n-type character. But compared with their alkyl substituted counterparts, fluorinated thiophenes demand high temperature growth or annealing to obtain a high crystallinity degree and thus good device performance. It indicates that fluoroalkyl substituted thiophenes need extra thermal energy to overcome the rotation energy barrier caused by the stiff fluoroalkyl chain to reach the planarity of the polyheterocyclic core. The complete and direct introduction of fluorine atoms onto the aromatic rings was reported by Sakamoto, Suzuki and co-workers in a series of thiophenes composed of various number of heterocyclic rings (Figure 1.6).[30-31] The highly planar molecules and good π-π stacking, however, do not give expected the high electron mobility because of the LUMO remaining too high.

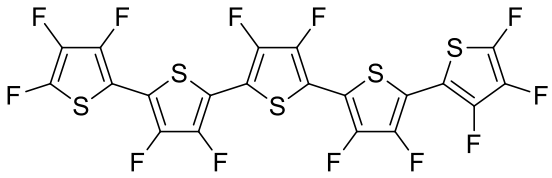

Figure 1.6: Perfluorinated oligothiophene

(3) Fluorinated oligophenylenes

Unsubstituted polymeric phenylenes are almost insoluble in common organic solvents, thus oligophenylenes with reduced length are targeted as materials that can be evaporated under high vacuum. Perfluorinated oligophenylenes were reported by Tokito, Taga and co-workers, covering linear and branched structures.[32-34] Among these materials, only Y-branched molecules can be evaporated as stable amorphous film which is favoured for good performance in OLEDs, while the other types of molecules are highly crystalline and insoluble. The mobility of Y-branched molecules was measured to be in the scale of 10^{-4} $cm^2V^{-1}s^{-1}$, which is relatively high for an amorphous electron-conducting film. Eventually, these materials are developed as electron injection and hole-blocking candidates owing to their low LUMO and HOMO levels.

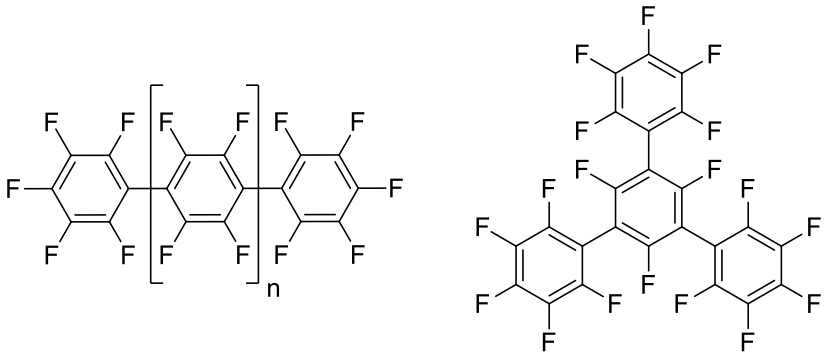

Figure 1.7: Perfluorinated linear and branched oligophenylenes

(4) Fluorinated acenes

Non-fluorinated acenes are p-type semiconducting materials with high mobility of holes. Fluorinated analogues were synthesised to obtain corresponding n-type materials. Perfluorinated pentacene was first prepared by the Suzuki group and evoked great interest for both physics studies and applications (Figure 1.8, left).[4] In the solid state, perfluoropentacene adopts a herringbone structure with an almost perpendicular angle, compared to an angle of 51.9° in pentacene. In addition, perfluoropentacene shows a close π-π stacking of 3.21 Å, which is shorter than the separation in graphite (3.35 Å). The close packing is ascribed by the authors to the electrostatic attraction between electronegative fluorine atoms and electropositive pentacene moieties. These features are expected to provide good charge transport abilities and the highest electron mobility of 0.11 $cm^2V^{-1}s^{-1}$ was achieved at optimised condition, which is comparable to the hole

mobility in pentacene. The development of n-type semiconductors with similar structure as the p-type ones enables the fabrication of organic analogues of CMOS. Partially fluorinated pentacenes with fluorination on one or both terminals were also made.[35] Close π-π_F stacking was observed in the crystal structures and the interplanar distance reduces with increased extent of fluorination. These materials should be n-type semiconductors as expected from their stabilised LUMO level, but are actually p-type from measurement in field-effect transistors (FETs). A trend was found that the hole mobility of this series of materials scaled with increased extent of fluorination and enhanced intermolecular interactions.

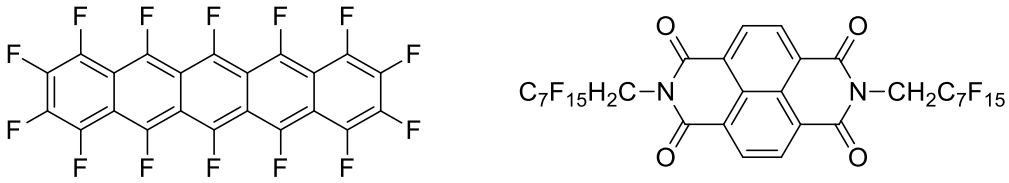

Figure 1.8 Left: fluorinated pentacene; Right: naphthalenetetracarboxylic acid diimides

The most promising n-type organic semiconducting materials have been found are naphthalenetetracarboxylic acid diimides (Figure 1.8, right).[36] While the FET device made from the nonfluorinated *N*,*N*'-bis(octyl)-1,4,5,8-naphthalenetetracarboxylic diimide can only preserve high electron mobility under high vacuum, the devices using semifluoroalkyl chain substituted analogs can be fabricated using solution casting and be operated in air with high electron mobilities of 0.01-0.06 $cm^2V^{-1}s^{-1}$.

(5) Fluorinated metal complexes

Mono-fluorinated Alq_3 analogues with various substitution positions were made by Shi *et al*.[16] They found that the material with fluorination at the C-5 position ($5FAlq_3$) has a red-shifted emission compared with that of the parent Alq_3 compound. They attributed this to the conjugation (electron releasing) effect from the electron pair on the fluorine atom to the HOMO density on the C-5, which leads to an increased HOMO and thus a decreased HOMO-LUMO gap. Substitution at the C-6 position does not have

conjugation effect, but only negative inductive effect is exhibited which decreases the HOMO and yields an increased band gap and a blue-shifted emission. The substitution at C-7 almost does not change the emission peak, which was accounted for by the author as a steric effect between the F atom and the O atom that decreases the conjugation. However, an alternative reason might come from a balance between the negative inductive effect and the positive mesomeric effect of the fluorine atom.

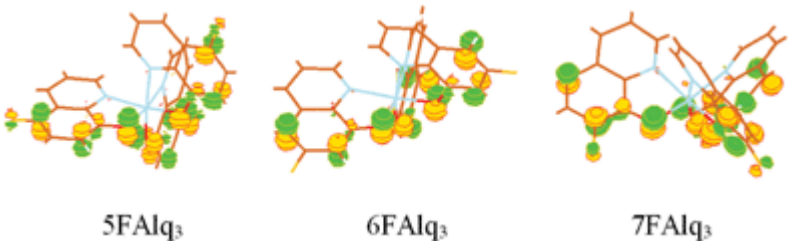

Figure 1.9: The HOMO of different mono-fluorinated Alq_3, adapted from literature[16]

Fluorination was also applied on some phosphorescent materials, such as Ir complexes. Ragni *et al* reported a series of Ir complexes based on fluorinated phenylpyridine-type ligands.[37] They utilised the electron withdrawing property of fluorine atoms to decrease the HOMO energy level and increase the HOMO-LUMO energy gap, thus obtaining blue phosphorescent complexes.

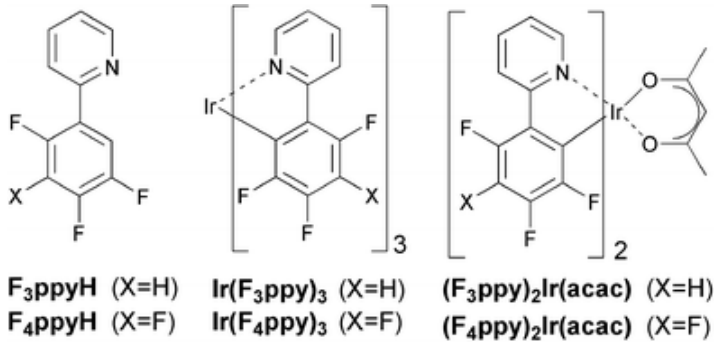

Figure 1.10: Fluorinated $Ir(Fnppy)_3$ and $(Fnppy)_2Ir(acac)$ complexes, adopted from literature[37]

1.5 Erbium complexes in optical amplifier

1.5.1 Optical amplifiers and waveguides

Optical fibre based telecommunication system dominate today's long distance data transmission networks. The whole system contains several optical integrated components such as amplifiers, splitters, couplers, multiplexers and de-multiplexers. When an optical signal propagates via an optical fibre for long distance, it is inevitable that the signal intensity gradually decreases because of Rayleigh scattering and absorption. To compensate for this transmission loss, optical amplifiers are needed to increase the signal intensity.

Optical amplifiers are usually in the form of a waveguide, which consists of a guiding core with a high refractive index and cladding layers with low refractive index. When the core is doped with active photoluminescent elements, new photons can be generated at the same wavelength and phase of the signal via stimulated emission, by pumping those elements with lasers at a shorter wavelength. In the silica waveguide amplifier, Er^{3+} ions are used as the active element, which gives emission at 1.5 μm to match the low loss transmission window of silica. This type of amplifier is called an *erbium-doped waveguide amplifier* (*EDWA*). The first EDWA was first fabricated by Mears *et al* from the University of Southampton,[38] and since then the EDWA technology has seen very fast growth and application in the modern world.

However, the traditional silica-based fibres and erbium-doped waveguide amplifiers still have some disadvantages. The glass fibre is very thin (~1 μm diameter) and requires very skillful labour and professional equipments to couple these fibres to the terminal. Meanwhile, the erbium concentration in glass matrices that can be achieved is limited. And the cross-sections for direct photoexcitation of lanthanide ions are low because of the forbidden nature of f-f transitions, so that relatively long length of fibre doping is required along with high power pump lasers. This means that the devices will be very bulky and expensive, which is especially problematic for short distance 'fibre to

the home' applications.

The most promising solution for realising fibre-to-the-home is the application of plastic fibres and organic optical amplifiers. Lanthanide ions with organic chromophores can be photosensitised with much larger absorption coefficient and over a wider wavelength range. The concentration of erbium can also reach a higher level due to the generally good solubility of organic materials in polymer matrices. So it opens the possibility of developing low-cost and compact infrared emitting devices for optical communication.

The key problem needing to be solved is the vibrational quenching of the infrared signal by typical organic molecules and water, which is caused by the coupling of the ions' excited states with high energy oscillators, such as OH, NH and CH bonds. Halogenation, especially fluorination, of hydrogen-containing ligands has been proved to be one of the most effective ways to extend the lifetime of infrared emissive lanthanide complexes.[39-41]

1.5.2 Emission and sensitisation of Ln^{3+} complexes

The erbium ion has an electron configuration of $[Xe]4f^{11}$. Its 1.5 μm near infra-red (NIR) emission originates from the f-f transition $^4I_{13/2} \rightarrow {}^4I_{15/2}$. Because f shell electrons are buried under the 5s and 5d full shells, the 4f electrons and the transitions are well shielded thus insensitive to the environment, resulting in sharp emission bands. According to the Laporte rule, f-f transitions are forbidden because of conservation of parity. On the one hand, this forbidden nature gives the excited states of Er^{3+} ions long lifetimes, which is essential for achieving population inversion in optical amplification. On the other hand, the forbidden nature results in very poor direct absorption by the Er^{3+} ion. Thus sensitisation by a chromophore is needed, just like an antenna absorbing the energy and then passing it to the ion. Organic chromophores are attractive because they can have large absorption coefficients over a wide spectrum. The organic chromophores can either be chemically bonded with the Er^{3+} ion to form chelating complexes, or in close physical contact by means of co-evaporation. Depending on the distance, the

energy transfer from chromophore to the ion can be categorised into two types, Dexter mechanism and Förster mechanism. The general energy path for sensitising the Er^{3+} ion can be illustrated using a simplified Jablonski diagram (Figure 1.11).

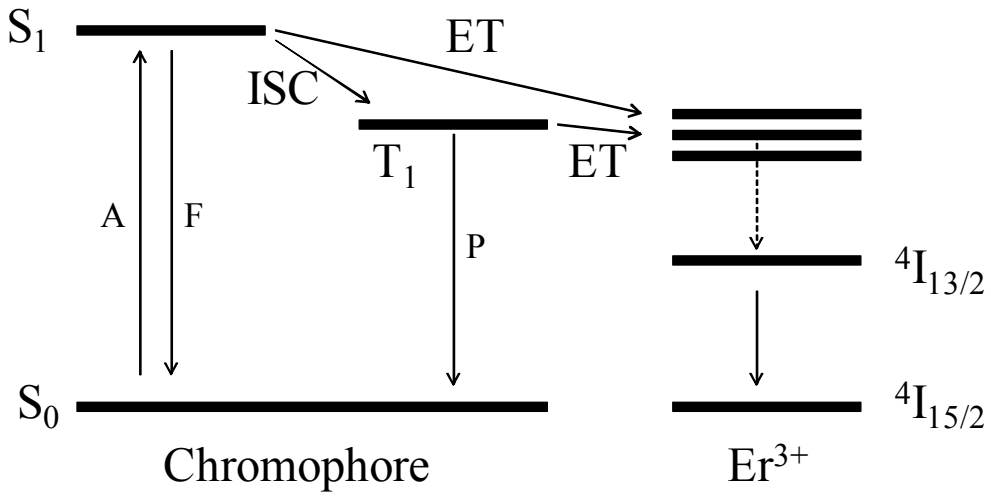

Figure 1.11: Schematic representation of sensitisation of Er^{3+} by an organic chromophore. S_0 or S_1 = singlet state, T_1 = triplet state, A = absorption, F = fluorescence, P = phosphorescence, ISC = intersystem crossing, ET = energy transfer

Firstly the chromophore is excited to its singlet state S_1, from where the energy can go through several paths. The singlet can decay to the ground state, or can be transferred to the triplet state T_1 via intersystem crossing (ISC), or either be transferred to the Er^{3+} ion directly. Since the singlet is short lived, the direct energy transfer from singlet to the metal ion is often not efficient. Therefore it is widely considered the chromophore-to-metal energy transfer is through the long lived triplet state.[42] If the chromophore is chemically bonded with the metal ion so that their orbitals are overlapped, the Dexter type energy transfer can take place involving a double electron transfer.[43] The energy transfer can also be realised when there is a certain distance between the chromophore and the ion via the Förster mechanism, in which the triplet state can have dipole or multipole interaction with the 4f orbitals.[44] This interaction requires a good match of the energy gap between the triplet state and the emitting level

of the erbium ion.

1.5.3 Development of fluorinated erbium complexes

A complete fluorination of the organic ligand, together with exclusion of water molecules from the coordination sphere, has shown great improvement in extending the luminescence lifetime of near infrared (NIR) lanthanide ions. Examples of perfluorinated lanthanide complexes with the best photophysical properties (lifetimes, quantum yields) are given here.

(1) Neodymium sulfonylaminate complexes[39]

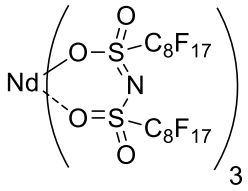

Nd complexes usually suffer from vibrational quenching in solvents of high vibrational frequency that contain OH or CH bonds. Hasegawa and co-workers reported a Nd complex of bis(perfluorooctylsulfonyl)aminate (pos), which gave the first observation of comparable emission efficiency (3.2%) in CH containing solvent (acetone) as that in corresponding deuterated solvent (d_6-acetone). Their Judd-Ofelt analysis indicates that the complex $Nd(pos)_3$ in acetone has a symmetric geometry and is free of coordinating solvent molecules. They calculated the electron density on O atoms and showed that the bis(perfluorooctylsulfonyl)aminate ligand has more negative O atoms than β-diketonates, which supports the stronger interaction between the ligand and the metal ions. They also calculated the Frank-Condon (FC) factor and found that sulfonyl groups have lower values than ligands having carbonyl groups, which leads to superior emission of the complexes of bis(sulfonyl)aminates. In conclusion, they attributed the long lifetime in $Nd(pos)_3$ to the strong chelating and bulky ligand attached with long perfluoroalkyl chains, which gives higher luminescent efficiency than other monodentate ligands or shorter chain ligands.

(2) Erbium tetrafluoroterephthalate[45]

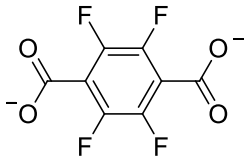

Chen and co-workers reported the first case of erbium-organic-framework (MOF) that is composed of a perfluorinated ligand. While the nonfluorinated analogue exhibits an overall structure of a pair of mutually interpenetrating nets, the perfluorinated one shows a structure of rod-packing framework. Neither of the as-synthesised nonfluorinated and perfluorinated compounds shows luminescence at room temperature because of coordinating and trapped uncoordinated solvent molecules. But they can be activated at 140 °C under vacuum, leading to a totally desolvated nonfluorinated compound and a partially desolvated perfluorinated compound. Although the activated fluorinated framework still has coordinating solvent molecules, it shows enhanced luminescence that is 3 times higher than its nonfluorinated counterpart.

(3) Erbium imidodiphosphinate derivatives

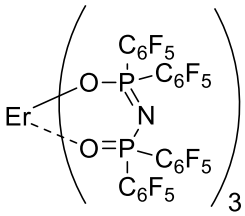

Two groups in UK have reported a perfluorinated shell structure around the lanthanide ion formed by the assembly of three perfluorinated imidodiphosphinate ligands (FTPIP).[40,46] This design not only removes all the X-H bonds of the ligands, but also shields the metal ion from the outside high frequency oscillators, such as water and other solvent molecules, thus leading to unprecedented long lifetimes and quantum yields for NIR emitting ions (Nd, Yb and Er) and yellow emitting Dy ion. However, for the other visible emitting lanthanide ions (Eu and Tb), the complete fluorination results in lower quantum yields compared to those non-fluorinated counterparts of $Eu(tpip)_3$ and $Tb(tpip)_3$. Pikramenou attributed the low yields of visible lanthanide emission to the quenching pathway through a low-lying intraligand π-σ* state at around 715 nm, which

adversely affects the sensitisation of visible emitting lanthanide ions.

What is remarkable about this ligand is that it gives among the longest lifetimes recorded for organic Nd, Er and Yb complexes, up to 1.1 ms for $Yb(ftpip)_3$ in deuterated acetonitrile for instance. However, for practical applications we would further desire visible chromophores combined to the ligands to enable sensatisation of lanthanide ions with low-energy visible light sources instead of a UV source.

(4) Erbium complexes of bis(pentafluorophenyl)phosphinate and bis(perfluoro-*p*-tolyl)phosphinate[41,47]

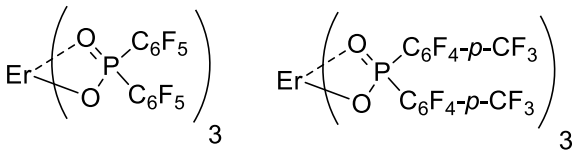

A few lanthanide complexes based on perfluorinated phosphinic acids have been prepared in our group, which are thermally stable, anhydrous chelates with Ln^{3+} ions such as Er^{3+} and Y^{3+}. A long lifetime of ~700 μs for the erbium complex has been achieved. This remarkably long lifetime was attributed to the absence of any C-H bonds in the chelating ligands and the exclusion of solvent molecules by the bulkiness of the ligand. It would be desirable to develop new analogues of the ligand to provide a chromophore in the visible range of the spectrum, and modify the ligand with additional substituent to increase the solubility and volatility of the complex.

(5) Erbium 3,4,5,6-tetrafluoro-2-nitrophenoxide[48]

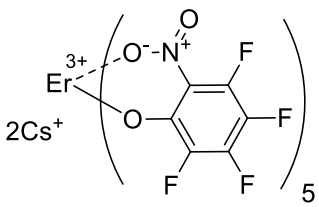

The orange coloured complexes of Cs_2LnL_5 (Ln=Er, Yb,

L=3,4,5,6-tetrafluoro-2-nitrophenoxide) have been prepared in our group. These complexes have moderate lifetimes of 20 μs for the Er complex, and 142 μs for the Yb complex, and the excitation spectra showed that the ligand is acting as a chromophore that absorbs light in the visible region. These complexes are soluble in organic solvents which allow them to be processed in solution.

1.6 Research aims and outline of thesis

Compared to the nonfluorinated parental molecules, fluorination can bring significant differences to both the structure and the physical properties. Although several examples of highly fluorinated hydrocarbons or heterocyclic compounds/polymers were reported, highly fluorinated metal complexes with band gap in the visible spectrum range are rare. Fluorinated metal complexes of phthalocyanines and porphyrins are known, but they only have emission in the deep red/NIR region (≥650 nm) with relative low efficiency. Instead of being used as emissive materials, they are more often used as semiconducting charge transport materials because of high charge carrier mobility.[49-51] Thus the first target of this project is to synthesise some new fluorinated metal complexes that possess band gaps in the visible region with low probability of nonradiative decay, which could lead to materials as efficient emitters or sensitisers. Apart from distinctive molecular packing and stabilised energy levels, another possible consequence of highly fluorination is the increased triplet generation and emission originating from enhanced spin-orbit coupling, which is going to be checked by the experimental results in this thesis.

To increase the chance of obtaining satisfying optoelectronic properties from the new fluorinated materials, the target molecules are based on several reported nonfluorinated molecules which already exhibit some desired properties, such as absorption of visible light and semiconducting behaviour. This part of work including materials design and synthesis will be introduced in Chapter 2.

Secondly, after synthesis and chemical characterisations, the crystal structures of the new compounds need to be examined, and DFT calculations are necessary to help understand the physical properties including absorption and photoluminescence. These results will be discussed in Chapter 3.

Furthermore, the material with the most promising properties will be applied to fabricate OLEDs. Some preliminary optimisations of the device structure are required to achieve satisfying electroluminescence intensity. The voltage-current-luminescence character, electroluminescence spectra, and lifetimes of the excited states should be measured. These results of device performance will be addressed in Chapter 4.

The details of the synthesis and the physical experiments will be described in Chapter 5 and Chapter 6, respectively.

Chapter 2 - Results and discussion part I: Synthesis and characterisations of fluorinated ligands and complexes

2.1 Introduction

In order to achieve a significant "antenna effect" to sensitise erbium ions, the chromophore has to be efficient at absorbing photons and then passing the energy to the metal ion. The chromophore can be connected to the metal ion by direct chemical bonds, or through simple mixing.

In the first case, if the ligand and metal ion are chemically bonded, there are several requirements for a good ligand candidate:

(1) being free of any high frequency oscillators like O–H, N–H and C–H bonds;
(2) having bulky groups to keep solvent molecules away from the metal ion;
(3) having enough binding atoms to satisfy the high coordination number;
(4) having a wide absorption band in the visible region with large absorption coefficient.

Benzothiazole derivatives are good candidates, because they are good at absorbing light with absorptivity exceeding 10^4 $M^{-1}cm^{-1}$; the benzothiazolyl part is an extended conjugated system and can obstruct access to the metal ion by solvent molecules; the N atom on the benzothiazole ring can also be used as a donor atom in combination with a second donor atom, typically oxygen. Fluorinated benzothiazole derivatives have been reported in the literature, so this existing knowledge provides a basis for the development of novel fluorinated ligands.

In this chapter, the synthesis of several different families of benzothiazole-derived ligands with varying amounts of fluorination and the formation of the corresponding

metal complexes will be discussed (Figure 2.1).

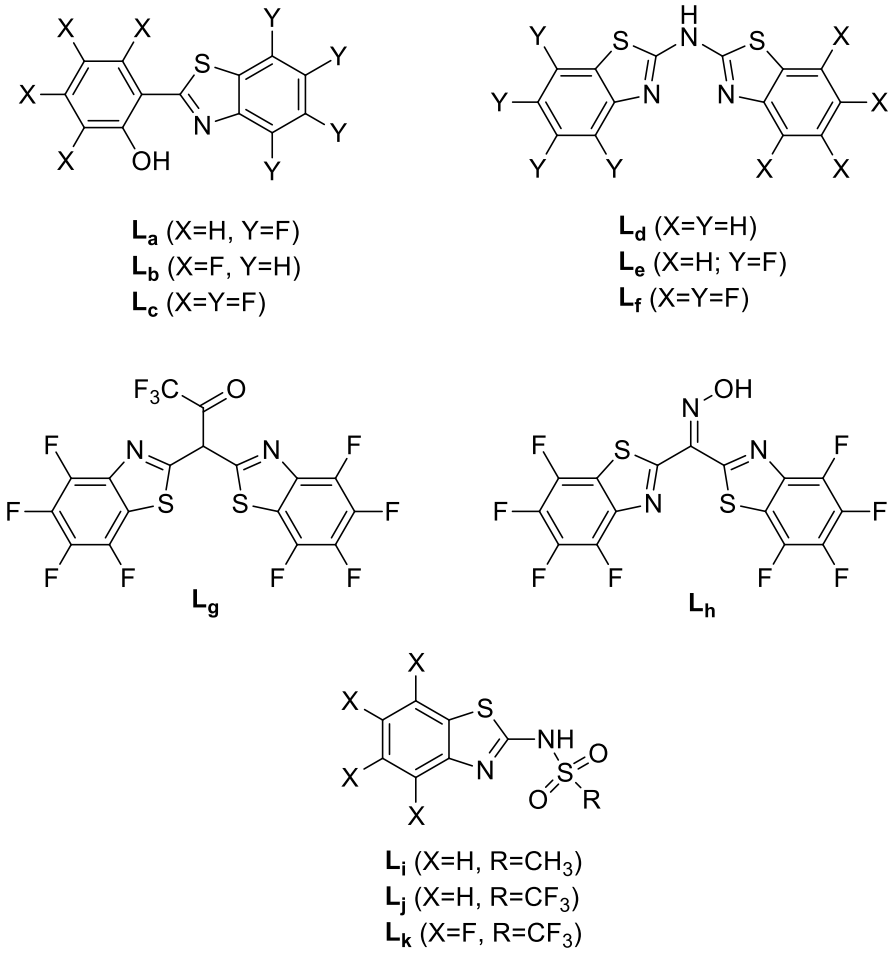

Figure 2.1: Different families of synthesis targets

2.2 Preparation of fluorinated 2-(2-hydroxyphenyl)benzothiazoles

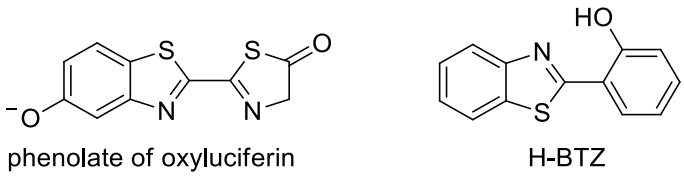

phenolate of oxyluciferin H-BTZ

Figure 2.2: Luminescent benzothiazole derivatives

The luminescence of benzothiazole derivatives is exploited both by Nature and by human technology. Thus phenolate of oxyluciferin (Figure 2.2, left) is responsible for light emission in fireflies and other bioluminescent insects,[52] whereas the zinc(II) complex of 2-(2-hydroxyphenylbenzothiazole) (H-BTZ, Figure 2.2, right) is an excellent white-light emitting material for organic light-emitting diodes (OLEDS).[53-54] The dimeric $[Zn(BTZ)_2]_2$ structure has five-coordinate zinc centres connected by bridging oxygen atoms from the BTZ ligands. Recently the effects of introducing additional alkyl, alkoxy and aryl substituents into the structure of ligand H-BTZ have been examined both experimentally and computationally, resulting in changes to the energies of molecular orbitals in the zinc complexes and shifts in the wavelengths of their maximum light emission.[55-56]

Recently, a patent (WO 2010/020352 A1) reported some other metal complexes of H-BTZ as electron transport materials, including a few lanthanide species. Katkova and coworkers[57] have reported near-infrared electroluminescence of lanthanide complexes with H-BTZ as ligand. The attractive luminescent and charge transport properties of these metal complexes with H-BTZ ligand encouraged us to explore the synthesis of the fluorinated 2-(2-hydroxyphenyl)benzothiazoles.

2.2.1 Synthesis of 2-(2-hydroxy-3,4,5,6-tetrafluorophenyl)-4,5,6,7-tetrafluoro-benzothiazole (6)

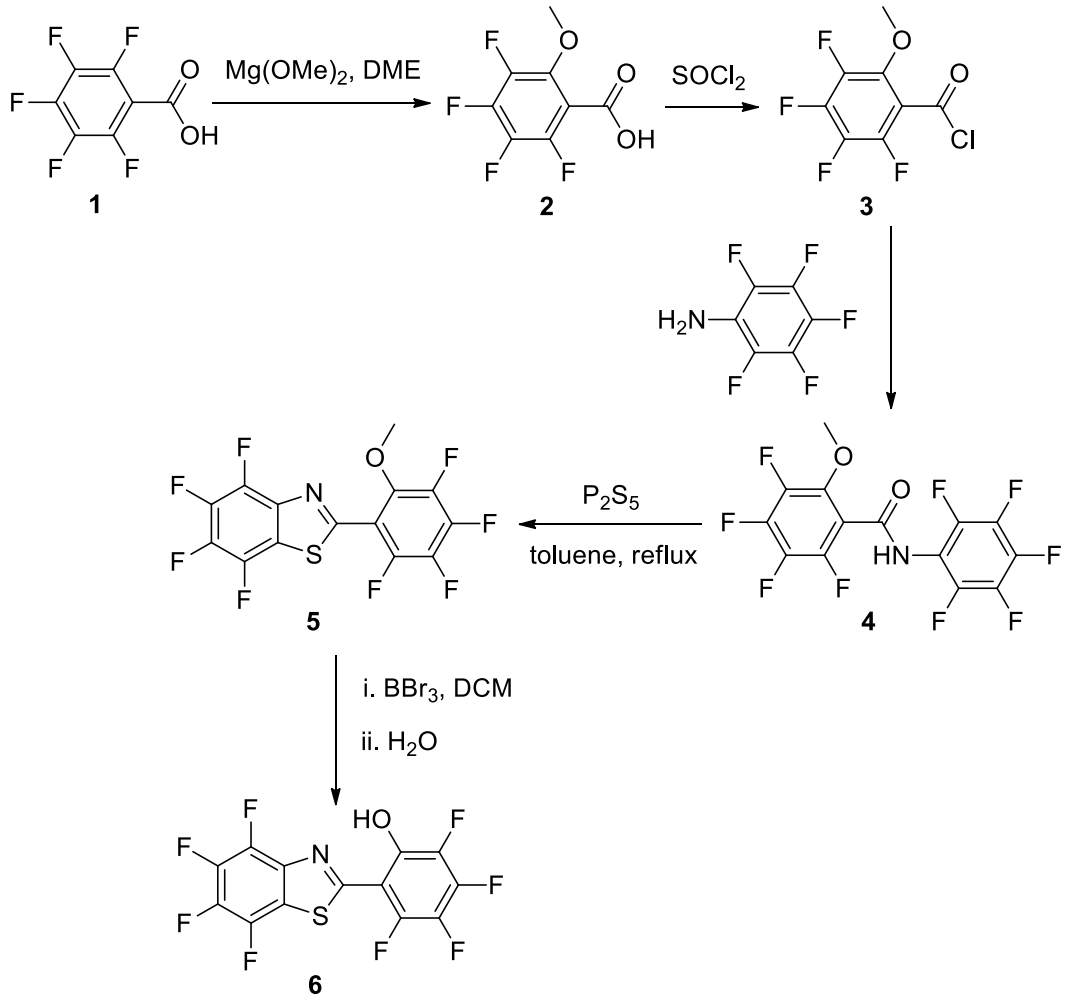

Scheme 2.1: Preparation of 2-(2-hydroxy-3,4,5,6-tetrafluorophenyl)-4,5,6,7-tetrafluoro-benzothiazole

2-Methoxy-3,4,5,6-tetrafluorobenzoic acid (**2**) was prepared according to the literature,[58] then without further purification was treated with thionyl chloride to give the acid chloride (**3**). Reaction of this chloride with pentafluoroaniline gave the amide (**4**), which was converted into 4,5,6,7-tetrafluoro-2-(2-methoxyphenyl)benzothiazole (**5**) by cyclisation with phosphorus(V) sulfide, followed by demethylation with BBr_3, to give the ligand 4,5,6,7-tetrafluoro-2-(2-hydroxyphenyl)benzothiazole (**6**).

2.2.2 Synthesis of 2-(2-hydroxyphenyl)-4,5,6,7-tetrafluorobenzothiazole (11)

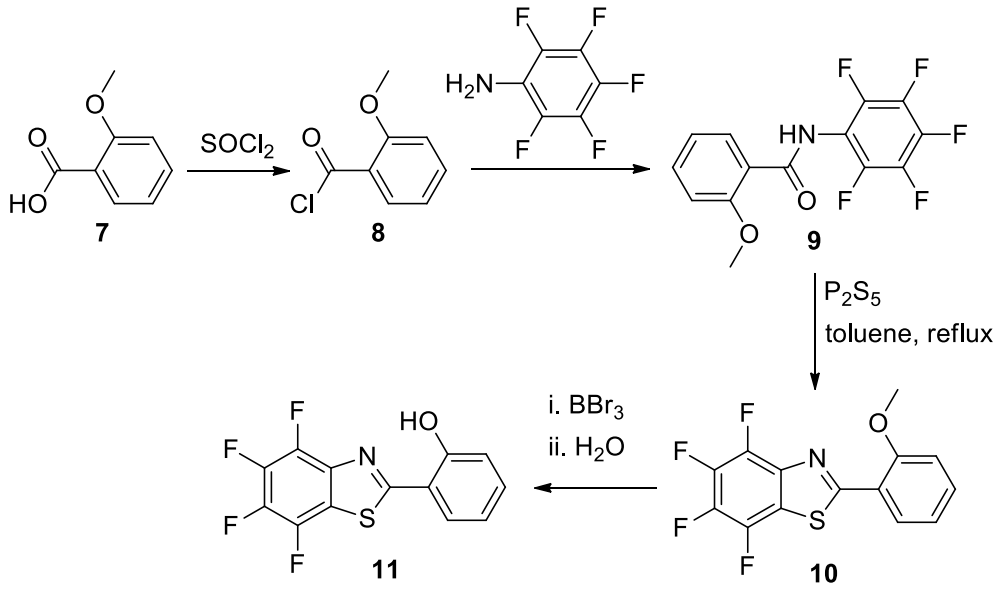

Scheme 2.2: Praparation of 2-(2-hydroxyphenyl)-4,5,6,7-tetrafluorobenzothiazole

The synthesis of half fluorinated ligand 2-(2-hydroxyphenyl)-4,5,6,7-tetrafluoro-benzothiazole (**11**) was similar to the fully fluorinated ligand, except that the acylation of pentafluoroaniline was performed using 2-methoxybenzoyl chloride, which was obtained from commercially available 2-methoxybenzoic acid and thionyl chloride.

2.2.3 Synthesis of 2-(2-hydroxy-3,4,5,6-tetrafluorophenyl)benzothiazole (15)

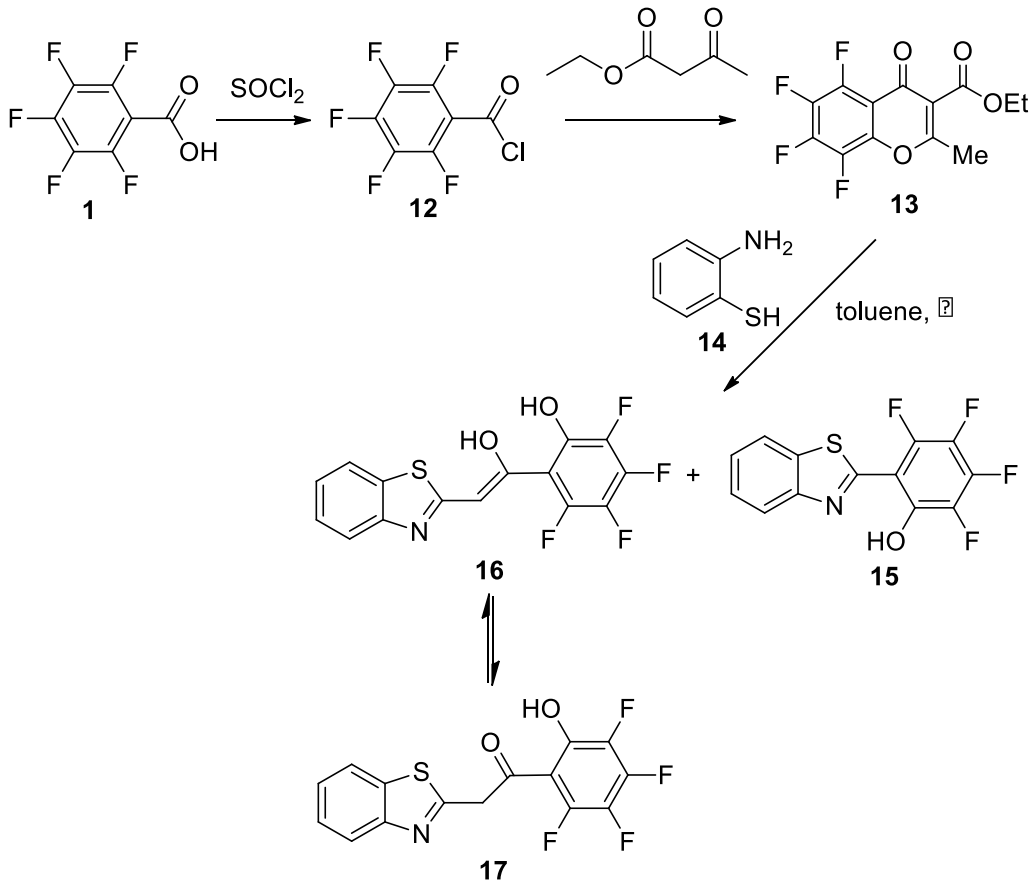

Scheme 2.3: Preparation of 2-(2-hydroxy-3,4,5,6-tetrafluorophenyl)benzothiazole (**15**, Route 1)

The preparation of 2-(2-hydroxy-3,4,5,6-tetrafluorophenyl)benzothiazole (**15**) has previously been reported by Bazyl' et al, by reaction of the 2-aminothiophenol **14** with the chromone **13**.[59] However, the literature ^{1}H NMR has two separate OH signals at low field and describes the entire aromatic region as one multiplet. When we repeated this preparation we isolated a low yield of material that had spectra consistent with ligand **15**, with just one OH signal and four distinct aromatic C-H environments in its ^{1}H NMR spectrum; the melting point was more than 30 degrees higher than the literature value, but ^{19}F NMR, elemental analysis, and high resolution mass spectrometry confirmed that we had isolated the correct structure. It is therefore likely that the material previously described by Bazyl' et al was not pure **15**. We also identified benzothiazole derivative **16** as a product of the reaction between **13** and **14**.

The keto form **17**, which is a tautomer of **16**, was not observed by NMR in deuterated DMSO solution. Three distinctive peaks with chemical shifts 6.75 (1H, C=CH), 13.59 (1H, OH), 15.63 (1H, OH) were assigned to the three non-aromatic protons in the enol form **16** (Figure 2.3), while the keto form **17** would only give two non-aromatic peaks in 2:1 ratio. A possible mechanism of producing compound **16** could be the successive addition and cyclisation of 2-aminothiophenol to the chromone (Scheme 2.4).

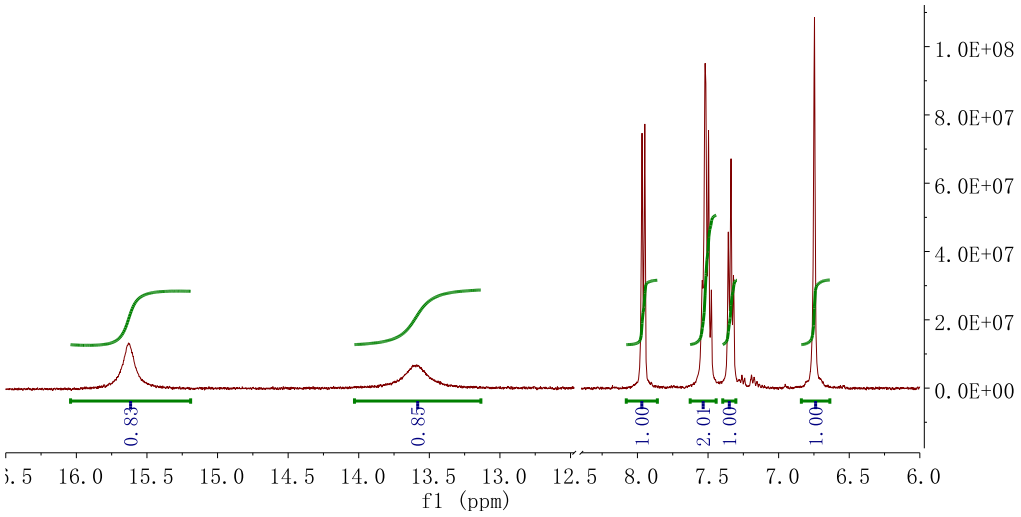

Figure 2.3: ^{1}H NMR of compound **16** in d_6-DMSO showing its enol form

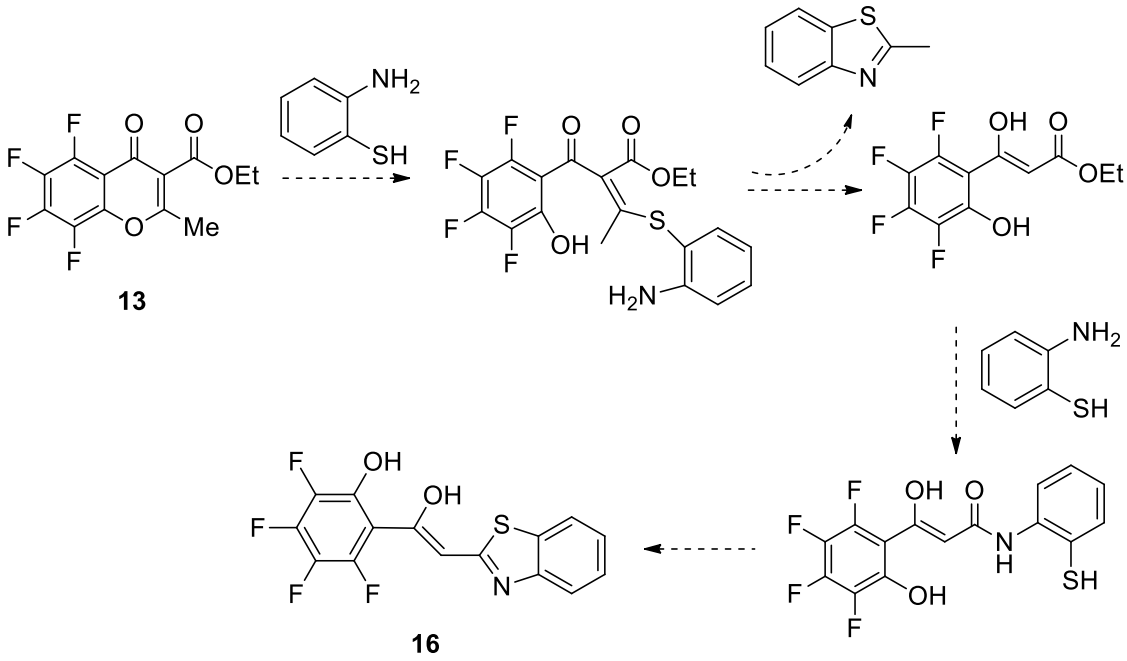

Scheme 2.4: A possible mechanism for producing compound **16**

In Route 1, the low yield of intermediate **13** limited the overall yield of the target, so an

alternative synthetic route was explored. In the attempt to increase the yield of **15**, we employed the general method[60] of condensing 2-aminothiophenol (**14**) with an acid chloride (Scheme 2.5), and reacted 3,4,5,6-tetrafluoro-2-methoxybenzoyl chloride, **3**, with 2-aminothiophenol, **14**, using NMP (*N*-methyl-2-pyrrolidone) as solvent. We were pleased to find that *O*-demethylation occurred under these reaction conditions, to give the required phenol **15** in a one pot reaction after quenching with water.

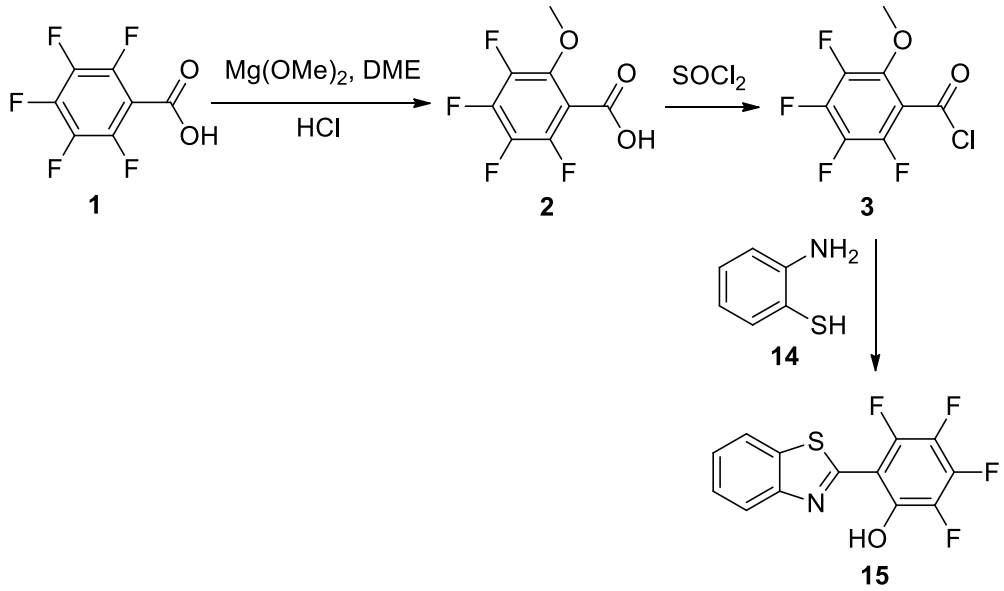

Scheme 2.5: Preparation of 2-(2-hydroxy-3,4,5,6-tetrafluorophenyl)benzothiazole (**15**, Route 2)

2.3 Preparation of bis(benzothiazolyl)amines

This series of ligands have structural similarities with the well known β-diketone type ligands. In β-diketones, O=C–C–C=O provides the chelating skeleton and chromophores can be attached to this skeleton as separated terminal groups R^1 and R^2, while in bis(benzothiazolyl)amines the chelating skeleton is N=C–N–C=N which is also embedded in the chromophore's framework and part of a conjugated structure.

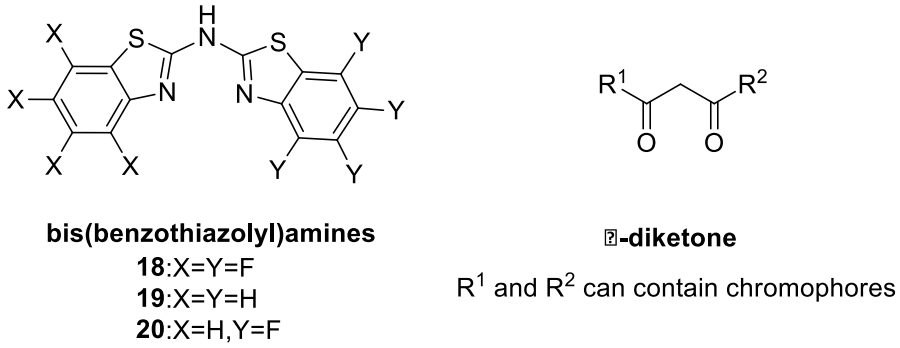

bis(benzothiazolyl)amines
18:X=Y=F
19:X=Y=H
20:X=H,Y=F

β-diketone
R^1 and R^2 can contain chromophores

Figure 2.4: bis(benzothiazolyl)amines and β-diketones

2.3.1 Preparation of perfluorinated bis(benzothiazolyl)amine (18)

1. Attempts to prepare perfluorinated bis(benzothiazolyl)amine via cyclisation

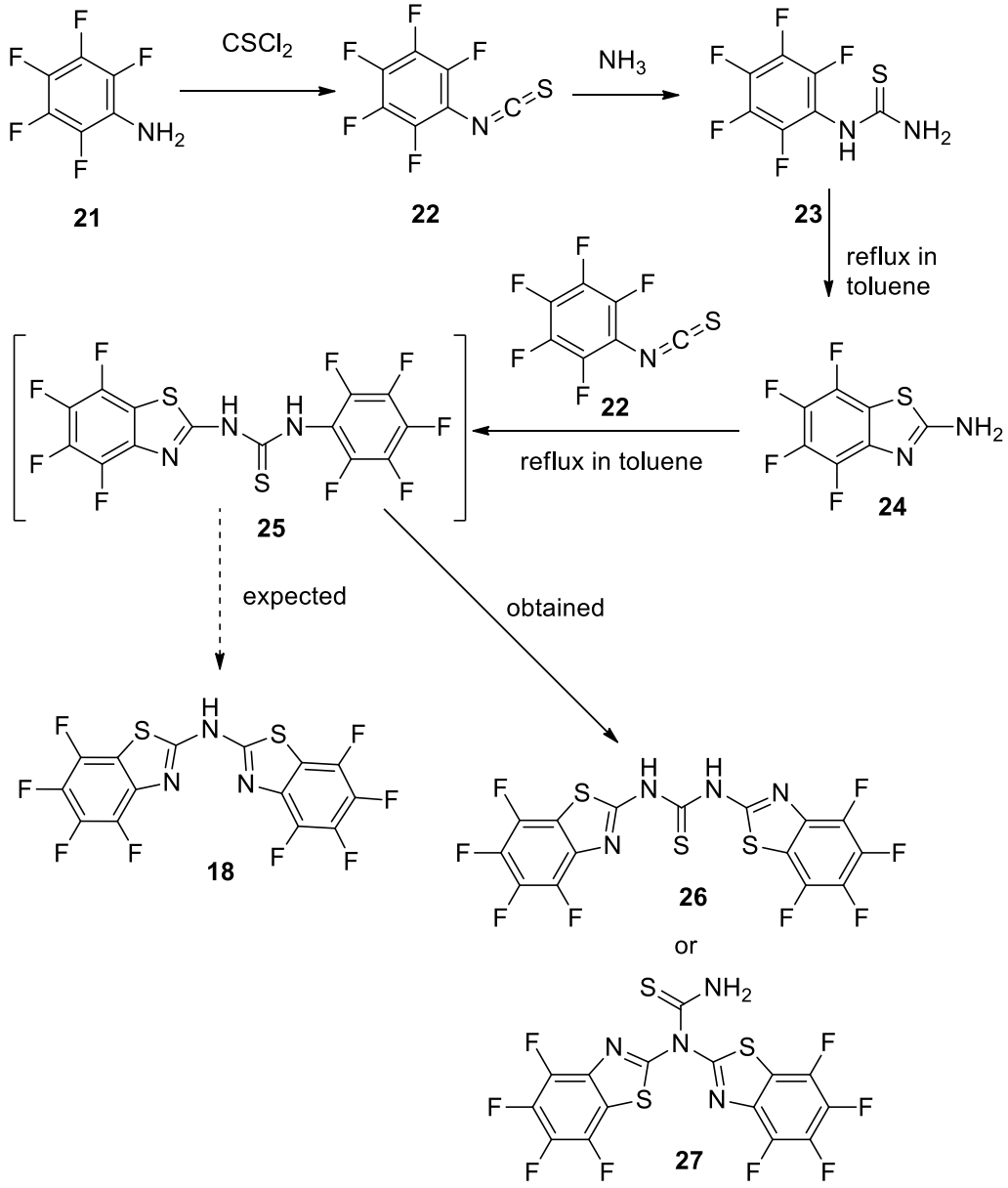

Scheme 2.6: Attempted preparation of bis(4,5,6,7-tetrafluorobenzothiazolyl)amine **18**

2-Amino-4,5,6,7-tetrafluorobenzothiazole (**24**) was prepared from pentafluoroaniline (**21**) in three steps according to literature procedures in which the benzothiazole ring system was formed by cyclisation of the thiourea (**23**).[61] It was envisaged that reaction of amine **24** with isothiocyanate **22** would then give a new thiourea **25**, which would readily cyclise to form the desired secondary amine ligand **18**. However, the reaction between 2-amino-4,5,6,7-tetrafluorobenzothiazole (**24**) and pentafluorophenyl

isothiocyanate (**22**) in refluxing toluene did not give the desired ligand **18**, but produced a precipitate which was deduced to be one of the two isomeric thioureas **26** and **27** from NMR and mass spectra. To identify which isomer the product is, the precipitate was subjected to hydrolysis by hydrochloric acid. After hydrolysis of the thiourea group, compound **26** would give 2-amino-4,5,6,7-tetrafluorobenzothiazole (**24**) as the product, while compound **27** would give the desired ligand **18** (Scheme 2.7).

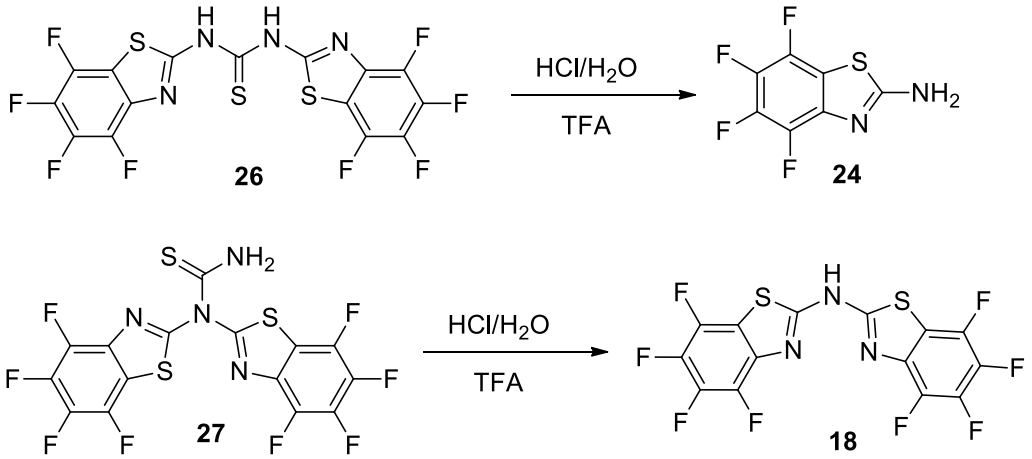

Scheme 2.7: Hydrolysis of the unknown precipitate

By comparing the TLC and analysing the fluorine NMR of product, it was found that 2-amino-4,5,6,7-tetrafluoro-benzothiazole (**24**) was produced and so it can be deduced that the precipitate was compound (**26**).

The reaction between 2-amino-4,5,6,7-tetrafluoro-benzothiazole (**24**) and pentafluoro-phenyl isothiocyanate (**22**) was also tried in refluxing DMF in an attempt to help the cyclisation of intermediate **25** and increase the reaction rate. However, upon refluxing for 5 days, DMF reacted as an electrophile with the amine starting material **24** to give the amidine **28** (Scheme 2.8). A small amount of tertiary amine **29** was also found among the by-products. It was supposed that DMF decomposed at high temperature and produced Me_2NH, which then added to the C=N bond of starting material **24** followed by loss of NH_3 from the addition intermediate to give **29**.

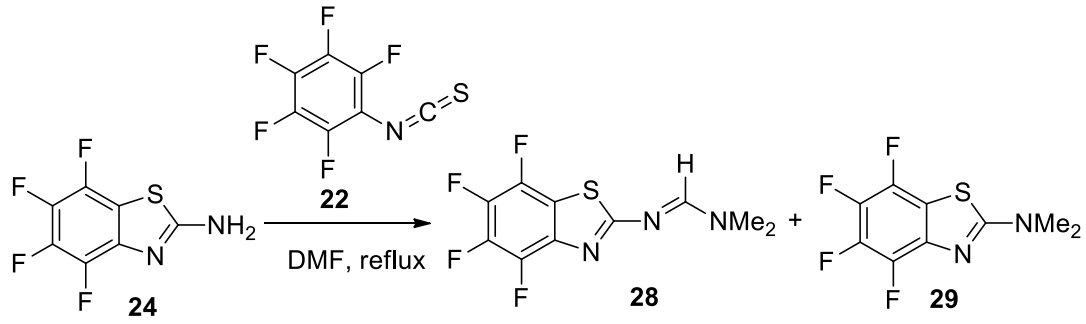

Scheme 2.8: Attempted preparation of ligand **18** in DMF

2. Successful synthesis of perfluorinated bis(benzothiazolyl)amine

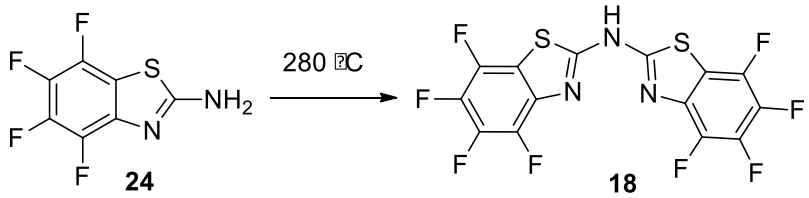

Scheme 2.9: Preparation of ligand **18** at high temperature

In work which will be discussed later in this chapter we discovered that the nonfluorinated bis(benzothiazolyl)amine could be prepared by simply heating 2-aminobenzothiazole at 250 °C in the absence of solvent. We adopted the same method for the fluorinated system (Scheme 2.9), but at a slightly higher temperature of 280 °C because of the slower reaction rate. It was much more difficult to get a high conversion of the starting material than in the case of the nonfluorinated counterpart and this was attributed to the following two reasons: the electron density on the amine nitrogen is decreased as a consequence of the electron withdrawing effect of fluorine atoms, so its nucleophilicity is weakened. In addition, the fluorinated starting material is much more volatile than the nonfluorinated analogue, which makes the starting material sublime out from the reaction mixture during the heating process. The latter problem can be minimised by creating a condensing zone in the middle of reaction vessel, with a temperature above the melting point of the starting material but not hot enough to sublime it. In this case, the melting point of starting material is about 200 °C, so the

condensing zone can be created having a temperature range of 200 – 280 °C. This can be realised by resting the bottom part the vertical reaction tube in an aluminium block, and wrapping the middle part with aluminium foil.

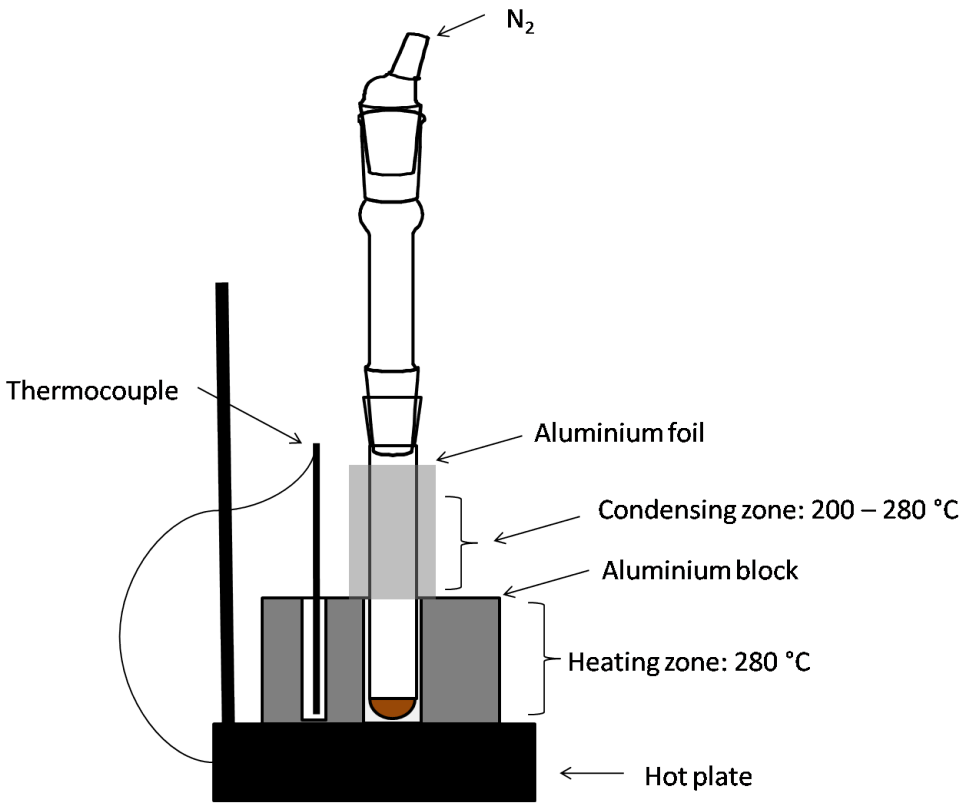

Figure 2.5: Apparatus for high temperature preparation of perfluorinated bis(benzothiazolyl)amine

2.3.2 Preparation of bis(benzothiazolyl)amine (19)

1. Preparation of bis(benzothiazolyl)amine via cyclisation

In order to have a comparison for the perfluorinated ligand and complexes to be made, the analogous nonfluorinated ligand was required. At first, this ligand was prepared according to the literature.[62] 2-Aminobenzothiazole (**30**) was reacted with phenyl isothiocyanate (**31**) to give 1-benzothiazol-2-yl-3-phenyl-thiourea (**32**), which was then cyclized using NBS in concentrated sulfuric acid to give the ligand bis(benzothiazolyl)amine (**19**).

However, this route via cyclisation using NBS was found to generate brominated by-product **33**. Due to the very similar properties of ligand **19** and by-product **33**, it was difficult to separate them to obtain a pure ligand. ^{1}H NMR showed that the brominated by-product could account for ~5% in the recrystallised product. Even after multiple purification steps, such as recrystallisation of the ligand and then sublimation of the prepared zinc complex, the presence of brominated analogue could still be detected by mass spectrometry. If the material is going to be used in (opto)electronic applications, then the presence of such impurities is undesirable.

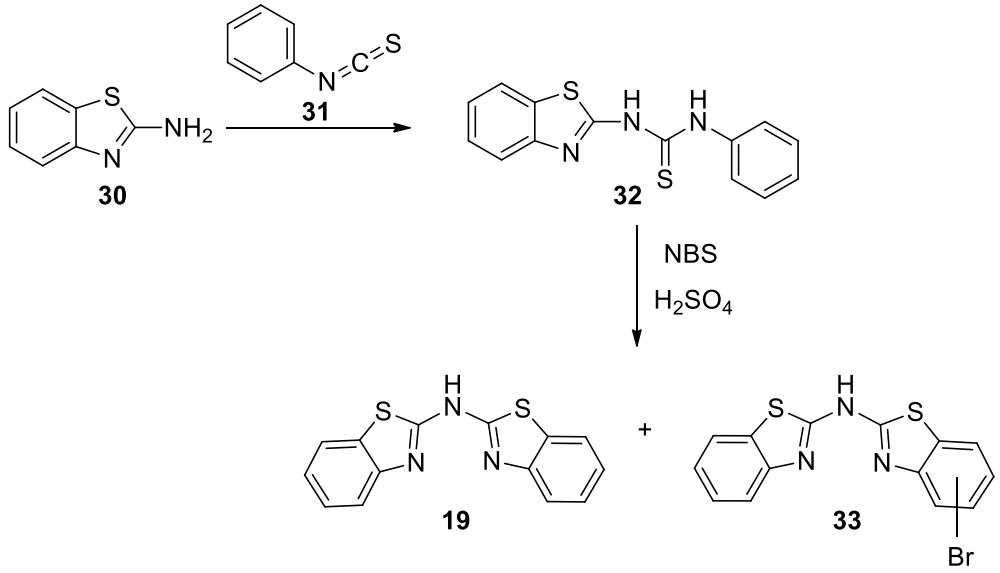

Scheme 2.10: Preparation of ligand **19** using NBS

2. Attempts to prepare bis(benzothiazolyl)amine via copper catalysed coupling reaction

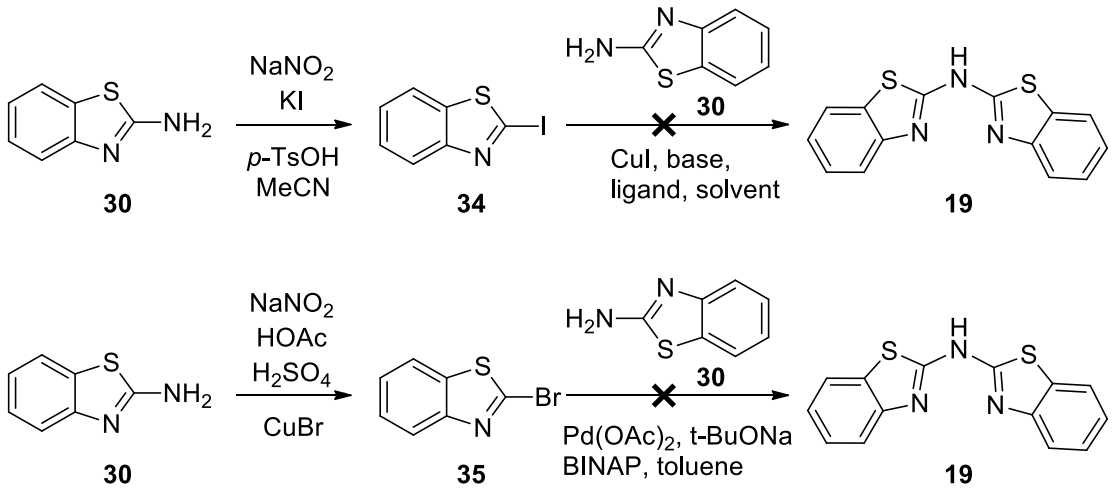

Scheme 2.11: Attempts to prepare ligand **19** using catalysed coupling reaction

To achieve the pure compound of bis(benzothiazolyl)amine (**19)**, other synthesis routes were tried using copper(I) catalysed coupling reactions (Scheme 2.11). The aryl halides in these reactions were made by Sandmeyer reactions according to literature procedures.[63]

Table 2.1: Conditions of attempted coupling reactions

Entry	catalyst	Ligand	Base	Solvent	Time	Temp
1	10 mol% CuI	proline	K_2CO_3	DMSO	24 h	80 °C
2	4 mol% CuI	2,2'-bipyridyl	t-BuOK	toluene	3.5 h	reflux
3	10 mol% $Pd(OAc)_2$	BINAP	t-BuONa	toluene	2h	reflux

However, none of these attempts gave the desired product but instead gave rather insoluble species. We suspect that the desired ligand would combine with the metal ion as soon as it was generated in the reaction mixture, then deactivate the catalyst and prevent the reaction going further. As a result, alternative synthesis routes were investigated to prepare ligand **19** in the absence of any metal catalyst.

3. Preparation of bis(benzothiazolyl)amine via high temperature reaction

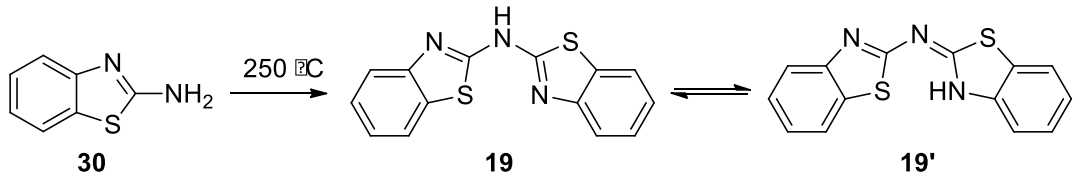

Scheme 2.12: Preparation of ligand **19** via high temperature reaction

The synthesis of the nonfluorinated ligand (**19**) has been reported by Wagner-Jauregg and was carried out under solvent-free conditions at 250 °C with catalysis by Pd/C.[64] However, when we repeated this preparation and compared it with a parallel experiment in the absence of Pd/C, we found the latter conditions still gave the pure product with complete conversion of the starting material after 1 h shown by TLC. Presumably this process involves nucleophilic addition by the primary amine group at the C-2 carbon of the benzothiazole, followed by irreversible loss of ammonia gas. The ^{1}H NMR spectrum of the product showed one broad peak at δ7.65 in the aromatic region, corresponding to the H-4 protons on the two benzothiazole rings, that were expected to give a doublet (Figure 2.6). We attributed this broadening to the tautomerisation of ligand **19** to **19'** (Scheme 2.12), which will bring some slight difference in the environment experienced by the two H-4 protons that are closest to the N-3 nitrogen atoms. This tautomerisation was also observed in the ^{1}H NMR and the crystal structure of half fluorinated analogue, which will be introduced later in this chapter (^{1}H NMR) and next chapter (crystal structure).

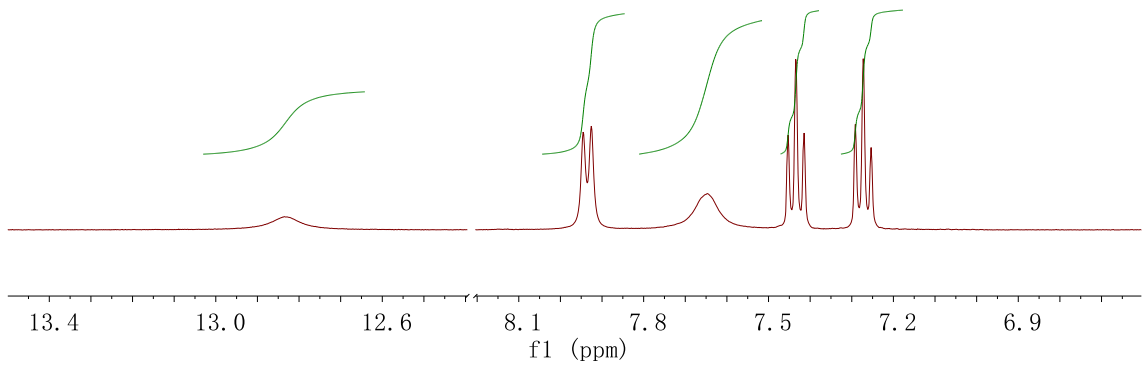

Figure 2.6: ^{1}H NMR (400 MHz) of ligand **19** in DMSO-d_6

2.3.3 Preparation of half fluorinated bis(benzothiazolyl)amine (20)

*1. Preparation of half fluorinated bis(benzothiazolyl)amine **20** using NBS*

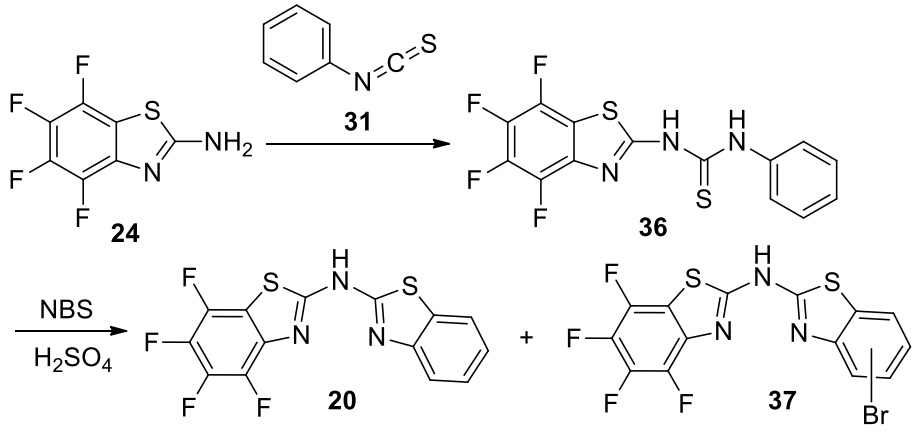

Scheme 2.13: Preparation of half fluorinated bis(benzothiazolyl)amine using NBS

This route of preparing half fluorinated bis(benzothiazolyl)amine (**20**) is the same as the one initially used to prepare the nonfluorinated version using NBS to effect cyclisation. Unsurprisingly, the ligand was obtained with the brominated compound **37** as the by-product. The brominated by-product was found in the mass spectrum, which showed two peaks located at m/z 432.9 and 434.9 respectively with nearly same intensity, while the ligand **20** lies at m/z 355.0. The difficulty of separating them makes this route unsatisfactory and other synthesis routes were therefore explored.

*2. Attempt to prepare half fluorinated bis(benzothiazolyl)amine **20** using 2-iodophenyl isothiocyanate*

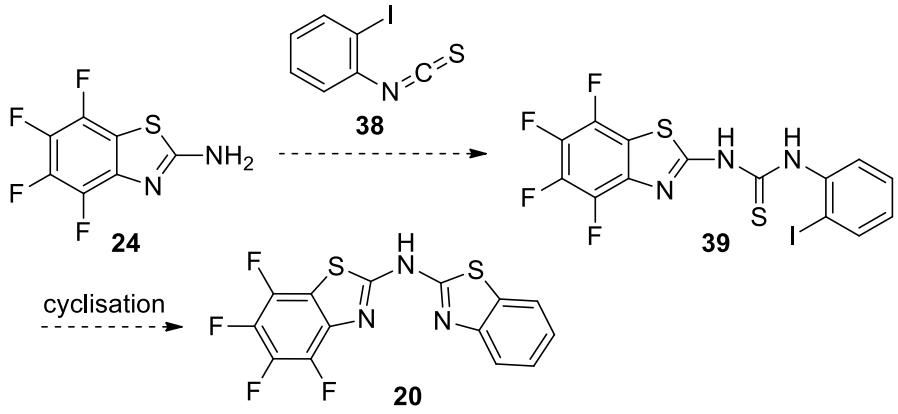

Scheme 2.14: Attempted preparation of half fluorinated bis(benzothiazolyl)amine using 2-iodophenyl isothiocyanate

In order to use an intramolecular nucleophilic substitution method to cyclise a thiourea derivative to form a benzothiazole ring, and avoid the problem of bromination when using NBS as the cyclization reagent, amine **24** was treated with 2-iodophenyl isothiocyanate (**38**) in the hope of getting the halogenated thiourea intermediate **39**. If this step had worked, the thiourea should then cyclise to give the desired ligand **20**. However, it was found that 2-iodophenyl isothiocyanate (**38**) did not react with 4,5,6,7-tetrafluorobenzothiazole (**24**) at all after 24 hours of stirring in DCM/ether (2:1) at room temperature. Then the reaction was tried in refluxing toluene for 96 h, but still a large amount of the isothiocyanate starting material was present as indicated by TLC and FTIR.

3. Attempt to prepare half fluorinated bis(benzothiazolyl)amine via cyclizing fluorinated thiourea

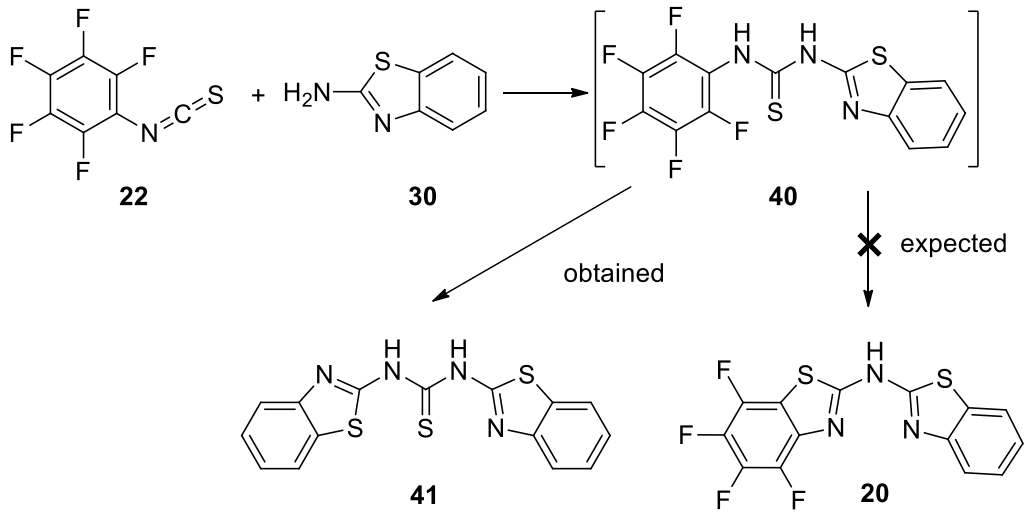

Scheme 2.15: Attempted preparation of half fluorinated bis(benzothiazolyl)amine via cyclising fluorinated thiourea (Route 1)

The ligand **20** is composed of a nonfluorinated benzothiazole and a fluorinated benzothiazole. Since the strategy of cyclising a thiourea to obtain the nonfluorinated benzothiazole did not work, cyclisation to form the fluorinated ring was examined. Thus a mixture of pentafluorophenyl isothiocyanate (**22**) and 2-aminobenzothiazole (**30**) was refluxed in toluene in an attempt to form the intermediate thiourea (**40)** and then the

ligand (**20)** in one pot. However, the precipitate obtained was identified as a nonfluorinated symmetric thiourea (**41**), implying loss of pentafluoroaniline as the by-product. This is considered as the consequence of the lower p*K*a and thus better leaving group ability of pentafluoroaniline compared with 2-aminobenzothiazole. Thus the simultaneous presence of 2-aminobenzothiazole (**30**) and the desired intermediate (**40**) was judged to be undesirable.

This led me to consider the attack of the fluorinated amine **30** on the nonfluorinated isothiocyanate **42** (Scheme 2.16). However, the yield of this reaction was extremely low; only 2% yield of desired product **40** was isolated. Meanwhile, the main product obtained was a fluorinated symmetric thiourea (**43**) with pentafluoroaniline attached to the thiocarbonyl. According to Lange's Handbook of Chemistry (15th Edition), the pK_{aH} of 2-aminobenzothiazole is 4.48; and the pK_{aH} of pentafluoroaniline is 0.3.[65] The reaction showed that the apparently better leaving group of pentafluoroaniline stayed with the thiocarbonyl. This result can not be explained simply on the basis of pK_a values, but may originate from an equilibrium driven by precipitation of the insoluble by-product.

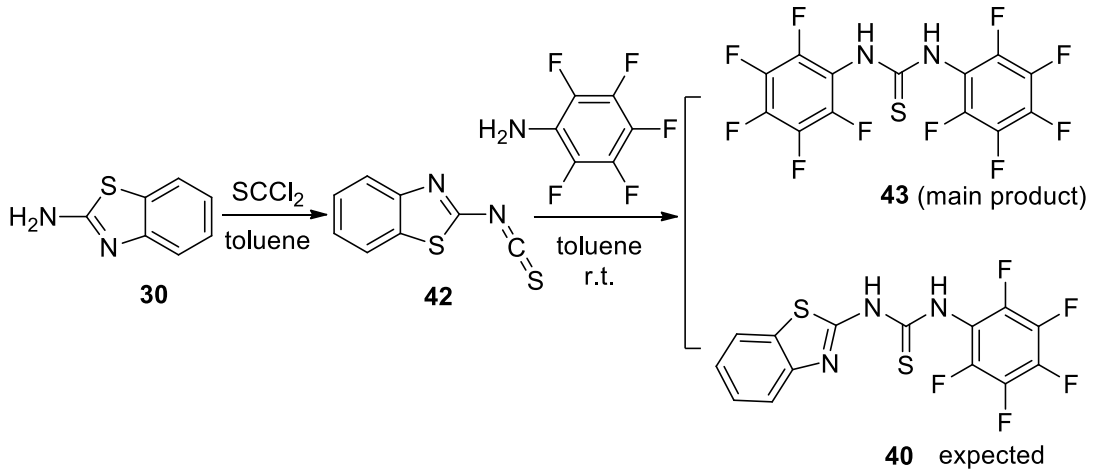

Scheme 2.16: Attempted preparation of half fluorinated bis(benzothiazolyl)amine via cyclising fluorinated thiourea (route 2)

*4. Preparation of half fluorinated bis(benzothiazolyl)amine (**20**) via high temperature reaction between amines **24** and **30***

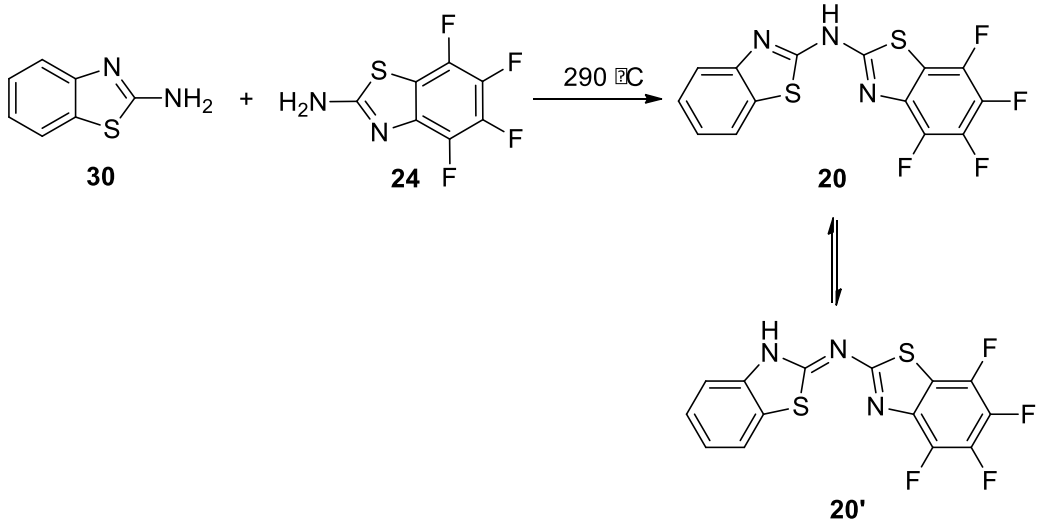

Scheme 2.17: Preparation of half fluorinated bis(benzothiazolyl)amine (**20**) via high temperature reaction

Inspired by our previous success of preparing the symmetric bis(benzothiazolyl)amines, **18** and **19,** by using high temperature self-condensations of the corresponding primary amines, we wondered if we could use the same method for preparing the asymmetric one by a crossed condensation (Scheme 2.17). There was a concern that each of the two starting materials could react either with itself or with the other amine to give mixtures of nonfluorinated, perfluorinated and half fluorinated bis(benzothiazolyl)amines. However, it was hoped that the electron rich nonfluorinated 2-aminobenzothiazole **30** might preferentially act as a nucleophile and attack the electron deficient fluorinated counterpart, the better electrophile, to give the half fluorinated product.

For the first trial, the two starting materials **30** and **24** were mixed by grinding, and the mixture was heated in a vertical tube under protection of nitrogen. The desired half fluorinated product was indeed generated, but only in a low yield of 17%. As expected, the other by-products were the nonfluorinated and perfluorinated bis(benzothiazolyl)amines. The nonfluorinated bis(benzothiazolyl)amine **19** was the

main by-product, while the perfluorinated amine **18** was much less abundant. The origin of the low yield could be the uneven mixing of two starting materials, and the high volatility of the fluorinated starting material which evaporates at high temperature and disturbs the original 1:1 ratio of two starting materials. In order to increase the yield, the two starting materials **30** and **24** were mixed in solution followed by evaporation of the solvent. In addition, to maintain an approximate 1:1 ratio of two starting materials, the same apparatus was used as for the preparation of the perfluorinated bis(benzothiazolyl)amine, with a condensing zone above the heating zone to return the evaporated fluorinated 2-aminobenzothiazole back to the reacting mixture. After adopting these measures, the yield of half fluorinated product was increased to 42%. Similar to the nonfluorinated ligand **19**, the tautomerisation of the ligand **20** to **20'** was also observed. The ^{1}H NMR showed a broad peak at δ7.59 corresponding to the H-4 proton. The structural evidence for this tautomerisation will be discussed in the next chapter.

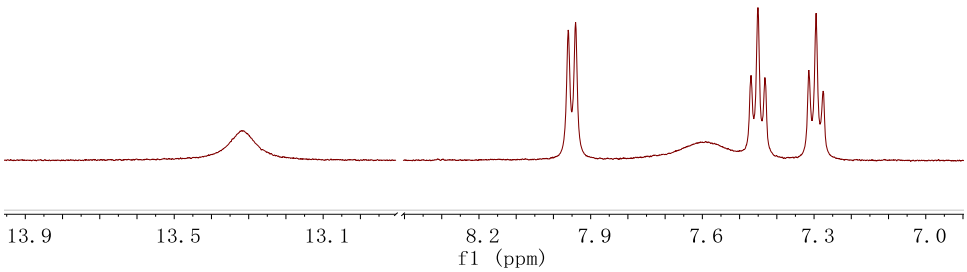

Figure 2.7: ^{1}H NMR (400 MHz) of ligand **20** in DMSO-d_6

2.4 Preparation of bis(perfluorobenzothiazol-2-yl)methane (47)

A few transition metal complexes of bis(perfluorobenzothiazol-2-yl)methane, the nonfluorinated analogue of **47,** have been reported in the literature, such as the Co, Ni, Cu and Zn complexes.[66] So we were interested in making the fluorinated compound **47**. The anion derived from this ligand still has one proton attached to the central carbon, which would be expected to act as a quenching source to reduce the lifetime if the erbium complex were made. However it may be possible to carry out further synthesis to replace the proton with other groups which can provide a donor atom such as O or N (e.g. to form the potential ligands **48** and **49)**.

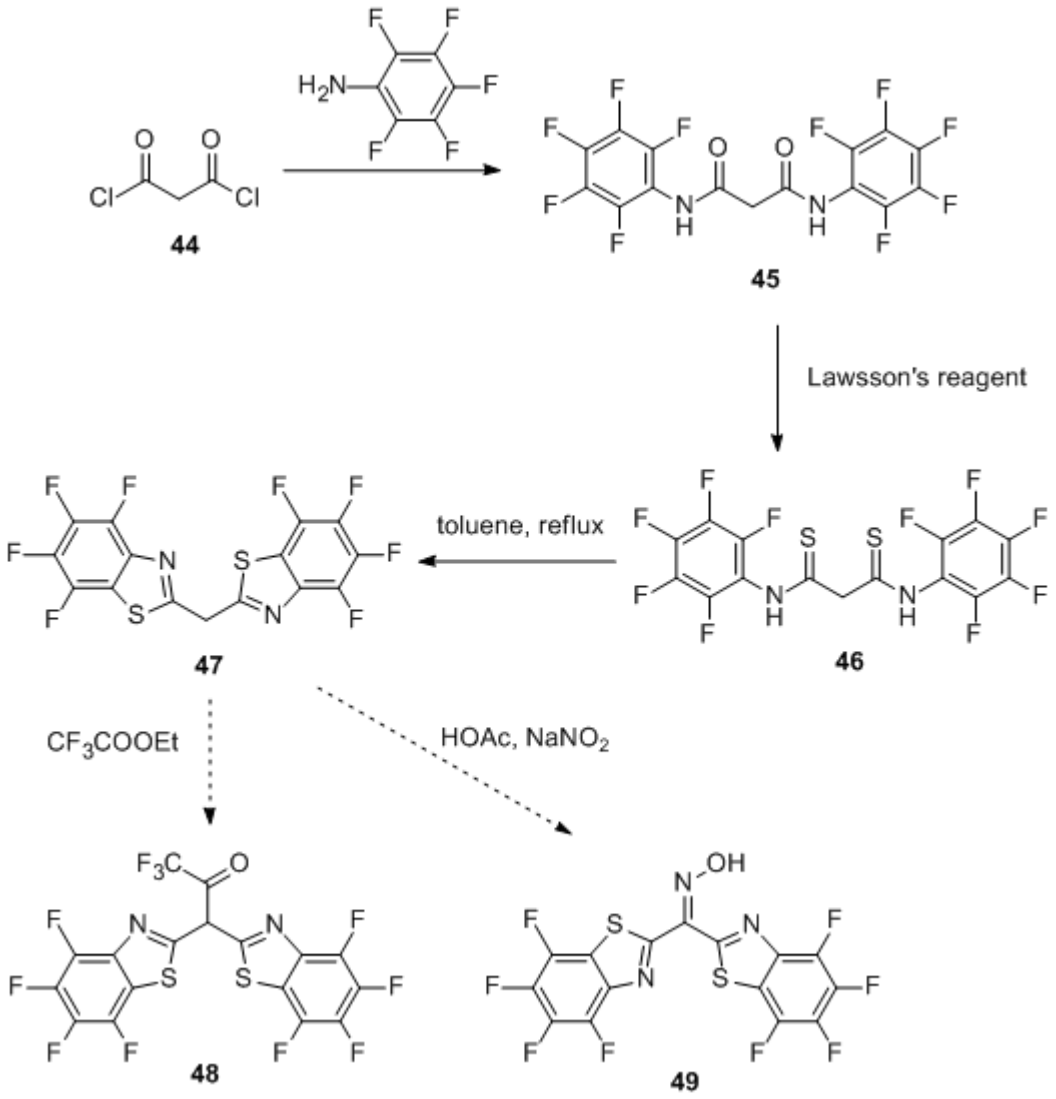

Scheme 2.18: Preparation of bis(perfluorobenzothiazol-2-yl)methane derivatives

Malonyl dichloride **44** was firstly converted into *N*,*N*'-bis(pentafluorophenyl)-malonamide **45** by treatment with four equivalents of pentafluoroaniline. When the malonamide **45** was refluxed with P_4S_{10} in toluene in an attempt to get the cyclised bis(tetrafluorobenzothiazolyl)methane **47** in one pot, only a small amount (3%) of desired product was isolated while many other coloured by-products were formed. So a two-step method was adopted instead. Firstly the intermediate dithiomalonamide **46** was prepared using Lawesson's reagent,[67] then isolated by flash chromatography, followed by refluxing in toluene to provide the cyclised compound bis(tetrafluorobenzothiazolyl)methane (**47**). However, time did not permit further investigation, thus compounds **48** and **49** remain as future targets.

2.5 Preparation of *N*-(benzothiazol-2-yl)methanesulfonamides

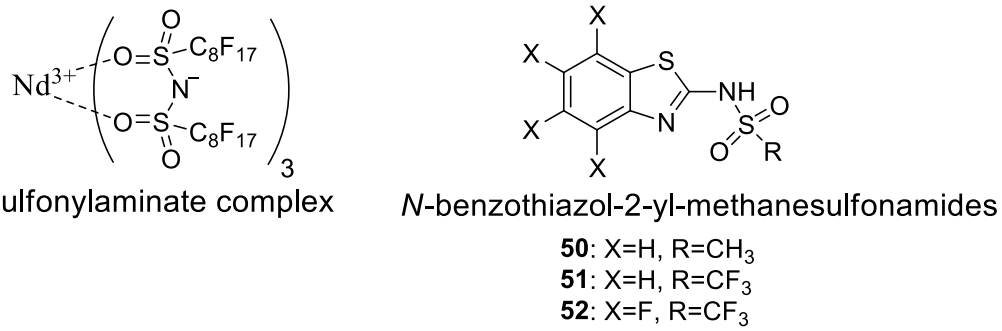

sulfonylaminate complex

N-benzothiazol-2-yl-methanesulfonamides

50: X=H, R=CH_3
51: X=H, R=CF_3
52: X=F, R=CF_3

Figure 2.8: Comparison of new benzothiazole based sulfonamide ligands with existing sulfonylaminate ligand

Hasegawa and co-workers reported the Nd complex of a fluorinated chelating ligand, bis(perfluorooctylsulfonyl)aminate[39] (Figure 2.8). Calculation was performed on the neodymium complex and that author concluded that the sulfonylaminate ligand binds more strongly with metal ions than β-diketonates because of its much more negative O atoms. In the neodymium complex the ligands are capable of excluding solvent molecules from the coordination sphere of the metal, thus giving a comparable emission efficiencies (3.2 %) for the Nd complex in CH containing solvent (acetone) and deuterated solvent (acetone-d_6).

However, such a ligand does not have an effective chromophore that can harvest photons. So we intended to replace one half of the sulfonylaminate ligand with a benzothiazole group, which can provide both a chromophore and a donor nitrogen atom. This ligand can be fully fluorinated on the benzothiazole (X=F) and the alkyl chain ($R=C_nF_{2n+1}$).

The synthesis was straightforward: *N*-benzothiazol-2-yl-methanesulfonamides **50**–**52** were obtained in one step by reaction of the corresponding 2-aminobenzothiazole with methanesulfonyl chloride or trifluoromethanesulfonic anhydride. The attempted synthesis of zinc and erbium complexes of these ligands will be introduced later in this chapter.

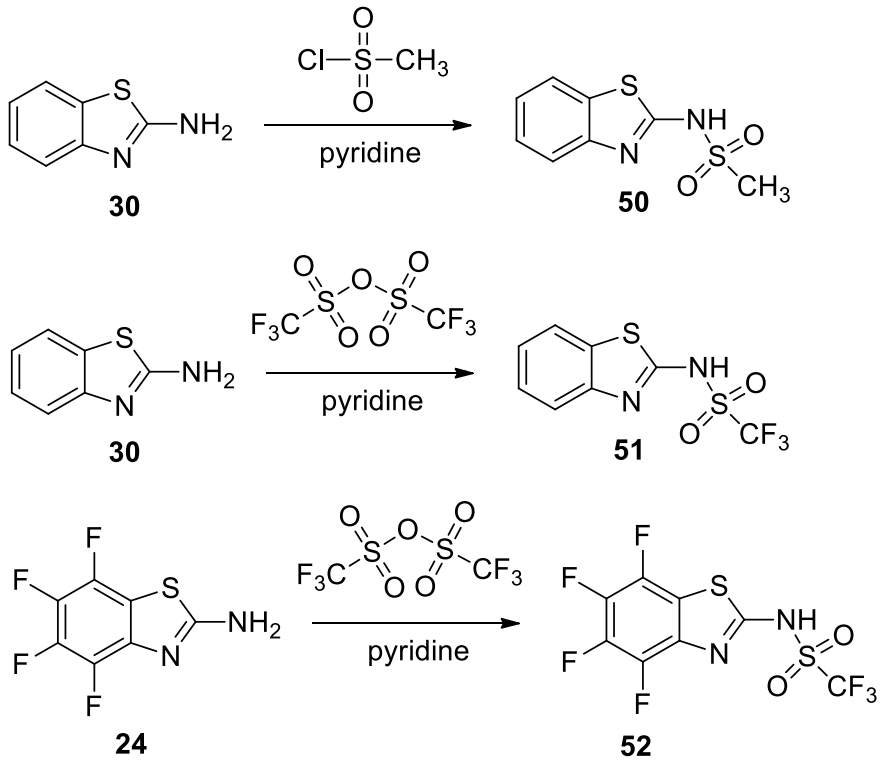

Scheme 2.19: Preparation of *N*-(benzothiazol-2-yl)methanesulfonamides

2.6 Preparation of zinc complexes

2.6.1 Preparation of zinc complexes of fluorinated 2-(2-hydroxyphenyl)-benzothiazoles

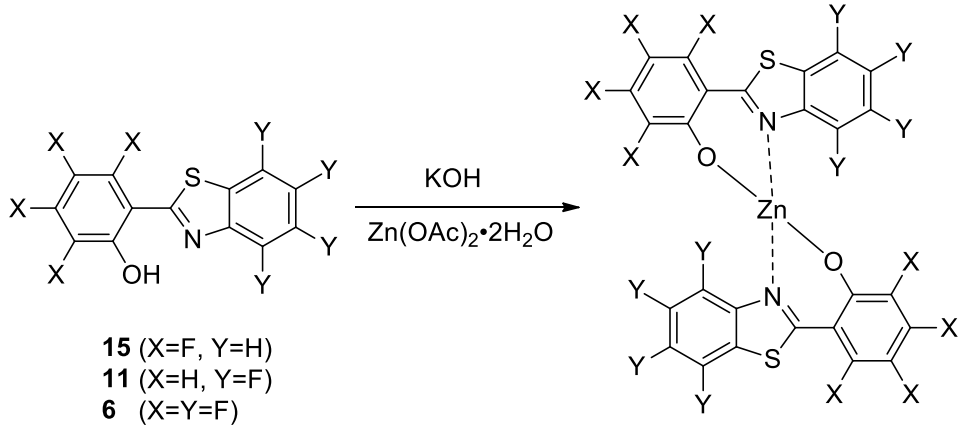

15 (X=F, Y=H)
11 (X=H, Y=F)
6 (X=Y=F)

53 (X=F, Y=H)
54 (X=H, Y=F)
55 (X=Y=F)

Scheme 2.20 Preparation of zinc complexes of fluorinated 2-(2-hydroxyphenyl)benzo-thiazoles

The zinc complexes **53** and **54**, which are fluorinated analogues of $Zn(BTZ)_2$, precipitated from methanol upon mixing solutions of zinc(II) acetate and potassium salts of the ligands. Complex **55** is comparatively soluble in methanol, and so was prepared by precipitation from aqueous solution.

2.6.2 Preparation of zinc complexes of bis(benzothiazolyl)amines

The zinc complex of nonfluorinated bis(benzothiazolyl)amine has previously been reported by Tellez *et al*.[68] The authors also described a few other metal complexes such as cobalt, nickel and mercury species. The crystal structure of the zinc complex they reported has a half DMSO solvent molecule per zinc complex molecule. This DMSO can coordinate strongly with the zinc ion, which was indicated by our observation of a DMSO adduct in the mass spectrum of a sample that was prepared following the same procedure reported by Tellez, crystallized from DMSO and then sublimed at 270 °C under high vacuum ($<10^{-6}$ mbar).

Considering that the presence of solvent molecules around the metal, especially when coordinated, can influence the complex's electron distribution and thus luminescence properties, we are interested to obtain solvent-free complexes. To achieve a solvent-free sample, we avoided using strongly coordinating and relatively involatile solvents, such as DMSO and DMF, in the preparation and purification process. The preparation of nonfluorinated, half fluorinated and perfluorinated zinc complexes were all performed using the same method (Scheme 2.21). An ethanol solution of ligand was mixed with an ethanol solution of zinc acetate dihydrate, and then the mixture was refluxed for several minutes to give the product as a precipitate, which was filtered off, washed with boiling ethanol a few times and dried.

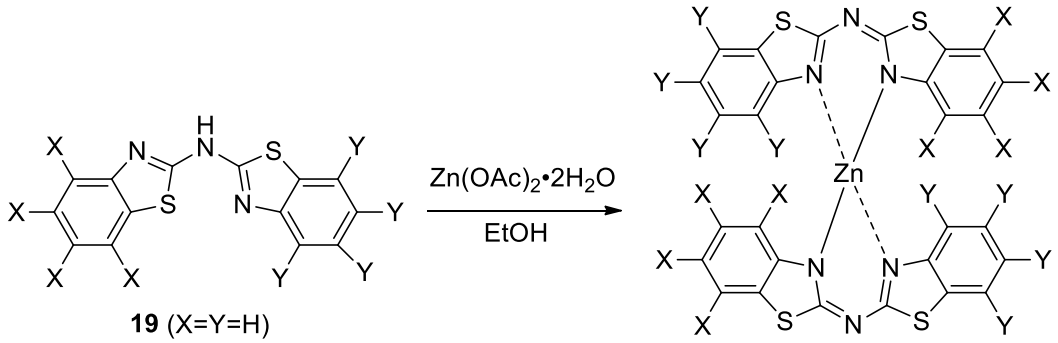

19 (X=Y=H)
20 (X=H; Y=F)
18 (X=Y=F)

56 (X=Y=H)
57 (X=H; Y=F)
58 (X=Y=F)

Scheme 2.21: Preparation of zinc complexes of bis(benzothiazolyl)amines

All the zinc complexes have very poor solubility in normal organic solvents except hot DMSO, so these complexes were purified by sublimation instead of crystallisation from DMSO. The sublimation technique was also used to grow single crystals for X-ray diffraction. These zinc complexes have been well characterised by NMR, IR and high resolution mass spectra. The crystal structures of the complexes will be discussed in the following chapter.

2.6.3 Attempted preparation of zinc complexes of *N*-(benzothiazol-2-yl)methanesulfonamides

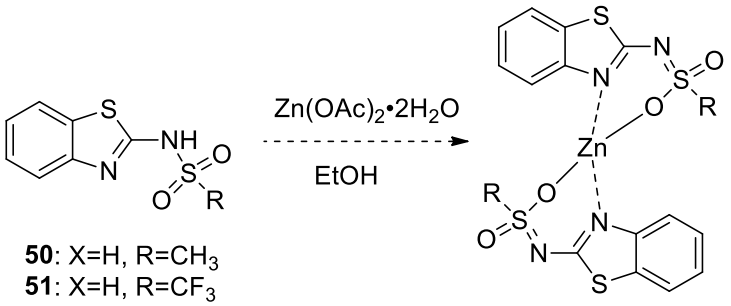

Scheme 2.22: Attempted preparation of zinc complexes of *N*-benzothiazol-2-yl-methanesulfonamides

For both ligands **50** and **51**, a solution of ligand in ethanol was mixed with a solution of zinc acetate dihydrate in ethanol and then the mixture was refluxed for half an hour. There was no precipitate formed during the refluxing, and then the solvent was removed by evaporation. The resulting solid was recrystallised from MeOH to give a white crystalline powder, which was characterised by melting point and IR. It was found that the obtained powder has almost identical melting point and IR peaks as the ligand.

Although this type of ligands did not combine with zinc to form stable complexes, they may prefer to combine with some other metal ions with their multiple combining sites, including two oxygen atoms, two nitrogen atoms and a sulfur atom. The work of trying other metal species may be carried out in the future.

2.7 Preparation of erbium complexes

2.7.1 Preparation of erbium complex of 2-(2-hydroxyphenyl)benzothiazole

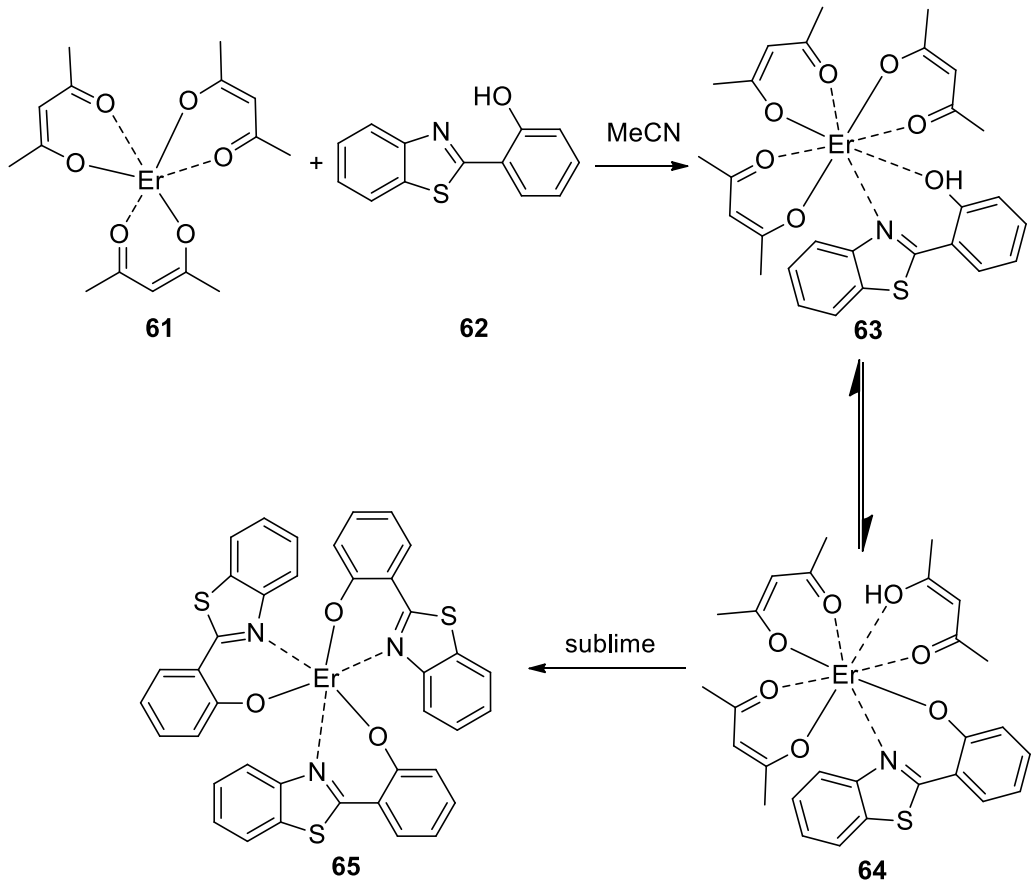

Scheme 2.23: Preparation of erbium complex of 2-(2-hydroxyphenyl)benzothiazole (All the complexes are drawn as mononuclear structures for simplicity, but they may be multinuclear.)

According to a patent containing the preparation of various metal chelates based on 2-(2-hydroxyphenyl)benzothiazole and 2-(2-hydroxyphenyl)benzoxazole (WO 2010/020352 A1), hydrated rare earth acetylacetonates can be used as useful precursors for preparing the corresponding phenolate complexes. The yttrium complexes are given as examples, so we decided to make the erbium analogue using a similar method. After adding the solution of $Er(acac)_3$ hydrate to the solution of ligand **62** in MeCN, a pale pink precipitate formed. IR showed the complete disappearance of water molecules in the newly obtained complex. Immediate measurement of the freshly made NMR sample indicated that the phenol ligand exists as a neutral form without deprotonation of –OH (Figure 2.9, top).

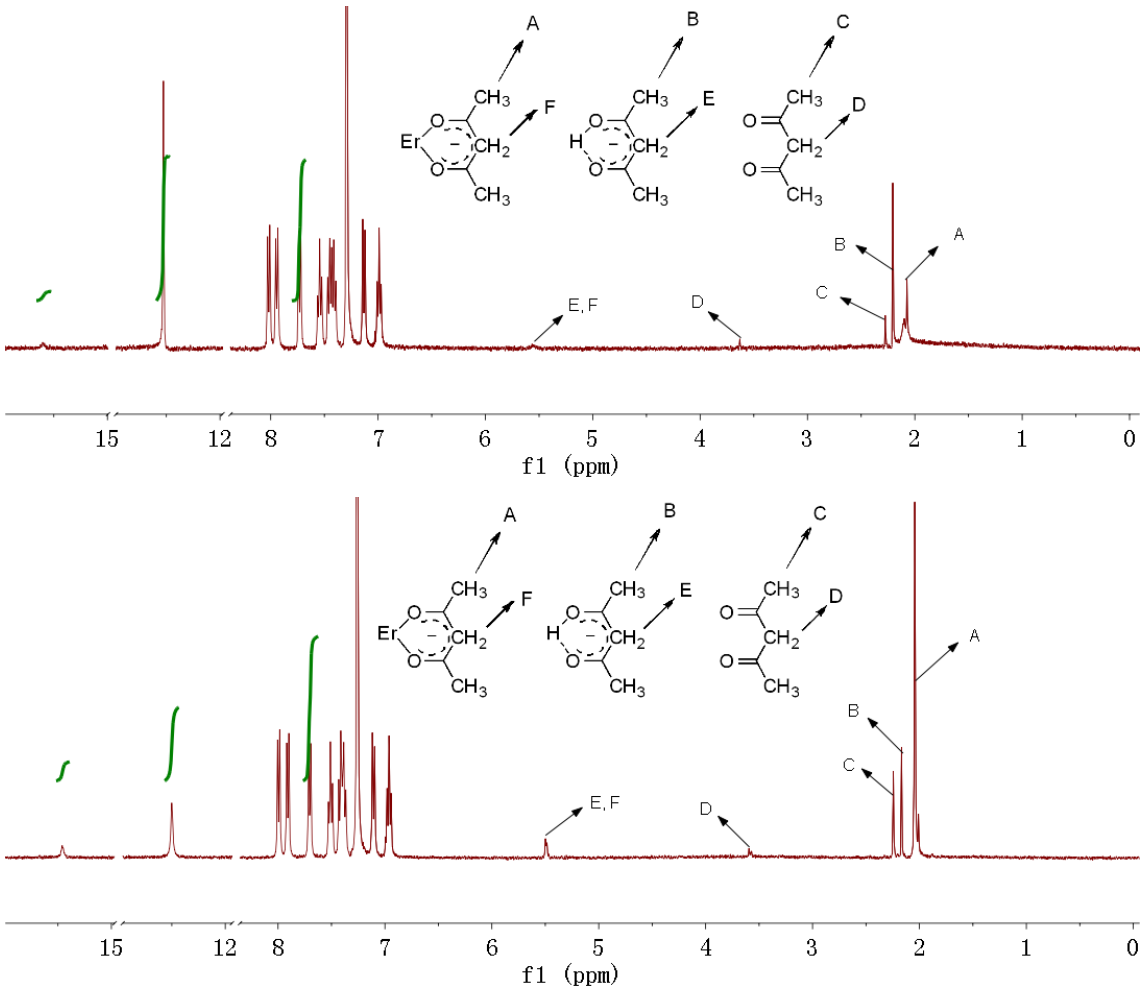

Figure 2.9: ^{1}H NMR spectra (400 MHz) of $Er(acac)_3(H\text{-}BTZ)$ in $CDCl_3$.
Top: fresh sample; Bottom: aged sample 96 h after preparation

However, it was discovered that the NMR sample changed its colour from the original pale pink to yellowish the next day. The yellow colour became deeper after aging for more time. As the potassium salt of the same phenol ligand also has a yellow colour, a proton transfer process was suspected to have happened in the NMR sample. An NMR spectrum of the same sample 96 h after preparation also suggested that a partial proton transfer took place (Figure 2.9, bottom). The peak at δ_H12.50 corresponding to the phenol –OH has shrunk to about the half of the previous integration compared to an aromatic proton at δ_H7.73, while a new peak emerged at δ_H15.46 which can be assigned to the enol –OH proton. Interestingly after concentration the yellow solution turned back to a pale pink powder again. So it is assumed this proton transfer is induced by a phase transition. In the mass spectrum a number of erbium containing species were

observed: $Er(acac)_3^+$, $Er(acac)_2(H\text{-}BTZ)^+$ (H-BTZ represents 2-(2-hydroxyphenyl)benzothiazole), $Er_2(acac)_5^+$ and $Er_2(acac)_4(H\text{-}BTZ)^+$ etc, suggesting that the complex may exist as a multinuclear structure and the proton can be with either of the two ligands.

While the proton transfer happened in the solution phase, it might also happen in the solid phase if more energy was introduced. This complex was subjected to high temperature at high vacuum < 3×10^{-6} mbar. Two different components sublimed out at different temperatures. Firstly a white-pink solid sublimed at around 250 °C. After this process was complete, the solid residue at the hot end became yellow. Then as the temperature increased to 350 °C, some yellow solid sublimed. IR suggested that the white-pink solid was the anhydrous $Er(acac)_3$; this was extremely hygroscopic and became sticky after a few days when left in a sample vial (even sealed). The yellow solid showed a similar IR pattern to the zinc complex made from the same ligand 2-(2-hydroxyphenyl)benzothiazole. The high resolution mass spectrum indicated the existence of the $Er(BTZ)_3^+$ species (BTZ represents the anion of H-BTZ ligand), but the diketone ligand was not removed completely and the species $Er(acac)(BTZ)_2^+$ was also observed.

2.7.2 Preparation of erbium complexes of 2-(2-hydroxy-3,4,5,6-tetrafluoro-phenyl)-4,5,6,7-tetrafluorobenzothiazole (L_c)

Various methods were tried to make anhydrous $Er(L_c)_3$ and $MEr(L_c)_4$ (M=alkali metal) complexes from the ligand 2-(2-hydroxy-3,4,5,6-tetrafluorophenyl)-4,5,6,7-tetrafluoro-benzothiazole (**6**). Only the formation of species $MErL_4$ could be observed without any water molecules coordinated to the metal ion.

1. *Attempted preparation of tris(2,3,4,5-tetrafluoro-6-(perfluorobenzothiazol-2-yl)phenoxy)erbium ($Er(L_c)_3$)using potassium salt in aqueous solution*

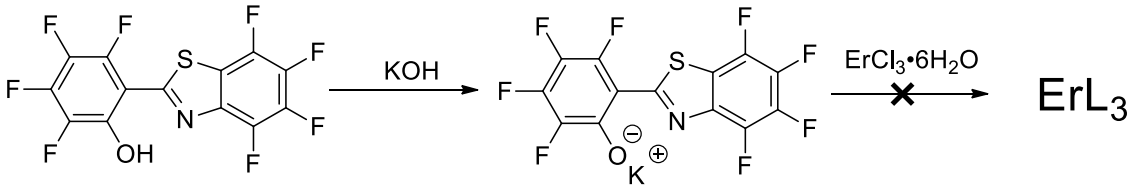

6 66 67

Scheme 2.24: Attempted preparation of tris(2,3,4,5-tetrafluoro-6-(perfluorobenzo-thiazol-2-yl)phenoxy)erbium

Firstly, attempts were made to prepare the erbium complex $Er(L_c)_3$ by using the same method as for the zinc complex $Zn(L_c)_2$, which was prepared in an aqueous solution. However, when a solution of $ErCl_3 \cdot 6H_2O$ was added to the solution of potassium salt KL, it was found that the free acid form of the ligand precipitated immediately. This is attributed to the Lewis acidity of Er^{3+}, which favours proton transfer from the coordinated water to the conjugate base of the ligand.

2. *Attempted preparation of anhydrous complex using erbium(III) bis(trimethylsilyl)-amide as precursor*

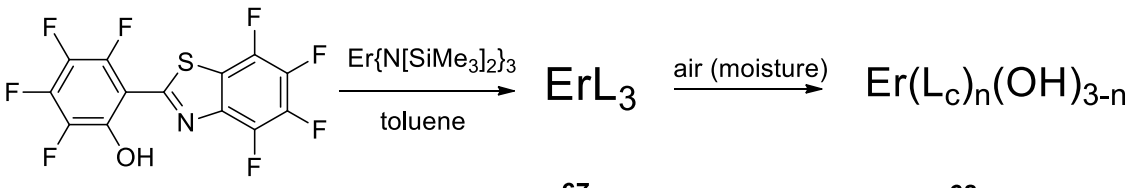

6 67 68

Scheme 2.25: Attempted preparation of anhydrous tris(2,3,4,5-tetrafluoro-6-(perfluorobenzo-thiazol-2-yl)phenoxy)erbium

Considering the adverse effect of water, we decided to prepare erbium complex in a dry organic solvent and use an anhydrous erbium precursor. Erbium(III) bis(trimethylsilyl)amide was used as the precursor, not only because it is anhydrous, but also of the convenience of removing the by-product bis(trimethylsilyl)amine, which has a relatively low boiling point.

All the steps of the reaction were conducted under N_2 and a yellow precipitate was obtained. This yellow powder was characterised by IR soon after preparation. A high frequency –OH peak was observed at around 3600 cm^{-1}. It indicated that it is not easy to obtain an anhydrous tris erbium complex from this perfluorinated ligand. Three such ligands can only provide six coordination sites to the erbium ion, which usually demands more donor atoms to saturate its high coordination number (9 ~ 12). Unless the ligand is bulky enough to prevent other coordinating species from approaching, as is the case when three ftpip ligands forming a shell around the ion, it is difficult to prevent water or other solvent molecules from becoming coordinated to the erbium ion. Another approach for using ligand **6** to make a coordinatively saturated homoleptic complex is to combine more than three ligands with the metal ion to provide more than six binding sites.

*3. Preparation of caesium tetrakis(2,3,4,5-tetrafluoro-6-(perfluorobenzothiazol-2-yl)phenoxy)erbate(III) (**70**) using the caesium salt of ligand*

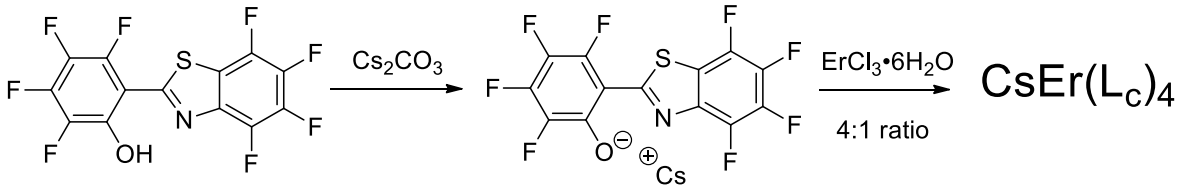

Scheme 2.26: Preparation of erbium complex $CsEr(L_c)_4$ using the caesium salt of ligand

In order to have more than three ligands to combine with the metal to obtain an anhydrous complex, a counter cation has to be introduced to balance the extra negative charge when four anionic ligands are coordinated with Er^{3+}. Caesium ion was chosen because its large size/charge ratio makes it easier, compared with other alkali metal ions, to overcome the solvation energy when forming the complex molecule from the solvated ion. For example, $Cs[Er(HFA)_4]$ (H−HFA = 1,1,1,5,5,5-hexafluoro-2,4-pentanedione) was reported as an anhydrous structure even when it was prepared from aqueous solution.[69]

The ligand HL_c (**6**) was firstly converted to its caesium salt CsL (**69**) by reacting with Cs_2CO_3, and purified by washing with $CHCl_3$ to remove excess ligand, and dried before use. Then to a solution of CsL in acetonitrile was added the solution of $ErCl_3 \cdot 6H_2O$ in methanol. If the ratio of acetonitrile/methanol were high enough, then the solution would become cloudy as the by-product CsCl is insoluble in MeCN and precipitated. The suspension was filtered and concentrated by evaporation. The resulting solid residue was extracted with MeCN and then filtered. After the filtrate was concentrated, an orange film could be obtained on the inside surface of the flask. This product was characterised by MALDI mass spectroscopy. At the *m*/*z* of 1646 it showed the presence of the species $Er(L_c)_4^-$. But semi-quantitative energy-dispersive X-ray spectroscopy (EDX) gave a much lower atomic percentage of Er^{3+} than Cs^+, indicating this product was still a mixture. Attempts to obtain pure product by recrystallisation from various solvents were not successful, which only gave crystal of the CsL salt. However, both IR and the relatively long photoluminescence lifetime about 29 μs proved the absence of water molecules in the coordination sphere of erbium. A detailed physical study of this material will be presented in the next chapter.

It was attempted to sublime this orange film at 350 °C under high vacuum ($<10^{-6}$ mbar). A red powder was seen condensed on the cool part of tube. The difference in colour of this red powder compared with the initial orange film indicated that some chemical reaction took place during the sublimation process. This red powder could be turned to liquid phase gradually over a wide temperature range from 130 °C to 160 °C, which suggested the red material was a mixture of several compounds. EDX of this red powder showed a very low atomic percentage of erbium in this mixture, which meant that the $CsEr(L_c)_4$ complex is not a good candidate for sublimation.

4. *Preparation of lithium tetrakis(2,3,4,5-tetrafluoro-6-(perfluorobenzothiazol-2-yl)phenoxy)erbate(III) (**72**) using the lithium salt of ligand **6***

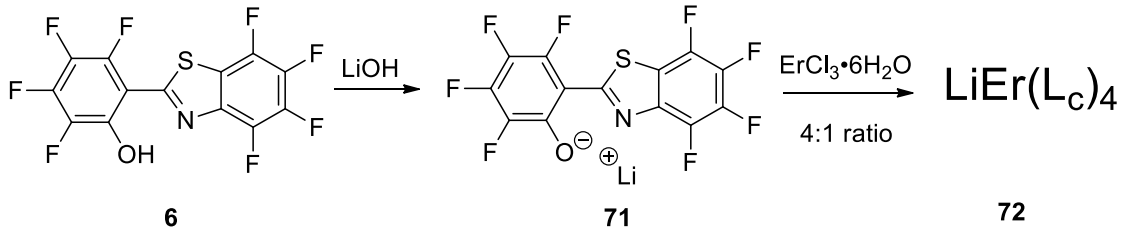

Scheme 2.27: Preparation of erbium complex $LiEr(L_c)_4$ using the lithium salt of ligand

The synthesis route was similar as that of making $CsEr(L_c)_4$, except that the base used here was the alkali hydroxide LiOH; and instead of using MeCN, DCM was used to extract the product. After concentration of the extract, a yellow powder was obtained. EDX only showed a very low atomic percentage of Er^{3+} in this yellow powder, indicating this yellow powder was still a mixture. And attempts to obtain a pure product by recrystallisation were not successful. However, after drying at 150 °C under high vacuum, this yellow powder showed no –OH peak in its IR spectrum, and a long photoluminescence lifetime of erbium about 50 μs.

2.8 Summary of Chapter 2

Three series of the target ligands have been synthesised (Figure 2.10), and two series of zinc complexes have been successfully prepared (Figure 2.11). The structures and photophysical properties of these zinc complexes will be the topic of the next chapter.

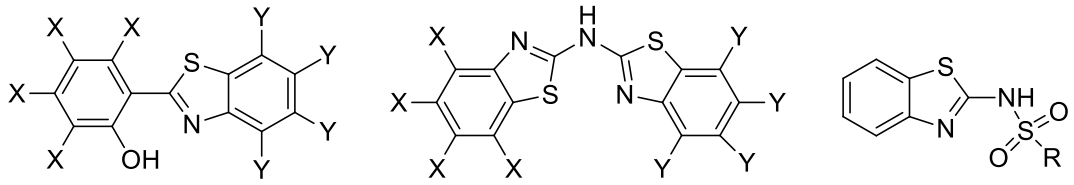

15 (X=F, Y=H)
11 (X=H, Y=F)
6 (X=Y=F)

19 (X=Y=H)
20 (X=H; Y=F)
18 (X=Y=F)

50: X=H, R=CH_3
51: X=H, R=CF_3

Figure 2.10 Successfully synthesised ligands

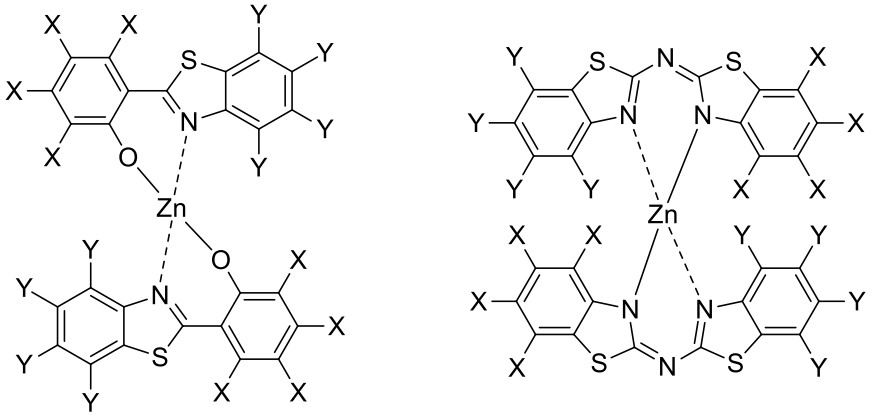

53 (X=F, Y=H)
54 (X=H, Y=F)
55 (X=Y=F)

56 (X=Y=H)
57 (X=H; Y=F)
58 (X=Y=F)

Figure 2.11 Successfully prepared zinc complexes

The synthesis of the target ligands of **48** and **49** have not been fully exploited till the end of this project. The synthesis of these two compounds will be carried out in our group in the future based on the successfully prepared intermediate **47** (Figure 2.12).

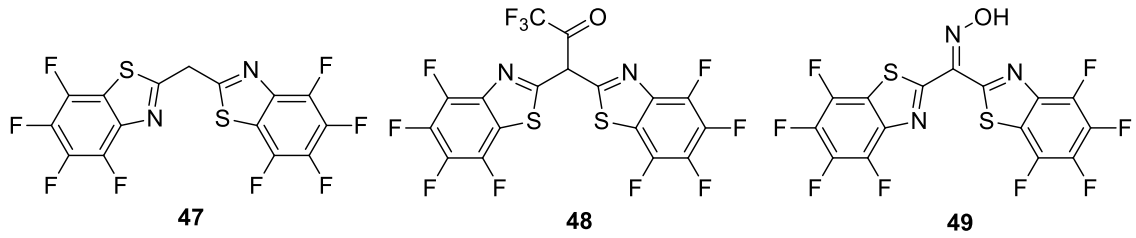

Figure 2.12 Intermediate compound **47** and its derivative potential ligands

Various methods were tried to prepare erbium complexes from the perfluorinated ligand HL_c(**6**). Only the tetrakis-ligand species $MEr(L_c)_4$ (M=Cs, Li) can be prepared as anhydrous materials. Although attempts to isolate a pure product of $CsEr(L_c)_4$ were not successful till now because of the difficulty of separating CsL_c and $CsEr(L_c)_4$, the mass spectrum was able to detect the existence of $Er(L_c)_4^-$ ion. Further efforts will be made to obtain the pure $CsEr(L_c)_4$ in the future work of our group.

Chapter 3 - Results and discussion part II: Structure and photophysical properties

3.1 Single crystal structures

3.1.1 Zinc complexes of fluorinated 2-(2-hydroxyphenyl)benzothiazoles

X-ray quality solvent-free crystals of the phenoxide complexes **53**, **54** and **55** were grown by vacuum sublimation. Single crystal X-ray diffraction studies were performed on all three metal complexes (Figure 3.1).

The reported structure of $[Zn(BTZ)_2]_2$ is dimeric,[53] with five-coordinate zinc ions. In a unit of $Zn(BTZ)_2$, besides the four binding atoms provided by two chelating ligands, the zinc centre is additionally bonded with another oxygen atom belonging to a neighbouring $Zn(BTZ)_2$ unit, thus forming the dimeric structure $[Zn(BTZ)_2]_2$. The four ligands in the dimeric $[Zn(BTZ)_2]_2$ can be categorized into two types: two nonbridging ligands that only chelate with one zinc ion, and two bridging ligands that bridge two zinc ions with their phenoxide oxygen atom.

In contrast to the nonfluorinated dimeric $[Zn(BTZ)_2]_2$, all three fluorinated zinc complexes are monomeric. The zinc ions are all four-coordinate with a roughly tetrahedral geometry, and have shorter Zn–O and Zn–N bond lengths than the five-coordinate $[Zn(BTZ)_2]_2$. The effect of fluorination in reducing nuclearity may be a consequence of the reduction in the Lewis basicity of the ligands. Similar observations have previously been reported *e.g.* for lanthanide perfluorarylthiolate complexes[70] and for Co(II) and Cu(II) pentafluorophenoxides.[71]

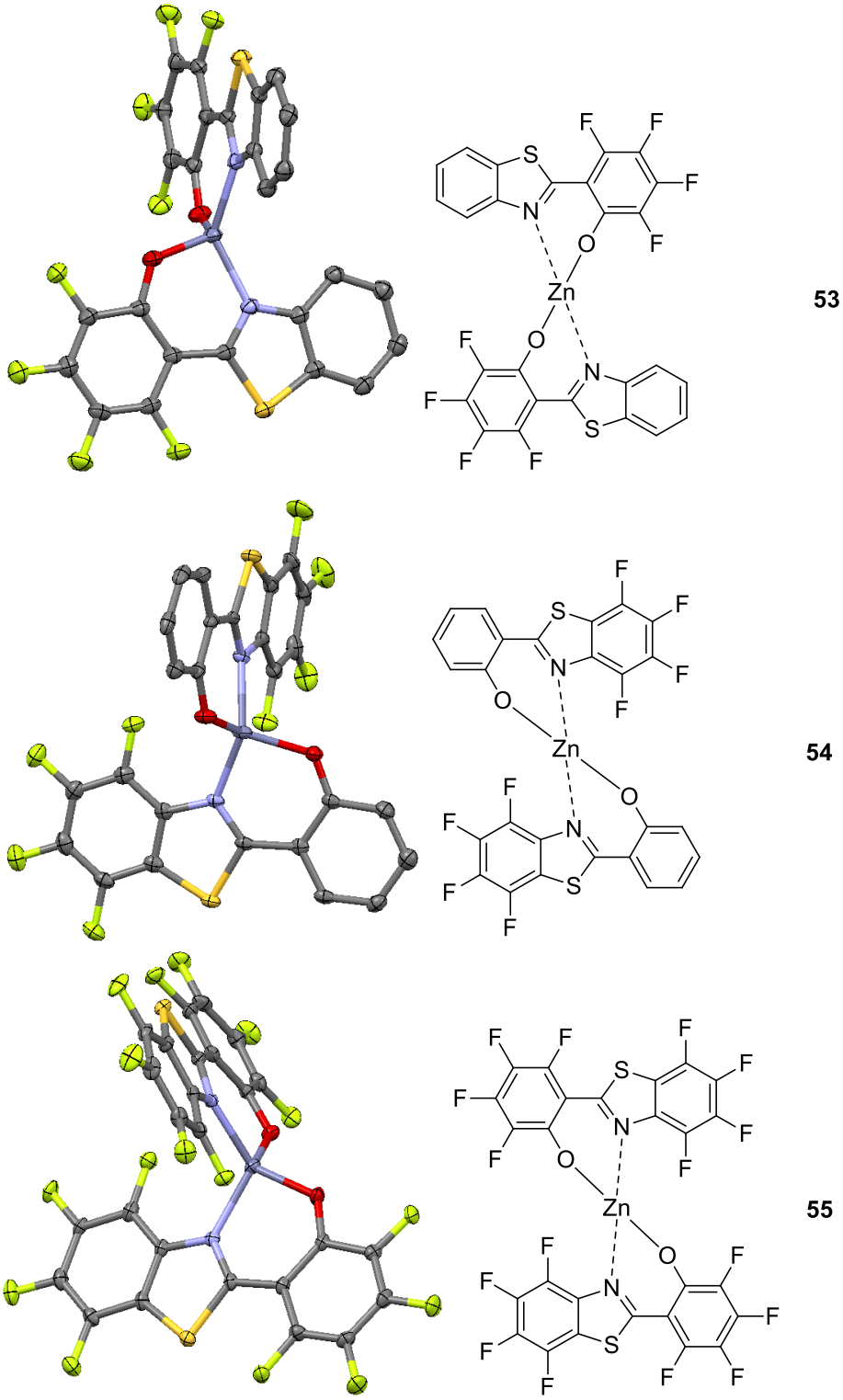

Figure 3.1: Molecular structures of phenoxide complexes **53** (top), **54 (**middle) and **55 (**bottom). Ellipsoids are shown at the 50% probability level

All three fluorinated zinc complexes are chiral molecules as they do not have a plane of symmetry or a centre of inversion. But they all exist as racemic crystals because each molecule is paired with an enantiomeric one through an inversion centre.

In these fluorinated complexes, their phenoxide rings are approximately coplanar with the benzothiazole rings within the same ligand. However, there are still obvious variations in the dihedral angles between the benzothiazole and the phenoxide rings among each of them (Table 3.1). Although these differences are small in value, they still may play an important role in affecting the extent of conjugation and physical properties. A correlation between the dihedral angles and the broadening of emission spectra was found, and will be discussed later in this chapter.

Table 3.1: Dihedral angles of phenolate zinc complexes

Complex	**$[Zn(BTZ)_2]_2$**	**53**	**54**	**55**
Largest benzothiazole-phenolate dihedral angle /°	12.7(5)	1.6(3)	3.4(6)	8.7(4)

3.1.2 Zinc complexes of fluorinated bis(benzothiazolyl)amines

X-ray quality crystals of the three amino complexes **56**, **57** and **58** were also grown by vacuum sublimation under similar condition as for the phenoxide complexes. Single crystal X-ray diffraction studies were performed on all three metal complexes (Figure 3.2).

The nonfluorinated zinc complex of bis(benzothiazolyl)amine has been reported as a solvated crystal $ZnL_2 \cdot 0.5DMSO$ by Téllez *et al.*[68] It is monomeric with the metal ion combined with four imine N atoms in a distorted tetrahedral geometry. The N–metal bond length is ca. 1.986(4) Å, and bite angle is ca. 93.0(2)°.

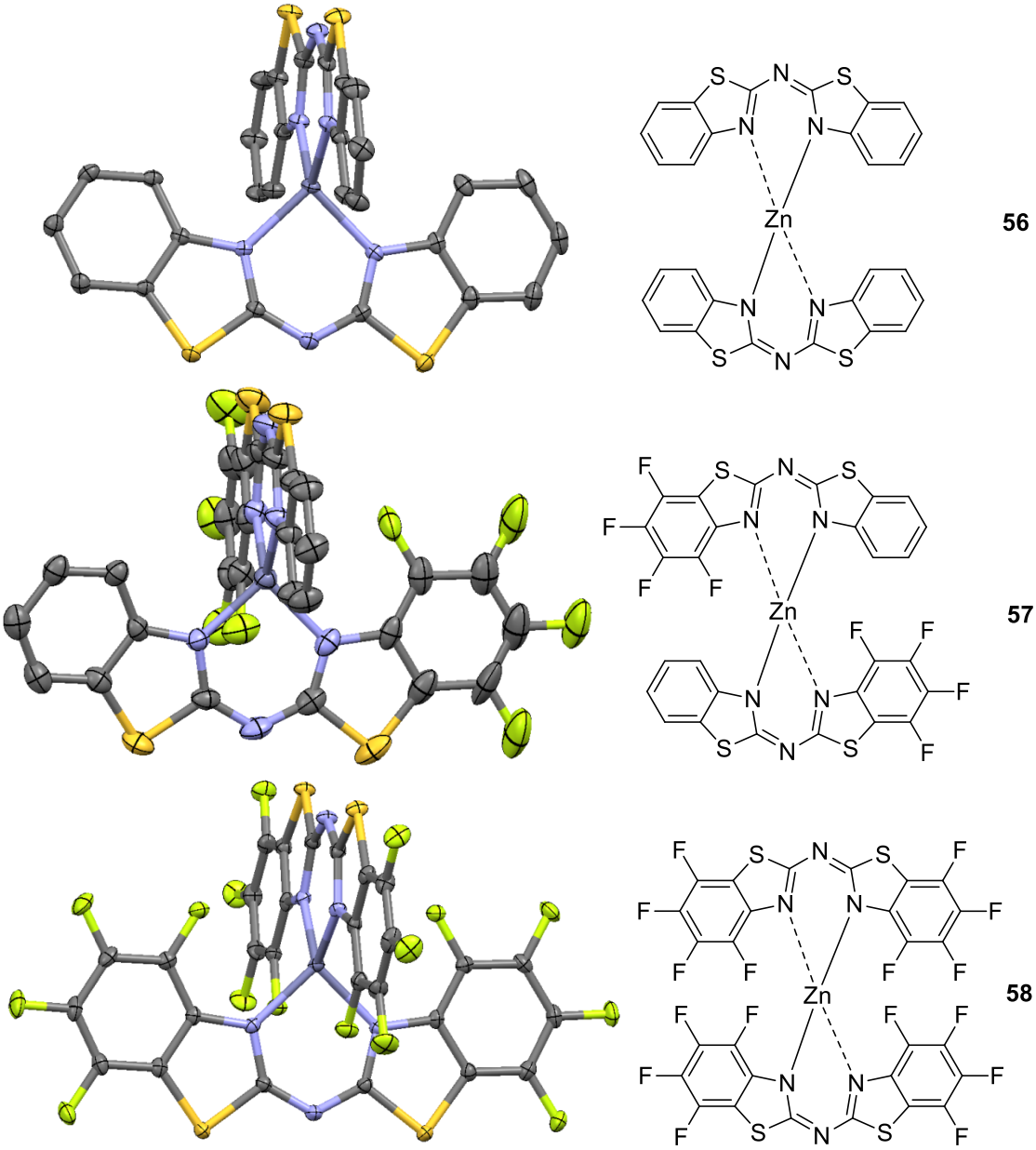

Figure 3.2: Molecular structures of zinc bis(benzothiazolyl)amide complexes **56** (top), **57 (**middle) and **58 (**bottom). Ellipsoids are shown at the 50% probability level

In comparison with the solvated zinc complex, our solvent-free complex **56** shows various but similar N–metal (II) bond lengths ranging from 1.978(2) Å to 2.005(3) Å with an average of 1.992(2) Å, and an average bite angle of 92.4(9)°. The variety of bond lengths and angles in complex **56** arises from the presence of two inequivalent environments for the four molecules in a unit cell.

The half fluorinated chiral molecule **57** crystallises as a monomeric structure. The average N–metal (II) bond length is 1.992(3) Å, and average bite angle is 94.0(1)°. There are also four molecules in the unit cell, but only one environment is present. All the molecules can be related by either an inversion center or a screw axis, indicating the half fluorinated complex **57** has higher symmetry than its nonfluorinated counterpart. However, this highly symmetric structure possesses some irregularity. There is a discrete static positional disorder associated with fluorine atoms in one ligand, which was refined by using SHELXX program facilities. The site occupancies for F(5) – F(8) were refined to 0.7, and 0.3 for F(5)' – F(8)'.

The perfluorinated chiral molecule **58** is also monomeric. The average N–metal (II) bond length is 2.007(2) Å, slightly bigger than those in **56** and **57**, and average bite angle is 93.3(1)°. There are two molecules in a unit cell that are related by an inversion centre.

In these zinc bis(benzothiazolyl)amide complexes, the two benzothiazole wings within the same ligand are almost coplanar. However, there are still variations in the dihedral angles between the two wings in different complexes (Table 3.2). A common correlation between the dihedral angles and the broadening of emission spectra was found both in the phenolate complexes **53** – **55** and these amine complexes, and will be discussed later in this chapter.

Table 3.2: Dihedral angles of zinc bis(benzothiazolyl)amide complexes

Complex	**56**	**57**	**58**
Average [largest] benzothiazole-benzothiazole dihedral angle /°	3.4(2) [7.0(2)]	3.2(3) [3.6(3)]	2.8(2) [3.1(2)]

3.2 Impact of fluorination on solid state structures

Mixtures of arenes and perfluoroarenes with a 1:1 mole ratio,[72] as well as single substances such as 1,2,3,4-tetrafluoronaphthalene,[73] often adopt crystal structures containing parallel stacks of Ar(H) and Ar(F) rings. These π-π_F interactions, which are estimated to be stabilizing to the extent of 20 - 25 kJ mol^{-1}, provide a strong influence for directing molecular assembly but may be outweighed by other effects, including hydrogen bonding and steric repulsion.[74] One feature of these π-π_F interactions is the short interplanar distance, for example, the distance between benzene and perfluorobenzene in their 1:1 mixture is 3.36 Å,[75] and the distance between fluorinated and nonfluorinated ring planes in the crystal of 1,2,3,4-tetrafluoronaphthalene is 3.45 Å.[76]

The study of π-π_F interactions should provide a better understanding of the solid state properties of partially fluorinated organic semiconductor materials. For small molecule organic semiconductors, the physical properties are determined by two main factors: the electronic structure, and the spacial arrangement of the molecules. The material's electronic structure is related to the characters of its HOMO and LUMO, the properties of which will decide which type of carriers can be injected, and also the band gap that determines the luminescence colour. Meanwhile, the spacial arrangement and orientations of molecular π orbitals influence the charge transport ability as the carriers are transported via hopping through HOMOs or LUMOs.

Previous studies have modified the energy levels by substitution with electron donating or withdrawing groups. A systematic methyl substitution on the well known material Alq_3 showed that although fine tuning of emission could be achieved, the 'abrupt' introduction of a substituent which has a much greater size than the fringe H atoms can adversely affect intermolecular interactions and thus decrease charge mobility.[77] However, the incorporation of the small element F combined with method of complete substitution on an individual ring or the whole molecule may solve the problem. It has

been found that highly fluorinated molecules usually favour parallel stacking over herringbone stacking, and usually have closer packing between neighbouring layers.

Fluorination on aromatic rings has been applied to molecules of various shapes,[78] e.g. one dimensional rigid-rod type molecules such as phenylene-ethynylenes,[79] and two dimensional molecules like acenes[80-82] and thiophenes[83-84]. But in a system composed of three dimensional molecules such as the zinc complexes studied here, the situation becomes more complicated by the presence of more influential factors, such as electrical dipoles and stronger steric effects. The approximately tetrahedral geometry at the metal centre places the two ligands in two more or less mutually orthogonal planes, reducing the degrees of free movement for molecules and making it geometrically difficult to achieve π-π_F stacking. It is therefore of interest to examine the nature of the π-π interactions that occur within these series of zinc complexes.

3.2.1 Zinc complexes of fluorinated 2-(2-hydroxyphenyl)benzothiazoles

1. Nonfluorinated $[Zn(BTZ)_2]_2$

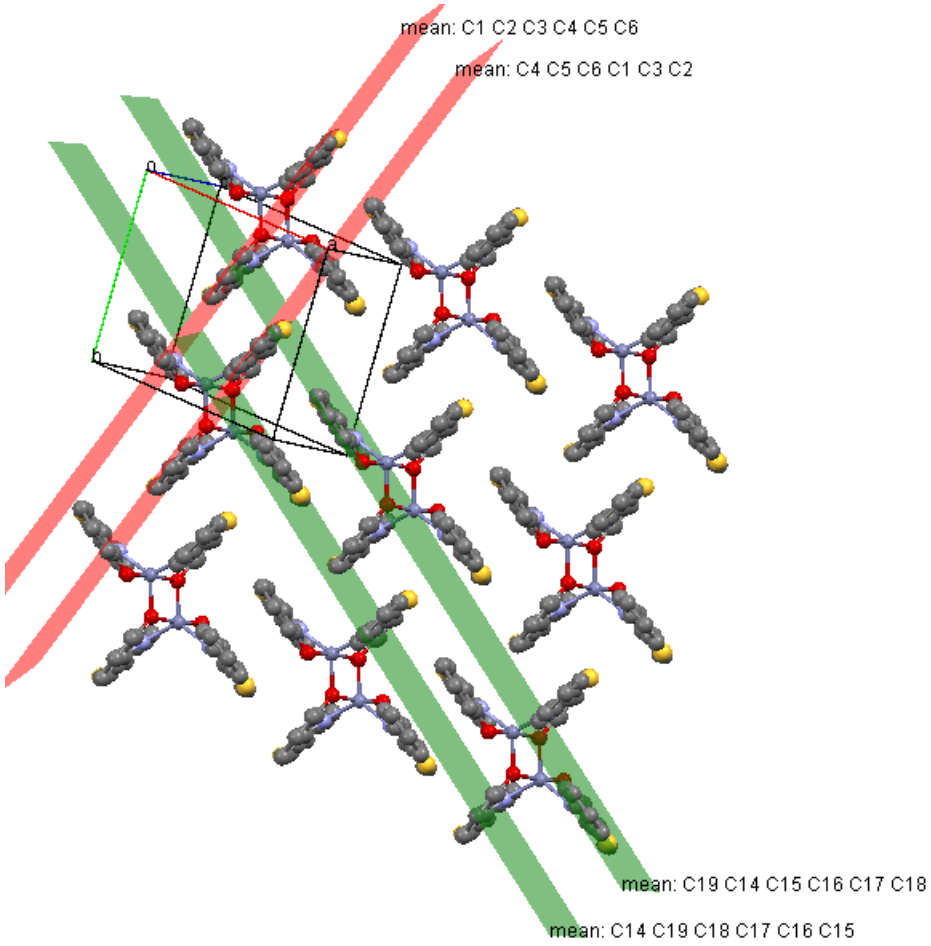

Figure 3.3: Packing of $[Zn(BTZ)_2]_2$[53]

In the dimeric $[Zn(BTZ)_2]_2$ unit there are four ligands. Each one faces an antiparallel ligand in the neighbouring $[Zn(BTZ)_2]_2$ unit. Thus every dimeric molecule is engaged in π-π interactions with four neighbouring molecules, forming an extended network with π-π stacking in two directions (Figure 3.3). All the ligands are stacked with the ligands of the same coordination type, bridging ligands with bridging ones and non-bridging ligands with non-bridging ones. The interplanar distances between ligands vary with the bridging type. The separation between bridging ligands is slightly smaller than the non-bridging ones.

When calculating the interplanar distance, the values obtained can differ depending on the atoms used to define the plane. For example, if the plane is defined by the six carbon atoms in the 'benzo' ring of benzothiazole unit, the distances between bridging ligands and non-bridging ligands are 3.61 Å and 3.77 Å respectively. However, if the plane is defined by the other six carbon atoms in the phenoxide ring, the separations for bridging and non-bridging ligands become 3.27 Å and 4.11 Å respectively. These differences arise from the twist of the ligand with a non-zero dihedral angle between the benzothiazole ring and the phenoxide ring. Therefore, the interplanar distances calculated in the following part of this chapter can only be used to evaluate the distance between two specific rings rather than two ligands. To be consistent, the 'benzo' rings are chosen for comparison of the interplanar distances in this chapter.

*2. Half fluorinated zinc complex **53** (fluorinated on phenoxide ring)*

In many cases of planar molecular systems, the π-π_F interactions can dominate molecular assembly with a large stabilizing force in absence of other strong effects, such as hydrogen bonding and steric repulsion. It is therefore interesting to see whether the π-π_F interactions still prevail in our fluorinated zinc complexes.

As with the dimeric $[Zn(BTZ)_2]_2$ that has an inversion centre between two $Zn(BTZ)_2$ components, fluorinated zinc complexes **53**, **54** and **55** also have inversion centres between two closest monomers, which pair together with π-systems facing each other in an antiparallel alignment and with terminal ligands extended like wings (Figure 3.4, top). It is noticeable that although these fluorinated molecules exist as monomers, between which there are no bridging bonds, they still adopt a structure based on pairs. So there must be a recognition force for each monomer to find its partner. In the following part of this chapter, discussion will be given on how monomers assemble to form pairs, and how these pairs further stack to build up the whole three dimensional network in crystals.

In the case of **53**, the two molecules in the pair have their ligands overlapped in a shoulder-by-shoulder manner with some offset, having one fluorinated phenoxide ring over its counterpart in the other molecule (Figure 3.4, top). The stacking of π_H-π_H and π_F-π_F is observed instead of the π_H-π_F interaction which is often seen in half fluorinated arenes. However, the stacking of the two ligands is not strictly parallel. The angle between the two planes, which are defined by the six carbon atoms in phenoxide rings, is around 10.8° (Figure 3.4, bottom). The separation between the centroid of a phenoxide ring and the plane defined by the carbon atoms in the facing phenoxide ring is 3.35 Å.

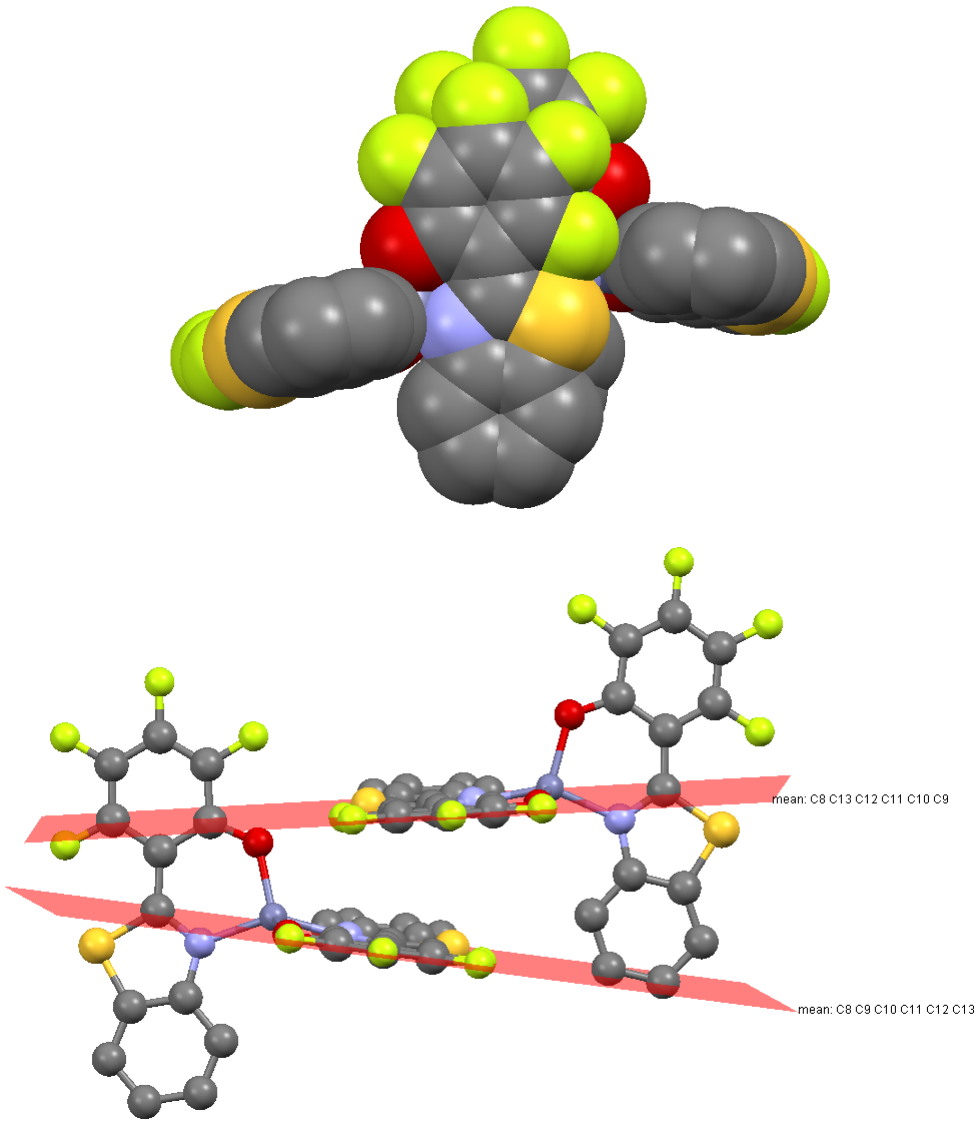

Figure 3.4: The enantiomeric pair in complex **53**

The pairs further extend through space to build up the three dimensional network. As *c* is the smallest edge of the unit cell, the stacking of molecules along the c axis will be denser than the other two directions. The translation along the c axis generates an infinite packing (Figure 3.5, top). The translation of pairs along this direction additionally generates π-π stackings in the direction perpendicular to the ligand plane (Figure 3.5, bottom).

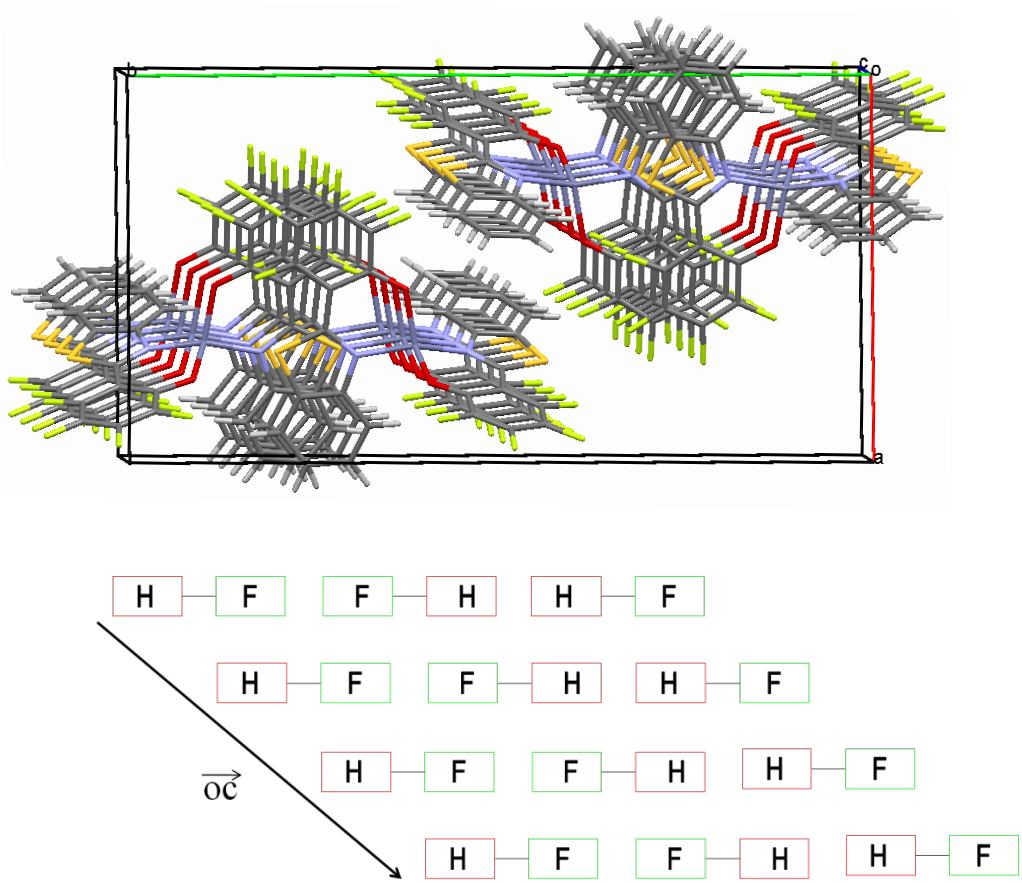

Figure 3.5: The packing of molecules in complex **53**

π_H-π_H, π_H-π_F and π_F-π_F interactions all exist within the stacks. Especially the π_H-π_H stacking is exhibited by an almost perfect superposition between two nonfluorinated 'benzo' rings in the benzothiazole units (Figure 3.6 left). The interaction between neighbouring π systems can be quantitatively analysed by the interplanar distance, which is the separation between two parallel planes defined by the six carbon atoms in a phenoxide ring or a 'benzo' ring in the benzothiazole unit. The interplanar distance is

calculated to be 3.63(1) Å, which is nearly identical with the distance between the centroids of two overlapping 'benzo' rings (calculated as 3.64(1) Å).

The π_F-π_F interaction is not as perfect as the π_H-π_H interaction, but still has a very good overlap with only a little offset (Figure 3.6, middle). The interplanar distance between two fluorinated rings is 3.28(1) Å, while the distance between the two rings' centroids is 3.47(1) Å.

For the π_H-π_F interaction, the overlapping is less well aligned compared with the previous two interactions (Figure 3.6, right). The interplanar distance of the π_H-π_F interaction can not be calculated the same way as π_H-π_H or π_F-π_F interactions, because the plane defined by the nonfluorinated 'benzo' ring and the plane defined by the fluorinated phenoxide ring are not parallel with the other. So the stacking can be only roughly considered as the distance from the centroid of phenoxide ring to the plane defined by the 'benzo' ring, which is calculated as 3.41(1) Å.

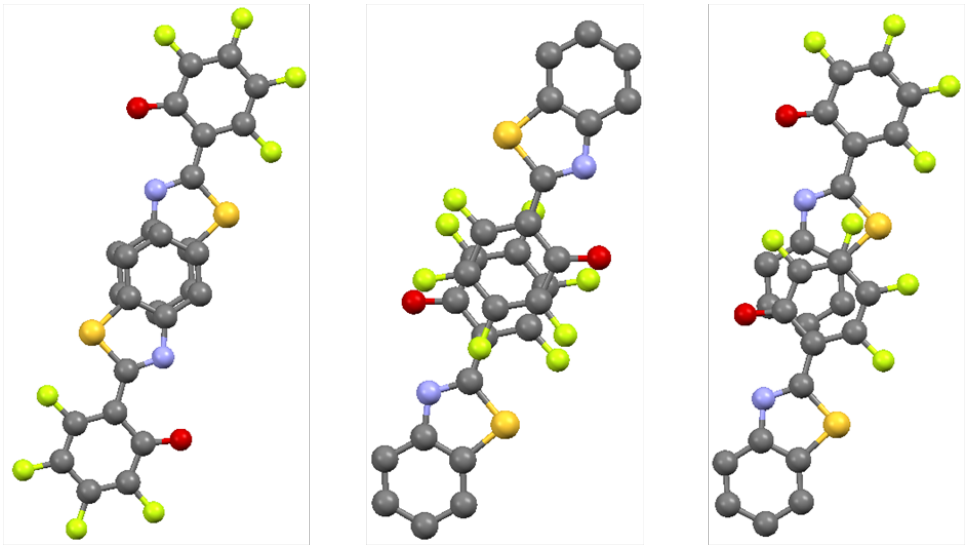

Figure 3.6: π_H-π_H, π_H-π_F and π_F-π_F interactions in complex **53**

3. Half fluorinated zinc complex ***54*** *(fluorinated on benzothiazole ring)*

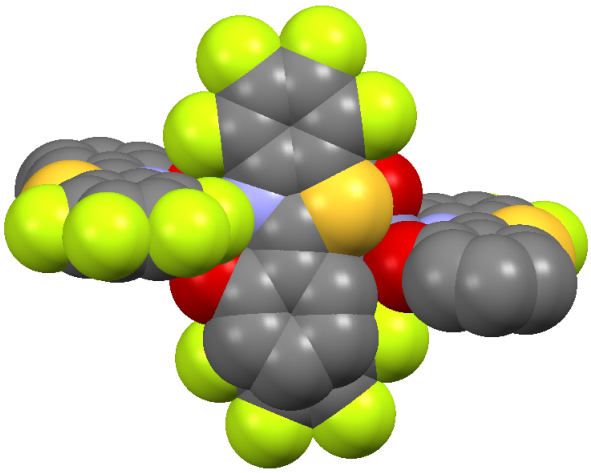

Figure 3.7: the unit pair in complex **54**

In complex **54,** two closest monomers form a pair with the nonfluorinated phenoxide ring facing the fluorinated benzothiazole ring, forming π_H-π_F interactions (Figure 3.7). The separation is calculated to be 3.23(1) Å between planes defined by the six carbon atoms in 'benzo' ring (3.25(1) Å between planes defined by the six carbon atoms in phenoxide rings), while the distance between the centroids of the fluorinated 'benzo' ring and the nonfluorinated phenoxide ring is 3.65(1) Å.

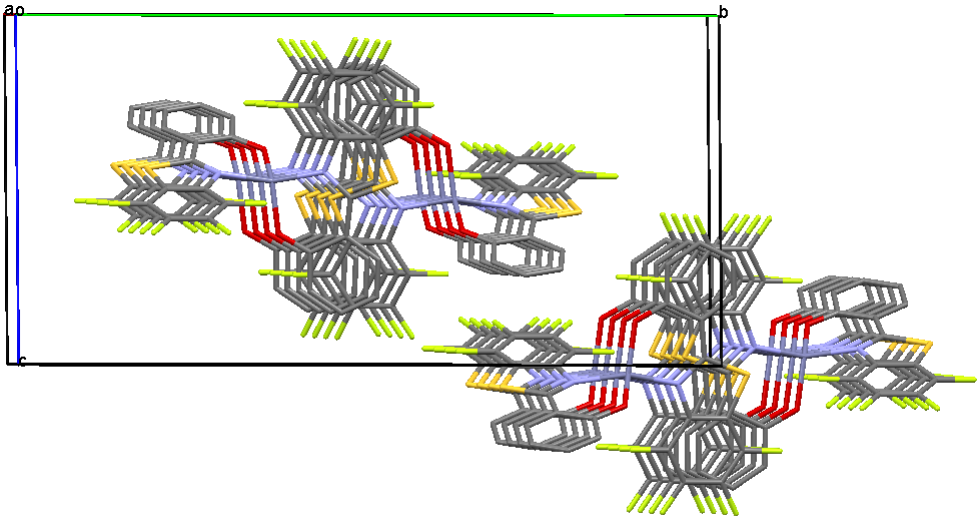

Figure 3.8: The packing of complex **54** along $\overrightarrow{oa}$ axis

The pairs of monomers further extend along the $\overrightarrow{oa}$ axis to build up the infinite network (Figure 3.8). This translation along $\overrightarrow{oa}$ direction generates stacking featuring π_H-π_F interactions between neighbouring pairs, in the direction perpendicular to the

'wing' ligands of the pair (Figure 3.9, top). This π_H-π_F interaction is represented by a very good overlap of the nonfluorinated phenoxide ring and the fluorinated 'benzo' ring (Figure 3.9, bottom), with two centroids almost superposed and the C–H and C–F bonds of the opposing rings staggered. The distance between the centroids of two opposing rings is 3.41(1) Å, while the centroid of the nonfluorinated phenoxide ring is 3.32(1) Å distant from the plane defined by the six carbon atoms of the fluorinated 'benzo' ring.

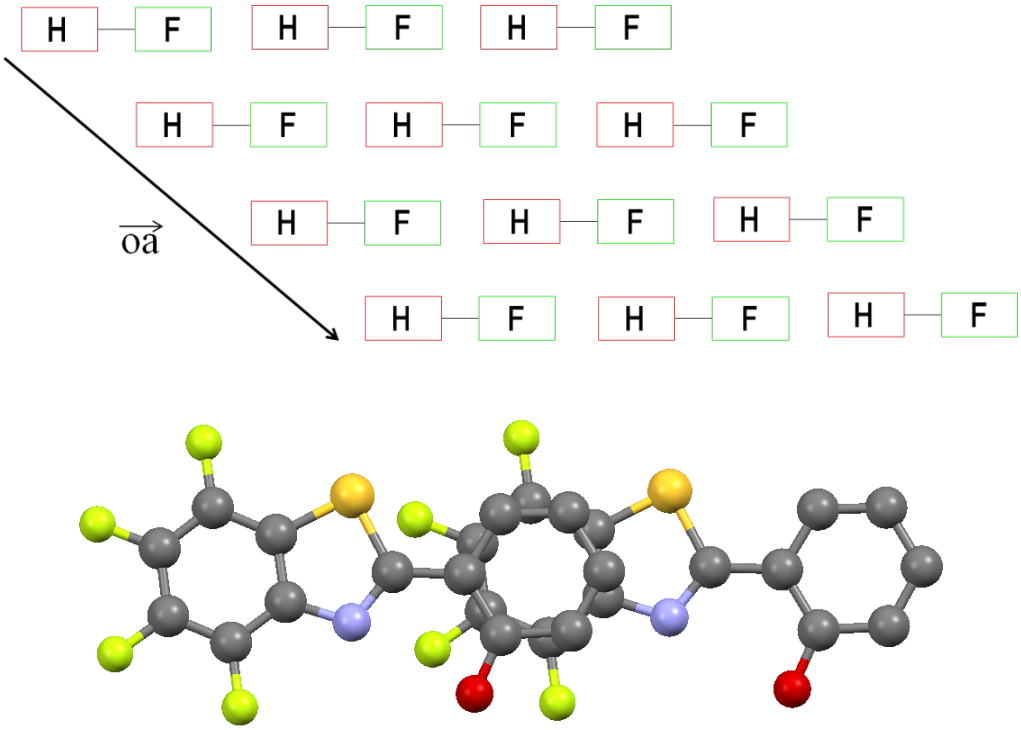

Figure 3.9: The packing between neighboring pairs: stacking of 'wing' ligands generated by translation through $\overrightarrow{oa}$ axis

Interestingly, π_H-π_F interaction was the only π-π interaction observed in the crystal structure of complex **54**, while π_H-π_H, π_H-π_F and π_F-π_F interactions all exist in the crystal packing of complex **53**.

4. Fully fluorinated zinc complex ***55***

In the fully fluorinated zinc complex **55**, two closest monomers also form a pair related by an inversion centre, giving a 'head to tail' packing manner with the phenoxide rings facing the benzothiazoles. The two confronting ligands are slightly offset so that the terminal electronegative fluorine atoms are approximately facing the electropositive carbon atoms (Figure 3.10). The separation is 3.21(1) Å between the centroid of phenoxide ring and the plane defined by the six carbon atoms of the facing 'benzo' ring in the benzothiazole unit.

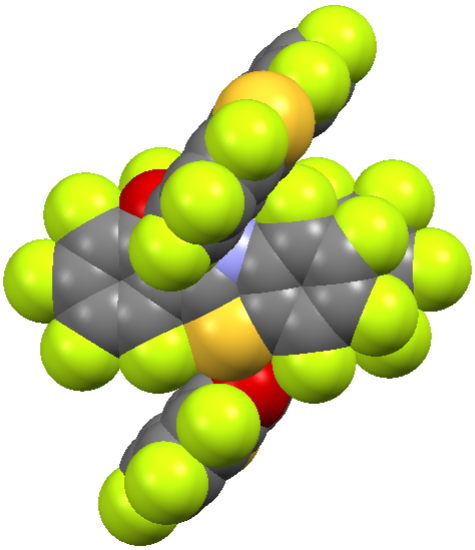

Figure 3.10: The enantiomeric pair in perfluorinated complex **55**

The enantiomeric pair extends along the $\overrightarrow{oa}$ axis to generate an infinite network (Figure 3.11). This $\overrightarrow{oa}$ translation further produces stacking of 'wing' ligands between two closest pairs (Figure 3.12), with the phenoxide ring facing the 'benzo' ring of benzothiazole unit in neighbouring molecule. Separation between wing ligands is 3.20 Å between planes defined by the carbon atoms in the phenoxide rings.

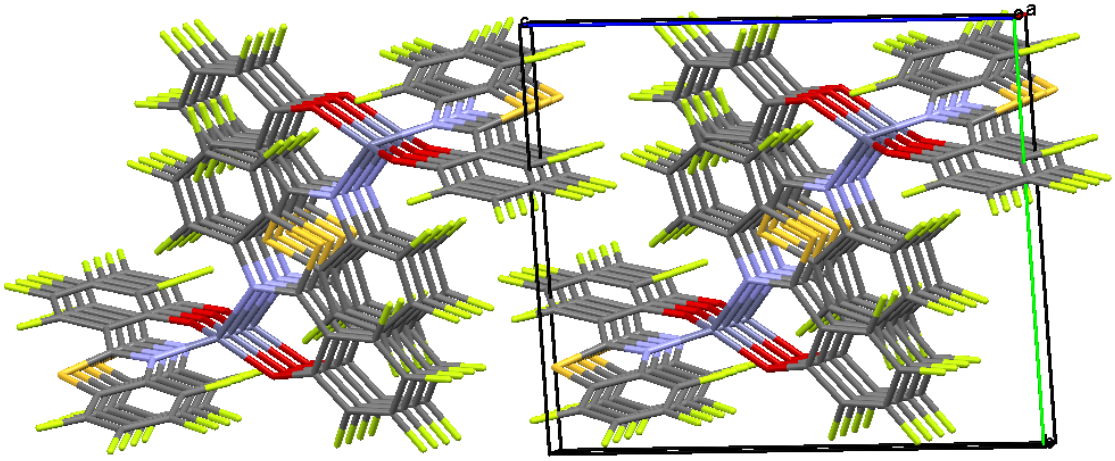

Figure 3.11: The packing of complex **55** along the $\overrightarrow{oa}$ axis

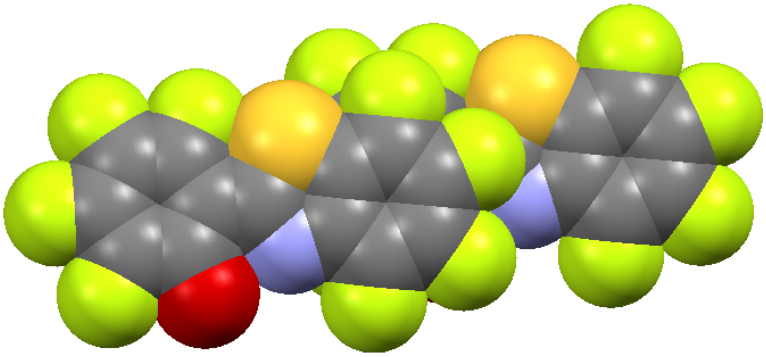

Figure 3.12: The packing between neighbouring pairs: stacking of 'wing' ligands generated by translation through the $\overrightarrow{oa}$ axis

In summary, the existence of stacked π-systems is a feature of all the phenoxide complexes. Despite the importance of π_H-π_F interactions in one dimensional (rod like) or two dimensional (planar) organic structures and its presence in half fluorinated complex **54**, this particular type of π-stacking is not the only one observed for half fluorinated systems such as **53**. However, *all* these three dimensional systems form centrosymmetric structures derived from chiral monomers. Thus the strongest influence in dictating the architecture of these crystals is the mutual recognition of enantiomers brought about by the favorable interaction of oppositely directed electrical dipoles, not the attraction of fluoroaryl groups for their fluorine-free counterparts.

3.2.2 Zinc complexes of bis(benzothiazolyl)amines

1. Zinc complexes of nonfluorinated bis(benzothiazolyl)amine

Nonfluorinated zinc complex **56** crystallises as a monomeric structure in a centrosymmetric space group (P–1). In contrast with the fluorinated phenolate complexes discussed earlier, there is not a pair composed of two monomers in this nonfluorinated zinc complex **56**, but a group of four molecules in a unit cell (Figure 3.13).

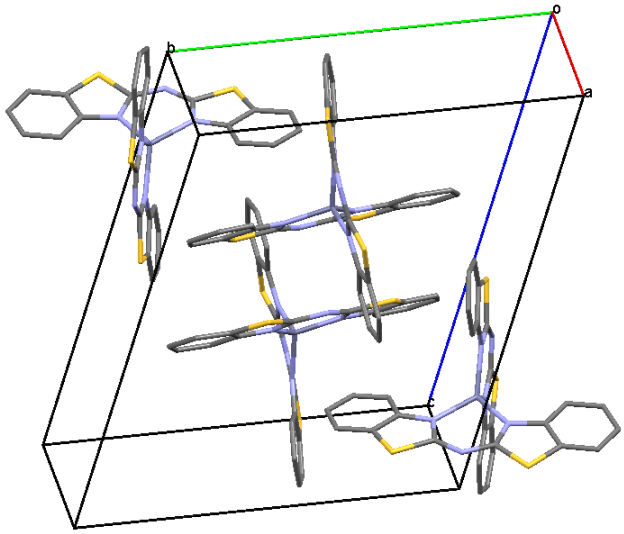

Figure 3.13: The unit cell in complex **56**

In such a group, the two molecules in the middle are relatively close, forming a pair with some partial stacking of their π orbitals (Figure 3.14, left). Compared with fluorinated zinc phenolate complexes **53** – **55**, the overlap of π orbitals in this pair of complex **56** molecules is much smaller, which could be due to the ligand's curved shape and steric effects that prevent two molecules getting closer (Figure 3.14, right). The interplanar separation is 3.55(1) Å between the two planes defined by carbon atoms in two 'benzo' rings related by the inversion centre.

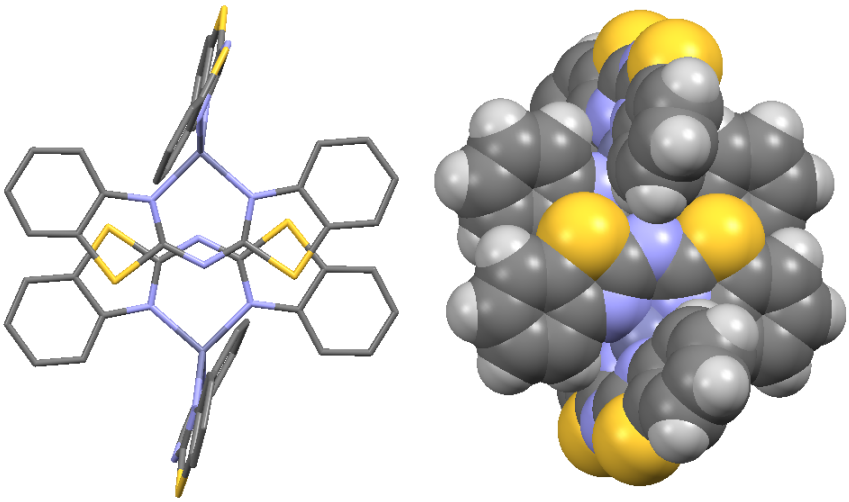

Figure 3.14: Stacking of two central molecules in the unit cell of complex **56**

Although the molecules at the corner of the unit cell are relatively remote from the central pair, they still possess some apparent π-π stacking with the central molecules, but the planes of the rings are far from being parallel. Figure 3.15 shows the 'benzo' ring of the corner molecule (right bottom) is facing the 'benzo' ring of one central molecule, with an angle of 23.5(2)° between the planes defined by the carbon atoms in the two facing 'benzo' rings.

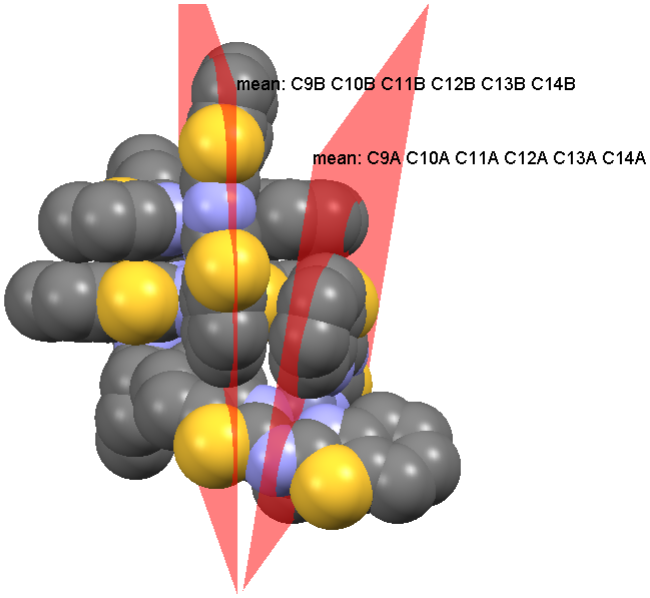

Figure 3.15: Stacking between a corner molecule and a central molecule

The two corner molecules locate roughly at 1 0 1 and 0 1 0 positions in the unit cell, so the close-packed direction in the crystal is [1 $\bar{1}$ 1]. Along this direction, one corner molecule has a π-π interaction with another corner molecule in the diagonally adjacent unit cell, with their terminal 'benzo' rings partially overlapped (Figure 3.16). The interplanar distance is 3.51(1) Å between the planes defined by the carbon atoms in the two confronting 'benzo' rings.

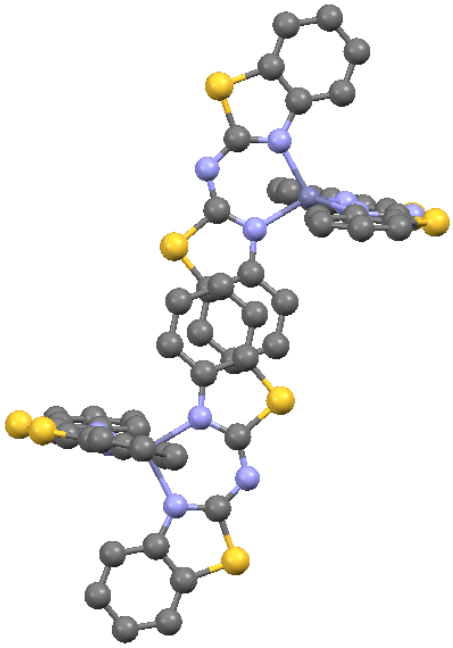

Figure 3.16: Stacking between corner molecules

2. Zinc complexes of half fluorinated bis(benzothiazolyl)amines

Half fluorinated zinc complex **57** crystallises as a monomeric structure in the space group $P2_1/n$. Although it also has four molecules in a unit cell (Figure 3.17), the same as the nonfluorinated complex **56**, there is only one molecule in the asymmetric unit. The other molecules can be generated by either an inversion centre or a screw axis.

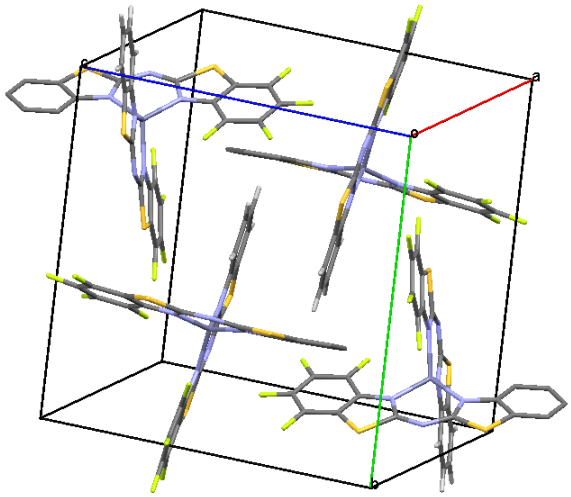

Figure 3.17: The unit cell in complex **57**

The two monomers in the centre of the unit cell are related by an inversion center, and have a small overlapping of their nonfluorinated 'benzo' rings showing π_H-π_H stacking (Figure 3.18, left), with a separation of 3.51(1) Å between the planes defined by the six carbon atoms in the two overlapping rings.

The molecules at the corner of unit cell also have some apparent π_H-π_F stacking with the central molecules, although the planes of the facing rings are far from being parallel. Figure 3.18 (right) shows the fluorinated 'benzo' ring of the corner molecule (right bottom) is facing the nonfluorinated 'benzo' ring of one central molecule, with an angle of 20.3(3)° between the planes defined by the carbon atoms in the two rings. The stacking between the corner molecule and the neighbouring central molecule is part of an infinite helix, in which the component molecules are related by a screw axis along the $\overrightarrow{ob}$ direction (Figure 3.19).

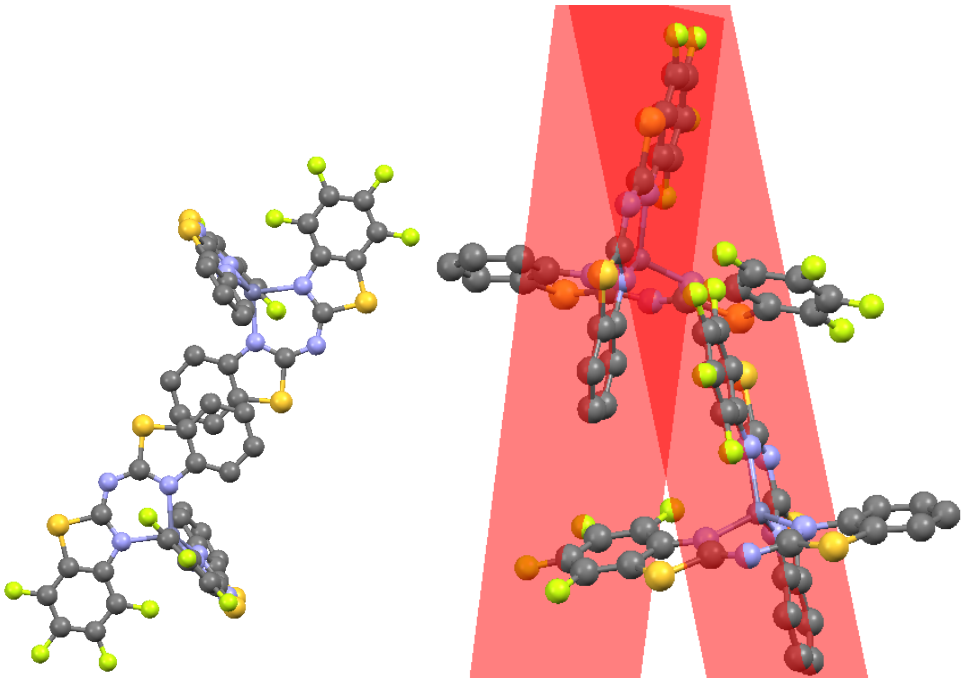

Figure 3.18: Left: Stacking between two central molecules of **57** showing π_H-π_H interaction; Right: Stacking between a corner molecule and a central molecule of **57** showing π_H-π_F interaction

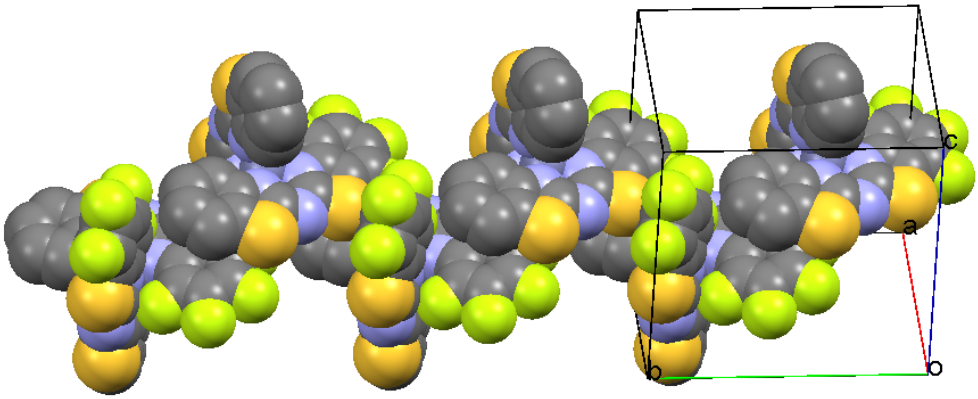

Figure 3.19: The helix along the $\overrightarrow{ob}$ direction with nonparallel stacking of nonfluorinated and fluorinated 'benzo' rings

The smallest edge length of the unit cell is *a*, so the translation along $\overrightarrow{oa}$ direction has denser packing of molecules than the other two directions. While the molecules along the $\overrightarrow{ob}$ direction only have one end of the ligands to interact with each other, the molecules along $\overrightarrow{oa}$ direction have both ends interacting with another one in the neighbouring cell. The two molecules are related by an inversion centre, and have the

nonfluorinated rings partially overlapped with fluorinated rings (Figure 3.20). The separation is 3.53(1) Å between the planes defined by the carbon atoms in two fluorinated 'benzo' rings.

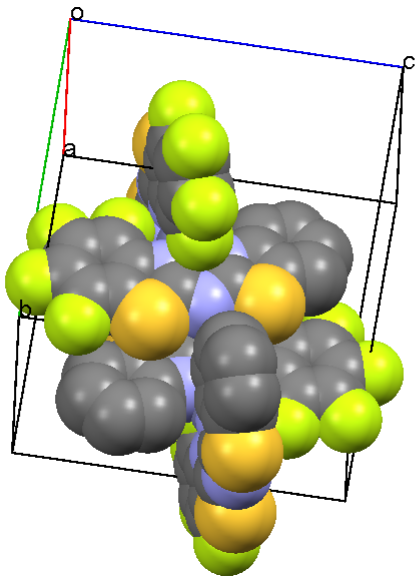

Figure 3.20: Packing of molecules along $\overrightarrow{oa}$ direction

3. Zinc complexes of perfluorinated bis(benzothiazolyl)amines ***58***

In the completely fluorinated zinc complex **58**, two monomers form a 'loose' pair with little overlapping (Figure 3.21). Their only physical contact is the adjacency of the sulfur atoms to the neighboring molecule's fluorine atoms, with an inter-atomic distance of 3.32(1) Å comparable with their sum of van der Waals radii (3.27 Å), while the interplanar separation is 3.30(1) Å between the two adjacent 'benzo' rings.

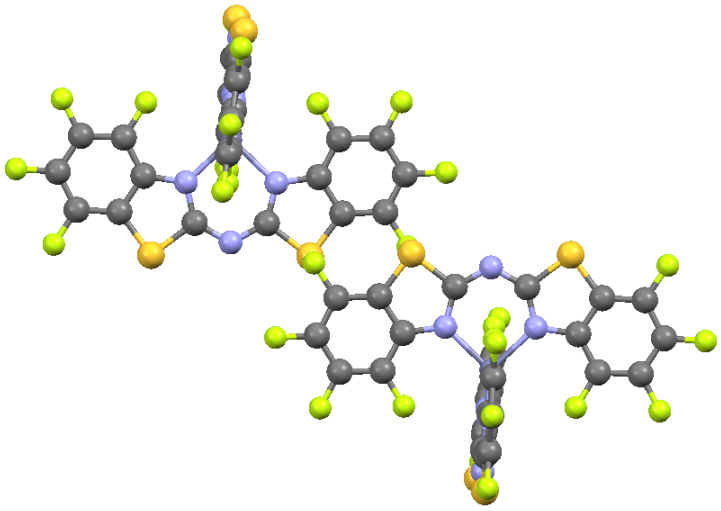

Figure 3.21: The pair of two closest molecules in complex **58**

Along the $\overrightarrow{oa}$ direction, the pair of molecules forms π-π interactions with its neighbouring pair, with two fluorinated 'benzo' rings stacking 'head to tail' (Figure 3.22, left). The average distance from the centroid of one 'benzo' ring to the plane defined by the opposite 'benzo' ring is calculated as 3.38(1) Å.

An almost identical stacking also exists in the perpendicular $\overrightarrow{ob}$ direction (Figure 3.22, right), with the same average separation of 3.38(1) Å between the centroid of one ring and the plane defined by the facing ring. The similarity of packing along the $\overrightarrow{oa}$ and $\overrightarrow{ob}$ directions arises from the triclinic structure's near-monoclinic features of unit cell parameters, with a = 10.281(5) Å, b = 10.321(5) Å and γ = 89.951(5)°. Detailed structural data can be found in the Appendix.

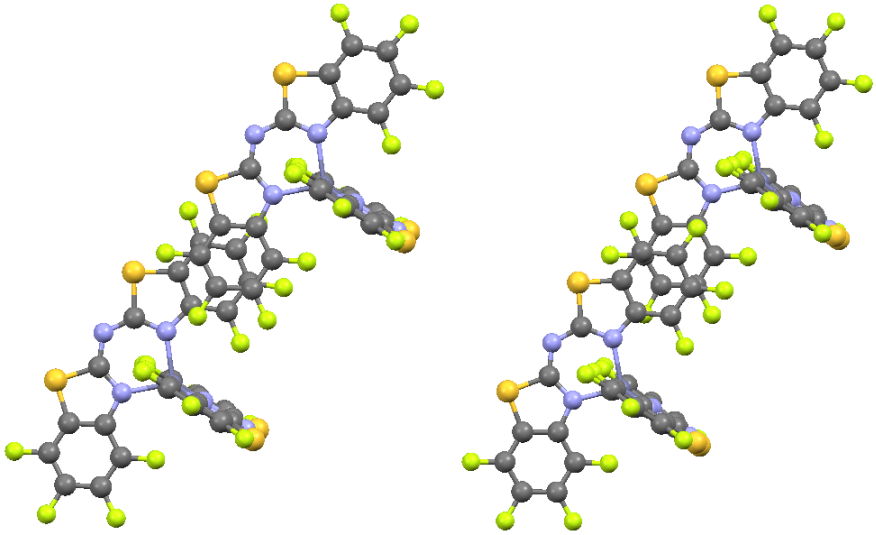

Figure 3.22: Stacking between pairs along the $\overrightarrow{oa}$ (left) and $\overrightarrow{ob}$ (right) directions

3.2.3 Half fluorinated bis(benzothiazolyl)amine (20): π-π_F stacking in the presence of hydrogen bonding

In examining the half fluorinated zinc complexes, we have seen how those three dimensional half fluorinated molecules stack in the presence of steric effects. In the case of a two dimensional half fluorinated ligand, the steric effect is much less prominent. But we can observe how the half fluorinated molecules stack in the presence of hydrogen bonding.

In the solid state, the half fluorinated bis(benzothiazolyl)amine stays as the tautomeric form **20'**, with the acidic proton attached to the thiazole N in the nonfluorinated benzothiazole ring rather than the middle bridging N (Figure 3.23). The acidic proton acts as the donor to form N–H···N type hydrogen bonding with the central N atom in the neighbouring molecule, with a H···N separation of 2.20 Å.

All the molecules in the crystal are linked by hydrogen bonds, forming planar pairs. Adjacent pairs are also coplanar, forming a sheet of molecules (Figure 3.24). The possible interactions between two neighbouring pairs are indicated by the short distance of C–H···F–C and S···F–C contacts (Figure 3.23). The H···F separation is as short as 2.49 Å, compared with the sum of van der Waals radii of 2.67 Å. The S···F separation is 3.13 Å, also shorter than the sum of van der Waals radii of 3.27 Å. The C–H···F–C interaction has been reported widely as a supramolecular assembly force.[17] The S···F interaction are much less reported, but was found in the thiophene–tetrafluorophenylene moiety[3] and identified by ^{19}F NMR in ((4-azido-2,3,5,6-tetrafluorophenyl)methylene)-bis(alkylsulfane) moiety.[85]

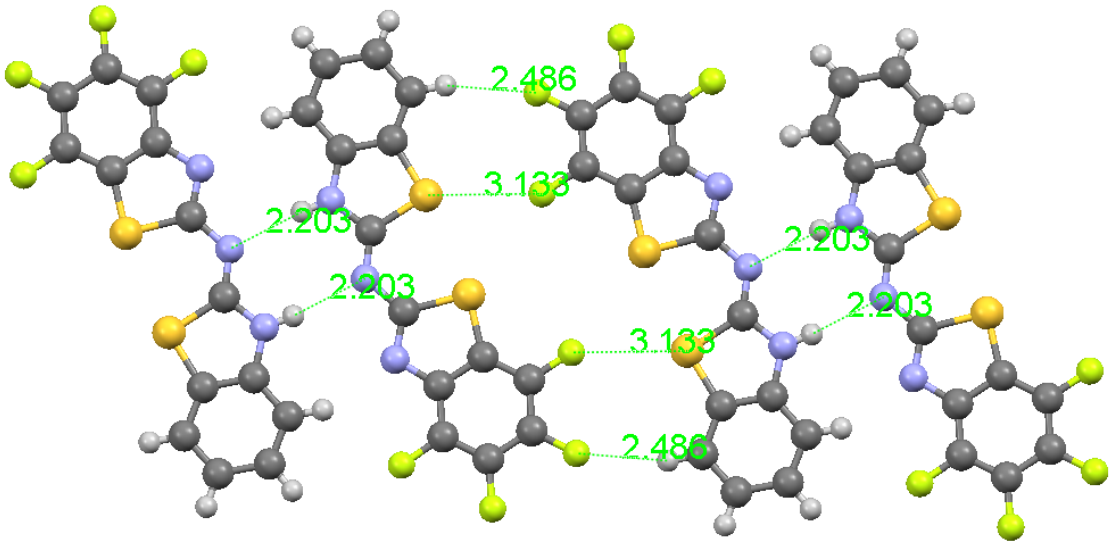

Figure 3.23: Hydrogen bond and possible interactions of C–H···F–C and S···F–C in the crystal of ligand **20'**

In the direction perpendicular to the molecular plane, sheets of molecules are stacked so that the fluorinated rings are overlapping with nonfluorinated rings with some offset (Figure 3.24). The interplanar distance is calculated as 3.55(1) Å between the planes defined by the six carbon atoms in two fluorinated 'benzo' rings.

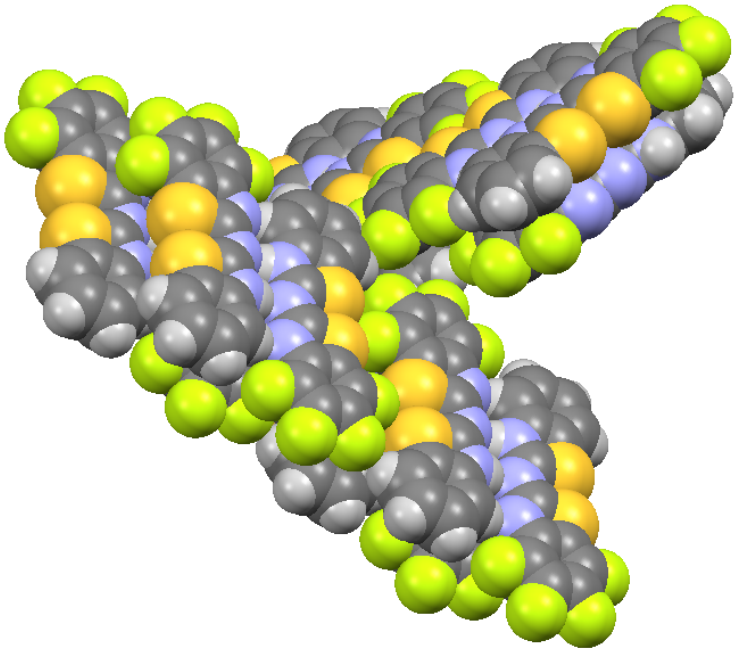

Figure 3.24: π_H-π_F interaction in the crystal of ligand **20'**

In summary, hydrogen bonding and π_H-π_F interaction exist simultaneously in the crystal of two-dimensional molecule **20'**. The hydrogen bonding, together with possible forces of C–H···F–C and S···F–C interactions, is responsible for assembly of neighbouring molecules to form planar sheets. The π_H-π_F interaction could facilitate the packing of molecular sheets to form infinite stacks.

3.3 Photophysical properties of zinc complexes

3.3.1 Photophysical properties of zinc complexes of fluorinated 2-(2-hydroxyphenyl)benzothiazoles

1. Solution phase absorption

The fluorinated zinc phenoxides **53**, **54** and **55** are yellow and have solution phase absorption spectra (recorded in DMSO) that are qualitatively similar to one another (Figure 3.25). All the phenoxides, including $[Zn(BTZ)_2]_2$, have their longest wavelength absorptions in the blue region. The absorption bands in the 350–470 nm range can be assigned to intraligand π–π* transitions, which is deduced from the distribution of HOMO and LUMO on the molecule that will be discussed in the following calculation part. The fluorinated phenoxides, which are mononuclear in the solid state, lack an absorption peak corresponding to the UV absorption of $[Zn(BTZ)_2]_2$ at 329 nm; this feature may be related to the ability of the latter compound to exist as a dimer in the solid. Extinction coefficients for the longest wavelength absorption bands in the partially fluorinated systems (**53** and **54**) were larger than either $[Zn(BTZ)_2]_2$ or fully fluorinated **55**; this is consistent with an enhanced transition dipole moment consequent on selective fluorination.

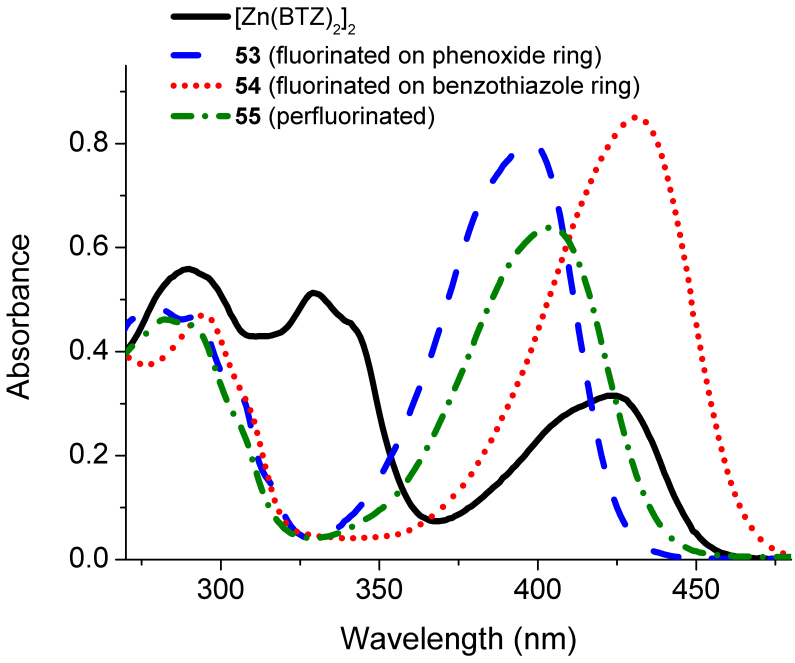

Figure 3.25: UV-visible spectra of zinc phenoxides $[Zn(BTZ)_2]_2$, **53**, **54** and **55** (2×10^{-5} M with respect to Zn^{2+}, solutions in DMSO)

2. Photoluminescence studies

Photoluminescence spectra were recorded on powders, thus avoiding the complications due to solvation in the solution phase measurements and interference effects in thin film studies.

The photoluminescence spectrum of each of the phenoxides $[Zn(BTZ)_2]_2$, **53**, **54** and **55**, excited at 368 nm, where there is an excitation peak, comprises a single broad peak in the visible region (Figure 3.26). Compared to emission from the nonfluorinated complex $[Zn(BTZ)_2]_2$ at 474 nm, tetrafluorination on the phenoxide ring, to give **53**, hardly changes the peak wavelength, but gives a broadened emission with the maximum at 476 nm. Tetrafluorination on the benzothiazolyl ring, to give **54,** leads to a red shift to 529 nm, whereas octafluorinated **55** shows an emission at 497 nm lying between the two tetrafluorinated complexes.

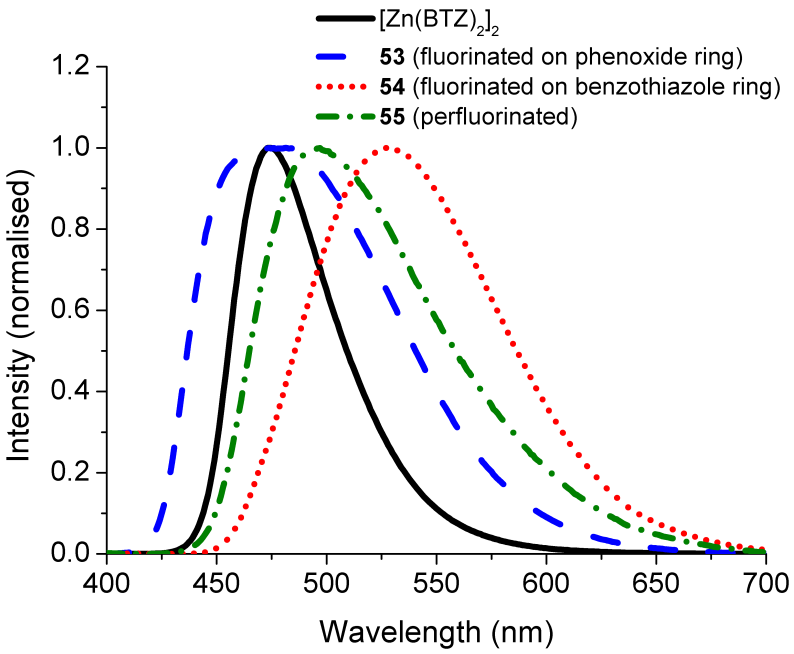

Figure 3.26: Photoluminescence emission spectra of powdered zinc phenoxides $[Zn(BTZ)_2]_2$, **53**, **54** and **55** upon excitation at 368 nm (excitation peak)

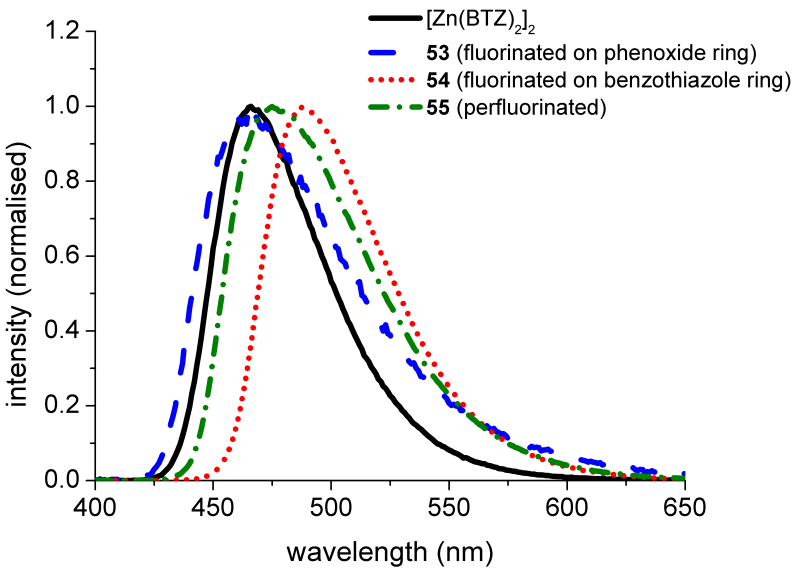

Figure 3.27: Photoluminescence emission spectra of zinc phenoxides $[Zn(BTZ)_2]_2$, **53**, **54** and **55** in DMSO solution upon excitation at 368 nm.

It is notable that the powder phase photoluminescence emission peaks of compounds **53-55** are broader than that of $[Zn(BTZ)_2]_2$; the differences in peak widths are much less marked in DMSO solution suggesting that this phenomenon is related to the structures adopted in the solid state. The compounds in which the phenoxide and benzothiazole rings are closest to coplanarity in the crystal, and so might be expected to have the most extensively delocalized π systems, are also the ones with the broadest emission peaks (Table 3.3).

Table 3.3: Inverse correlation between dihedral angles and photoluminescence full width at half maximum (FWHM)

Complex	**$[Zn(BTZ)_2]_2$**	**53**	**54**	**55**
Largest benzothiazole-phenolate dihedral angle /°	12.7	1.6	3.4	8.7
FWHM /nm	54	103	101	93

3. DFT calculation

The electronic structures of monomeric and dimeric forms of nonfluorinated $Zn(BTZ)_2$ were the subject of previous calculations.[86] The HOMOs are mainly localized on the phenoxide rings, whereas the LUMOs are less localized and spread over both the benzothiazole and phenoxide rings. In the case of the dimer the energy gap between the HOMO and LUMO is smaller than for the monomer; however, the HOMOs are located on the two bridging ligands, whereas the LUMOs are associated with the non-bridging ligands, so there may only be a low probability of a transition occurring between these particular orbitals.

Table 3.4: Calculated HOMO and LUMO energies for zinc phenolate complexes

	$Zn(BTZ)_2$	**53**	**54**	**55**
E_{LUMO}/eV	–1.79	–2.26	–2.19	–2.65
E_{HOMO}/eV	–5.39	–5.83	–5.68	–6.14
$E_{LUMO\text{-}HOMO}$/eV	3.60	3.58	3.49	3.48

In Table **3.4** we present the results of our own DFT calculations for the monomer of $Zn(BTZ)_2$ and the series of fluorinated analogues. The forms of the HOMO and LUMO wavefunctions are exemplified in Figure 3.28 by the perfluorinated zinc complex **55**. While the HOMO is mainly localised on the phenoxide ring, the LUMO spread over both phenoxide and benzothiazole rings. Therefore the electronic transitions are expected to show some charge-transfer (CT) character involving electron density redistribution between the phenoxide ring and the benzothiazole ring. A typical behaviour of molecules possessing CT character is the shift of spectra under influence of solvents.[87] The significant difference of PL spectra at solid phase and solution phase observed in our experiment also indicated the CT in $[Zn(BTZ)_2]_2$ and the fluorinated analogues.

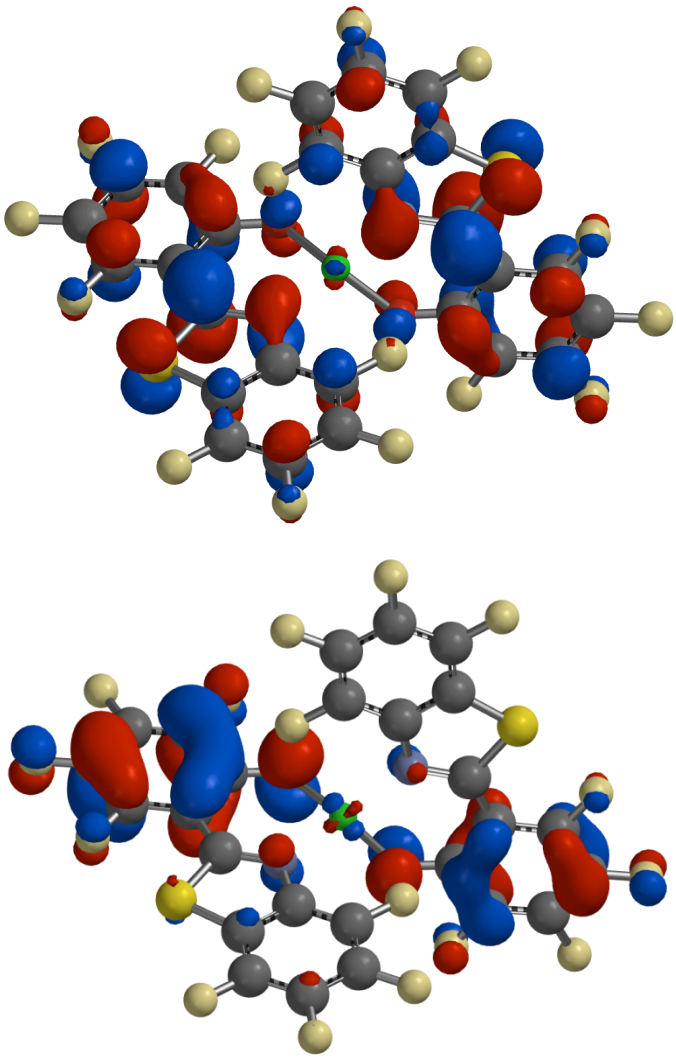

Figure 3.28: LUMO (top) and HOMO (bottom) of the fully fluorinated zinc phenoxide **55**

The relative shift of the emission spectra of fluorinated analogs compared with $[Zn(BTZ)_2]_2$ can also be rationalised by the influence of fluorination on the HOMOs and LUMOs. It is noticed that on the phenoxide ring there are distributions of both HOMO and LUMO, but on the benzothiazole ring there is only distribution of LUMO. Therefore the fluorination of the phenoxide ring, to give **53**, reduces both the HOMO and LUMO energies simultaneously, yielding an emission peak almost at the same wavelength as $[Zn(BTZ)_2]_2$. Fluorination of only the benzothiazole ring stabilizes the LUMO (delocalized over both rings) more than the HOMO (localized on the phenoxide ring), so that **54** has a decreased HOMO-LUMO gap compared with **53**, as is consistent with the red shift in both the absorption and photoluminescence spectra of **54**. Complete

fluorination in **55** is calculated to provide a HOMO-LUMO gap almost equal to that in **54**; however the absorption spectrum of **55** is blue-shifted relative to **54** and more closely resembles that of **53**. Photoluminescence from **55** is also blue shifted relative to **54**.

3.3.2 Photophysical properties of zinc complexes of fluorinated bis(benzothiazolyl)amines

1. Solution phase absorption

The zinc complexes of nonfluorinated, half fluorinated and perfluorinated bis(benzothiazolyl)amines are all colourless solids. They are monomeric in the crystal structure and show similar peak features, including shape, position, and comparable extinction coefficients in the UV region. The absorption bands in the 300–400 nm range can be assigned to intraligand π–π* transitions, which is deduced from the distribution of HOMO and LUMO on the molecule discussed in the following calculation part.

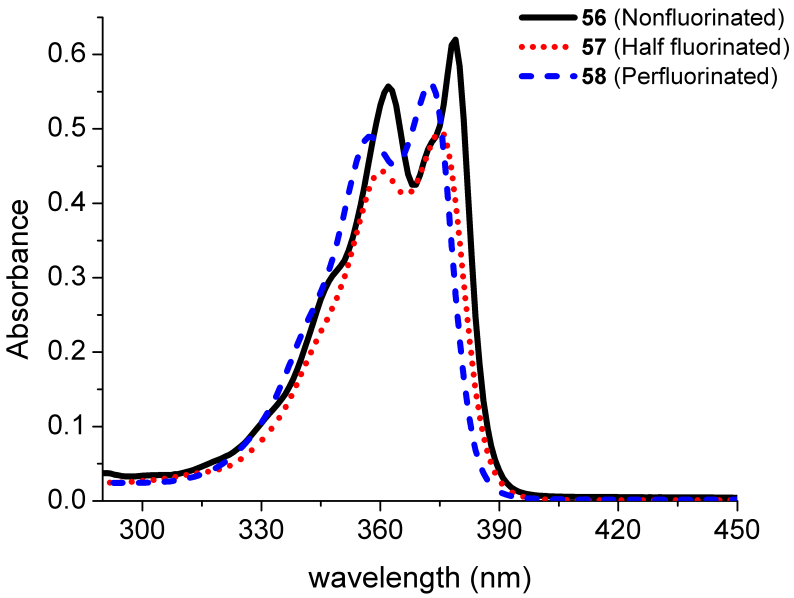

Figure 3.29: UV-visible spectra of zinc complexes **56**, **57** and **58** (5×10^{-6} M, solutions in DMSO)

2. Photoluminescence studies

Photoluminescence spectra were recorded on powders, thus avoiding the complications

due to solvation in the solution phase measurements and interference effects in thin film studies. Compared with the nonfluorinated zinc complex **56** having a narrow peak at 427 nm and a smaller shoulder around 440 nm, half fluorinated **57** leads to a large red shift showing a single broad peak at 482 nm, whereas perfluorinated **58** yields a broad emission showing some structure, with a central peak at 444 nm and shoulders at 427 nm and 468 nm (Figure 3.30).

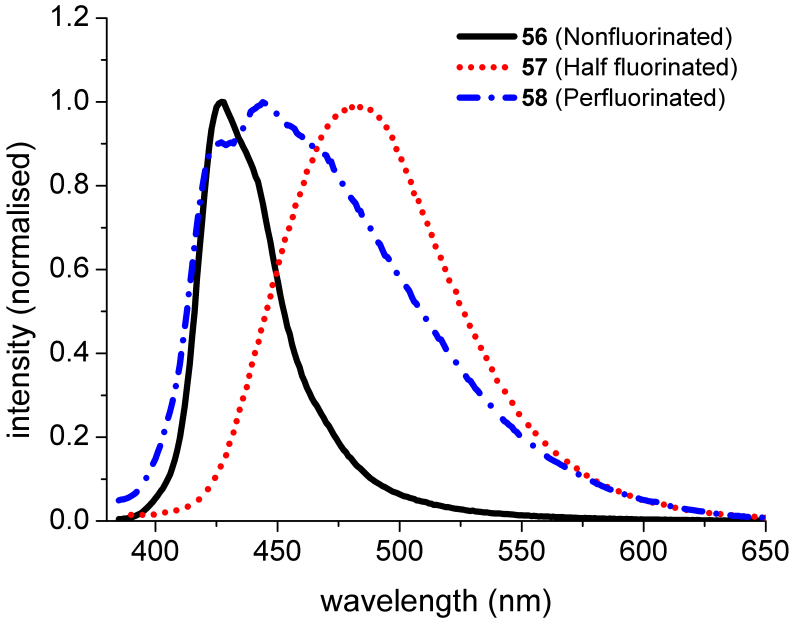

Figure 3.30: Photoluminescence emission spectra of powdered zinc complexes **56**, **57** and **58** upon excitation at 350 nm

It is notable that the powder phase photoluminescence emission peaks of fluorinated compounds **57** and **58** are broader than that of the nonfluorinated compound **56**. The full width at half maximum (FWHM) of **56** is only 37 nm, but the FWHM of **57** and **58** reaches 81 nm and 96 nm respectively. The compounds in which the two benzothiazole rings are closest to coplanarity in the crystal, and so might be expected to have the most extensively delocalized π-systems, are also the ones with the broadest emission peaks (Table 3.5). This is further evidence of the inverse correlation between dihedral angle and spectra width that we reported earlier.[88]

Table 3.5: Inverse correlation between dihedral angles and photoluminescence full width at half maximum (FWHM)

Complex	**56**	**57**	**58**
Largest dihedral angle /°	7.0	3.6	3.1
FWHM /nm	37	87	96

3. DFT calculation

Table 3.6 shows our DFT calculations for the series of zinc complexes of bis(benzothiazolyl)amines. Fluorination decreases the LUMO and HOMO energies by almost equal amounts. Tetrafluorination decreases LUMO and HOMO by about 0.35 eV, and octafluorination decreases them further by another 0.35 eV roughly. The calculation suggests almost identical band gaps for all three complexes, which is in agreement with their similar absorption curves. However, their powder phase emission spectra show apparently different features compared with each other, which is considered as the consequence of different molecular stacking and π-π interactions in the solid state. The forms of the HOMO and LUMO wavefunctions are exemplified in Figure 3.31 by the perfluorinated zinc complex **58**.

Table 3.6: Calculated HOMO and LUMO energies for zinc bis(benzothiazolyl)amide complexes

	56	**57**	**58**
E_{LUMO}/eV	–1.49	–1.85	–2.20
E_{HOMO}/eV	–5.51	–5.86	–6.20
$E_{LUMO\text{-}HOMO}$/eV	4.02	4.01	4.00

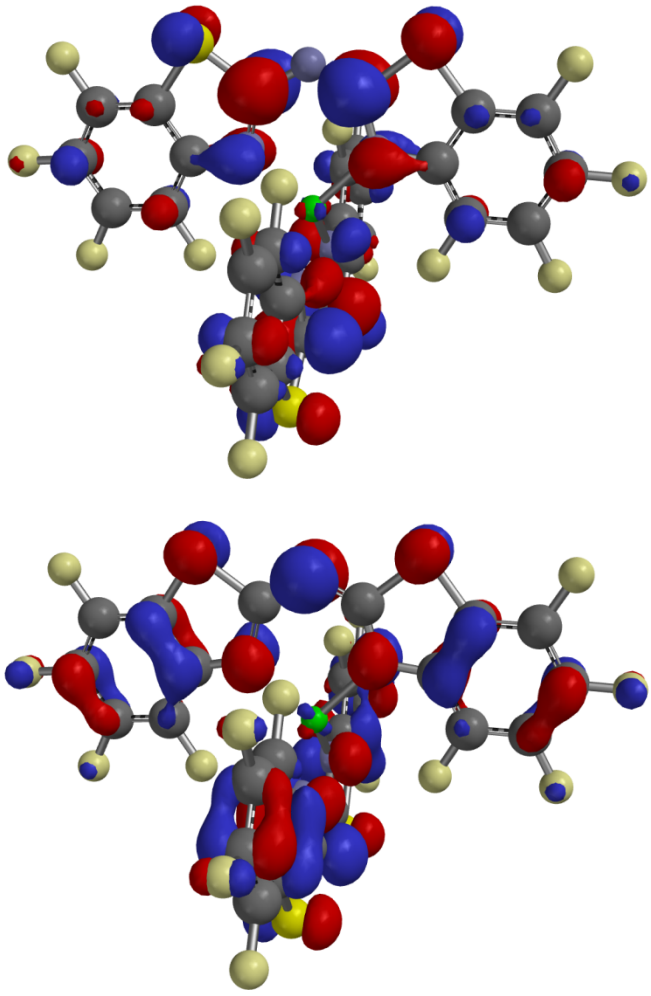

Figure 3.31: LUMO (top) and HOMO (bottom) of the fully fluorinated zinc bis(benzothiazolyl)amide complex **58**

3.3.3 Quantum yield measurement

Photoluminescence quantum yields were measured for all zinc complexes in their diluted DMF solution (4×10^{-6} M for zinc phenolates, and 1×10^{-6} M for zinc bis(benzothiazolyl)amides). Crystalline anthracene (1×10^{-5} M) in 95% EtOH was used as the standard solution with a known quantum yield of 0.27.[89] In order to minimise reabsorption and re-emission effects, all the solutions were diluted to a level that the integrated spectra and absorbance maintained a linear relationship (with absorbance smaller than 0.1 for most solution, but absorbance more than 0.1 was allowed if the

linear relationship can be maintained). Then the quantum yields Q_x were calculated using the expression:[90]

$$Q_X = Q_R \left(\frac{Grad_X}{Grad_R}\right)\left(\frac{{n_X}^2}{{n_R}^2}\right),$$

where Q is the quantum yield of the solution, *Grad* is the gradient of the fitted line of integrated spectra against absorbance, n is the refractive index of the solvents (1.43 for DMF, and 1.36 for 95% EtOH at around 20 °C), and the subscripts X and R refer the sample and standard respectively. The obtained values are listed in the table.

Table 3.7: Quantum yields for different zinc complexes

compounds	**standard**	**$[Zn(BTZ)_2]_2$**	**53**	**54**	**55**	**56**	**57**	**58**
quantum yield	0.27	0.69	0.05	0.50	0.44	0.40	0.004	0.02

3.4 Photophysical properties of erbium complexes

Although there is concern about the purity level and structural identity of all the erbium complexes made, some preliminary photophysical measurements were done on the purest sample we could get.

1. Tris[(benzothiazol-2-yl)phenoxy]erbium

The sublimed sample of tris[(benzothiazol-2-yl)phenoxy]erbium has the characteristic yellow colour, which resembles the potassium salt and zinc complex where the ligand is deprotonated. Time-resolved photoluminescence showed this compound has a lifetime of τ = 0.8 μs upon excitation at 520 nm. The short lifetime in the microsecond range is consistent with published lifetimes measured for erbium complex with containing C–H bond in the ligand.[91-93]

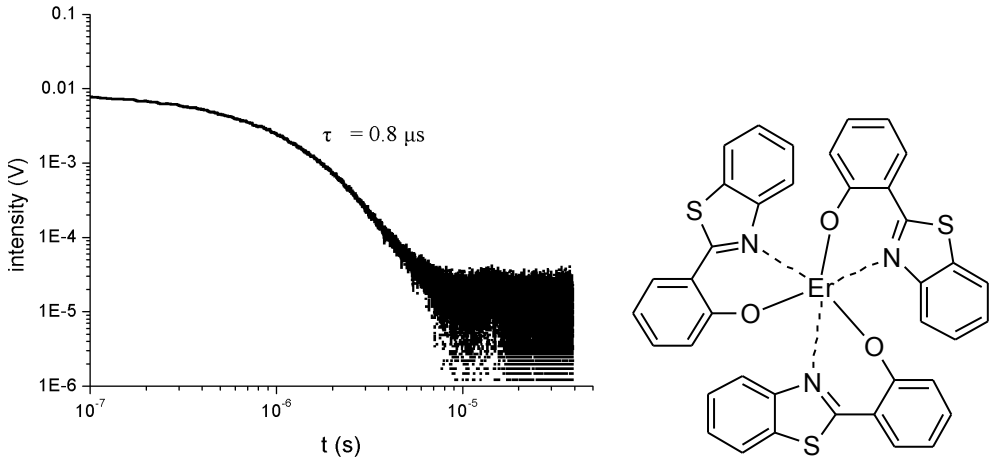

Figure 3.32: Lifetime of tris[(benzothiazol-2-yl)phenoxy]erbium

2. Caesium tetrakis[(4,5,6,7-tetrafluorobenzothiazol-2-yl)-3,4,5,6-tetrafluorophenoxy] erbate(III)

The orange coloured film-like caesium tetrakis[(4,5,6,7-tetrafluorobenzothiazol-2-yl)-3,4,5,6-tetrafluorophenoxy]erbate(III) has a much longer lifetime compared with the nonfluorinated erbium phenolate complex, with a lifetime of τ = 29 μs upon excitation

at 450 nm. This prolonged lifetime can be attributed to the exclusion of C–H bond in the coordinating ligands and the absence of solvent molecules.

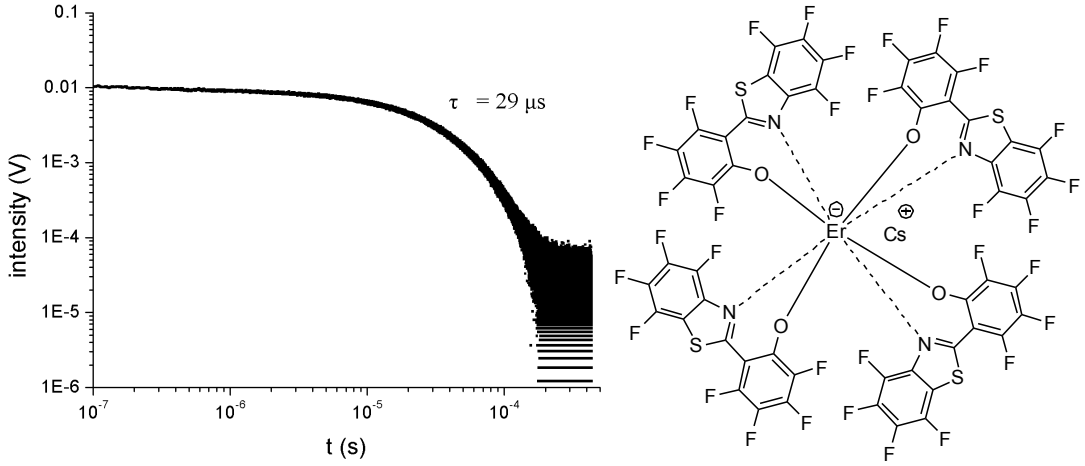

Figure 3.33: Lifetime of caesium tetrakis[(4,5,6,7-tetrafluorobenzothiazol-2-yl)-3,4,5,6-tetrafluorophenoxy]erbate(III)

3.5 Summary of Chapter 3

1. Crystal structures of six zinc complexes with different extent of fluorination (Figure 3.34) were obtained. Unlike the nonfluorinated complex of $[Zn(BTZ)_2]_2$ which has a dimeric structure, all the new structures are monomeric.

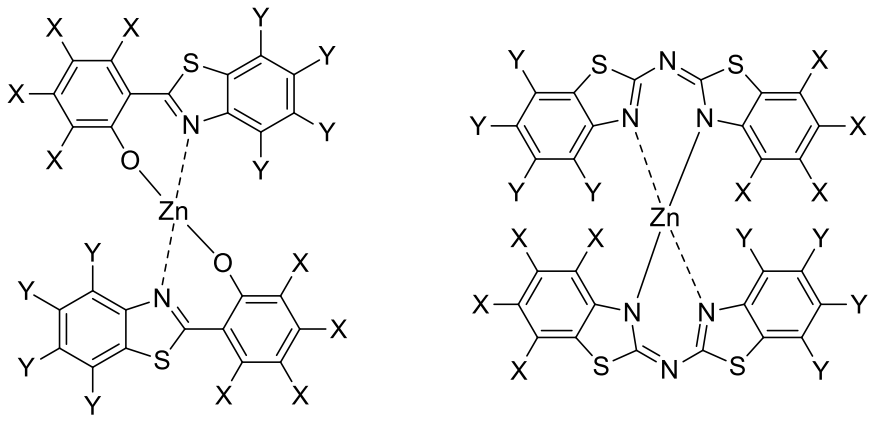

53 (X=F, Y=H)
54 (X=H, Y=F)
55 (X=Y=F)

56 (X=Y=H)
57 (X=H; Y=F)
58 (X=Y=F)

Figure **3.34** Monomeric zinc complexes

2. The molecular packing behaviour was analysed in all zinc complexes. Apart from the π_H-π_F stacking mode which has been found to be the dominant recognition force in those partially fluorinated or 1:1 mixtures of perfluorinated and nonfluorinated planar molecules, π_H-π_H and π_F-π_F stacking modes were also observed in the half fluorinated three-dimensional zinc complexes. We consider that the dipole-dipole interaction between enantiomers and the steric effect are combined to guide the molecular packing in these half fluorinated three-dimensional systems.

3. The ligand **20** was identified as its tautomer form **20'** in the crystal structure (Figure 3.35). Hydrogen bonding, and the possible C–H···F–C and S···F–C interactions assemble the neighbouring molecules into planar molecular sheets, while these molecular sheets are stacked by π_H-π_F interactions.

4. Fluorination stabilises the energy levels of HOMO and LUMO simultaneously but to different extent, depending on the location of fluorination and the distribution of HOMO and LUMO. The small differences between the decreased values of HOMO level and LUMO level cause subtle changes of the band gaps, which lead to the relative shift of the photoluminescence spectra. An inverse relation between the spectra broadening and the dihedral angle of neighbouring aromatic rings in a conjugated system has been found. A smaller dihedral angle leads to an increased FWHM.

Chapter 4 - Results and discussion part III: Application of perfluorinated zinc complex 55 in OLEDs fabrication

4.1 Use of perfluorinated zinc complex 55 as emissive material

In a fluorescent type OLED device, such as one using Alq_3 as the emissive layer, only singlet emission is allowed as a result of the selection rule. But for metal complexes of some heavy elements, the spin-orbit coupling can give rise to the mixing of singlet and triplet, therefore the triplet emission (phosphorescence) is allowed. There are already several phosphorescent materials making advantage of heavy transition metals, e.g. iridium and platinum complexes, to fabricate highly efficient OLEDs. However, these heavy metal elements are very costly because they are limited resources. The possibility of achieving phosphorescence by some other means would be desirable. In typical organic luminescent materials, many atoms are hydrogen which can be substituted by other atoms or functional groups. If all the hydrogen atoms are replaced with heavier halogen atoms, we can expect an enhanced intersystem crossing (ISC) rate, and thus an increased possibility of triplet emission. This approach may open a new direction to develop novel phosphorescent materials. The following part of this chapter will discuss the application of the perfluorinated zinc complex of 2-(2-hydroxy-3,4,5,6-tetrafluorophenyl)-4,5,6,7-tetrafluorobenzothiazole (complex **55**), which will be written as $Zn(F\text{-}BTZ)_2$, as an emissive layer in OLEDs.

4.1.1 Devices with structure ITO/TPD/$Zn(F\text{-}BTZ)_2$/LiF/Al and ITO/TPD/$Zn(F\text{-}BTZ)_2$/Alq_3/LiF/Al

In a standard device with the structure ITO (anode)/TPD/Alq_3/LiF/Al (cathode), TPD is used as the hole transport layer (HTL), and Alq_3 is used both as the electron transport layer (ETL) and the emissive layer (EML). Our first attempt of device fabrication was

based on this structure, and the thicknesses of different layers were ITO/ TPD (50 nm)/ $Zn(F\text{-}BTZ)_2$ (50 nm)/ LiF (1 nm)/ Al (100 nm). The current-voltage-light (I-V-L) characteristic of this device is illustrated in Figure 4.1 (top). The I-V curve showed a typical diode characteristic with a turn-on voltage at 1.4 V, from where the carriers began to be injected. However, the light output was not able to be detected by a power meter until the drive voltage reached 5 V, and the highest efficiency of this device was only 0.002%.

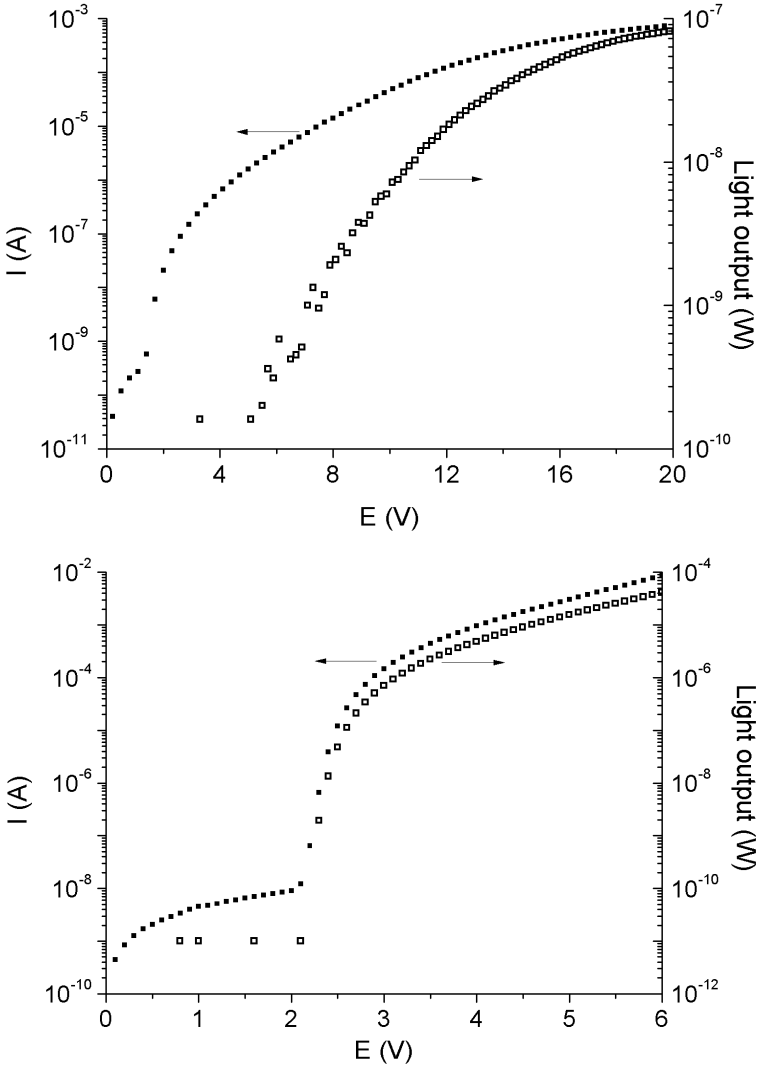

Figure 4.1 Top: I-V-L characterisation of device ITO/TPD/$Zn(F\text{-}BTZ)_2$/LiF/Al
Bottom: I-V-L characterisation of standard device ITO/TPD/$Zn(BTZ)_2$/LiF/Al

The possible causes for the device's poor performance could be the low charge mobility of the perfluorinated zinc complex and the energy barrier for holes at the

TPD/Zn(F-BTZ)$_2$ interface. These factors can substantially limit the current through the device, which in this case was about three orders of magnitude smaller than for the standard device at the same voltage (Figure 4.1, bottom). The HOMO levels for TPD and Zn(F-BTZ)$_2$ are -5.5 eV and -6.1 eV respectively,[88, 94] which give a 0.6 eV barrier for hole injection. This interface barrier could explain why the turn-on of the emission was more than 3 V higher than the turn-on of the current.

To improve the device performance, a layer of Alq$_3$ was added to the device structure to improve electron transport and confine carriers in the thin Zn(F-BTZ)$_2$ layer. So a device of ITO/TPD (50 nm)/ Zn(F-BTZ)$_2$ (20 nm)/ Alq$_3$ (50 nm)/ LiF/ Al was prepared.

Compared to the device of ITO/TPD/Zn(F-BTZ)$_2$/LiF/Al, the adoption of Alq$_3$ and reduction of the thickness of Zn(F-BTZ)$_2$ increased the device current by more than one order of magnitude (Figure 4.1), and the efficiency was improved to 0.004%. However, there was still a lag of the turn-on of emission after the turn-on of the current, suggesting that a reduction of the interface barrier for holes was required.

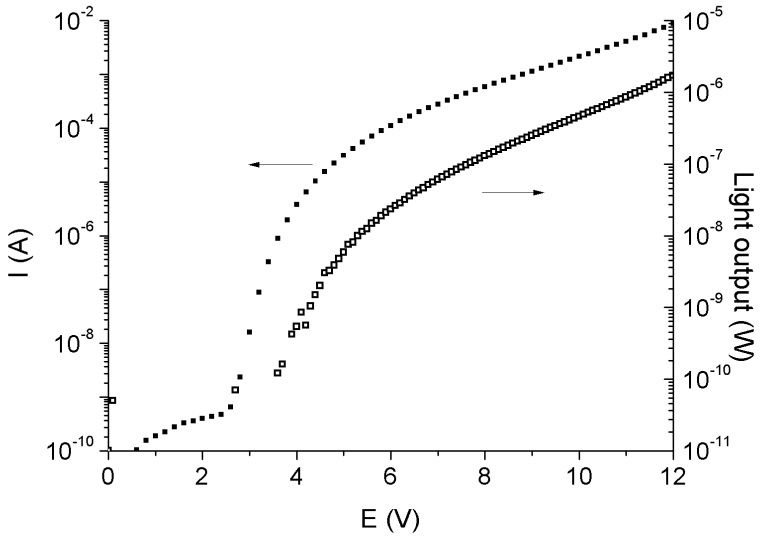

Figure 4.2: I-V-L characterisation of device ITO/TPD/Zn(F-BTZ)$_2$/Alq$_3$/LiF/Al

4.1.2 Devices with structure ITO/HMTPD/Zn(F-BTZ)$_2$/Alq$_3$/LiF/Al

The difference of HOMO levels between TPD and Zn(F-BTZ)$_2$ is as large as 0.6 eV. To reduce the barrier for injecting holes into Zn(F-BTZ)$_2$, a new HTL material with lower

HOMO level was demanded. The Thompson group reported a device in which they used the material HMTPD to transport and inject holes into the host material BCP that has a low HOMO level of -6.7 eV.[95] Therefore we expected that HMTPD could also be able to used to inject holes into our perfluorinated zinc complex. A device with the structure ITO/ HMTPD (50 nm)/ $Zn(F\text{-}BTZ)_2$ (20 nm)/ Alq_3 (50 nm)/ LiF (1 nm)/ Al (100 nm) was prepared. Its I-V-L characteristic showed the device's current and emission were almost turned on simultaneously at about 3.5 V (Figure 4.3, and the maximum efficiency was substantially improved to 0.02%. This improvement in emission intensity also enabled us to carry out more studies on the electroluminescence (EL).

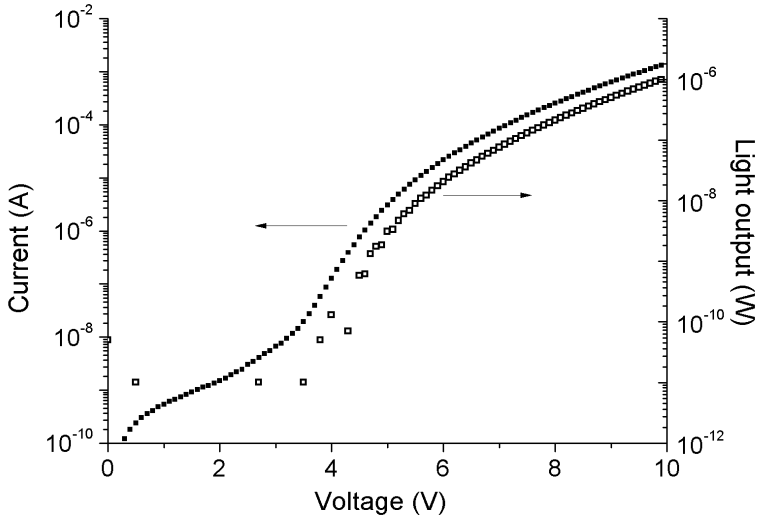

Figure 4.3: I-V-L characterisation of device ITO/HMTPD/$Zn(F\text{-}BTZ)_2$/Alq_3/LiF/Al

4.1.3 Transient electroluminescence of $Zn(F\text{-}BTZ)_2$

1. Influence of the device current on EL

The transient EL is measured when the device is just switched off. The exciton lifetime would simply be the detected lifetime of light output from the device if the current through the device vanished immediately after switching off. However, the actual situation is that the current through the device also has a lifetime, which is a consequence of the intrinsic capacitance and resistance of an OLED. Thus the current decay in the device also needs to be monitored and compared with the light decay. The set up for the transient measurements of current and EL are illustrated in the experimental section.

Only when the light decay is obviously longer (Figure 4.4, b) than the current decay (Figure 4.4, a), can it be confirmed that there is indeed a triplet related emission. If the light decay has almost the same lifetime (Figure 4.4, c) as the current decay, it would suggest that there is only singlet emission, which has a fast decay in the order of a few nanoseconds so that its decay curve follows the shape of current decay (usually a few hundreds of nanoseconds) very closely.

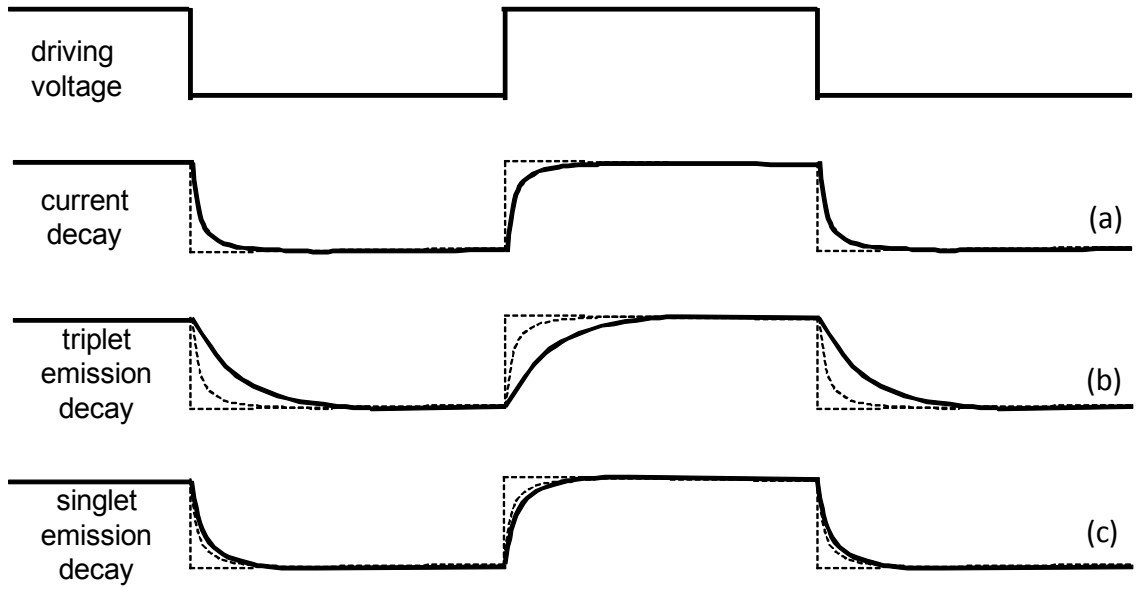

Figure 4.4: Expectations for the decay curves of (a) device current, (b) triplet emission and (c) singlet emission

The real current decay curve was, however, different from the ideal situation considered above. Instead of decaying from the steady working current (point W) to zero (point N) along the dashed line, the current first changed its direction, and then started to discharge from a negative value (point D) (Figure 4.5, left).

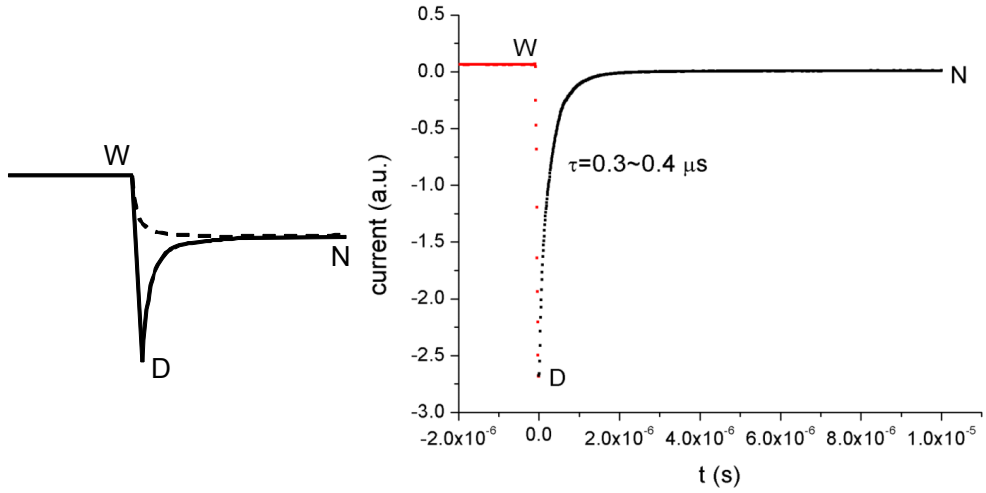

Figure 4.5 Left: Illustration of the device current decay; Right: Lifetime of the recorded current decay in device ITO/HMTPD/Zn(F-BTZ)$_2$/Alq$_3$/LiF/Al

This change of device current was due to the discharging process of the capacitor-like OLED, which has an opposite discharging current direction to the working current direction. The discharging process was fitted with an exponential equation and gave a lifetime of 0.3~0.4 μs (Figure 4.5, right). Considering the process of changing the direction of the current took about 0.1 μs, we believe any luminescence with lifetime longer than 0.5 μs should be derived from the triplet. But caution is needed when measuring the real EL lifetime. The resistor-capacitor (RC) decay of the EL measuring circuit must not be slower than the luminescence decay, especially when an ancillary resistor is used to amplify the signal.

2. EL spectra

Electroluminescence spectra of the device were recorded at various driving voltages (Figure 4.6). There are clearly two peaks in the spectra. The one at 510 nm is very close to the photoluminescence peak of the zinc complex at 497 nm, so we assign this to the

emission from the singlet. The other peak at about 612 nm occurs at substantially lower energy than the photoluminescence of any composing material in the device, and we ascribed it to the triplet emission, or phosphorescence, from the zinc complex.

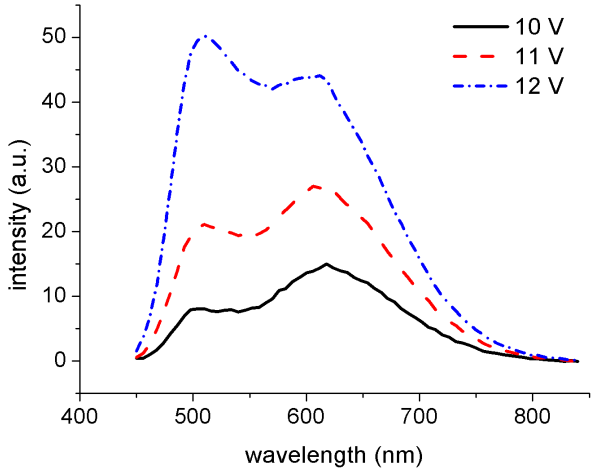

Figure 4.6: EL spectra of device ITO/HMTPD/Zn(F-BTZ)$_2$/Alq$_3$/LiF/Al at different driving voltage

It is noticeable that the intensity ratio of the two peaks varies substantially upon increasing of the driving voltage: the peak at 612 nm experienced a slower growth than the peak at 510 nm. Several reasons could cause the depression of triplet emission: the triplets can either be quenched by interaction with charge carriers (polarons),[96] or be quenched by other processes such as triplet triplet annihilation (TTA),[97] or can even dissociate into free charge carriers at some site in the material.[98]

3. Lifetimes of device EL

To verify the origin of the emission centered at 612 nm, an EL decay curve was recorded at the wavelength 612 nm (Figure 4.7). The fitting with a triple exponential decay function gave three components: 0.52±0.11 μs, 4.4±1.8 μs and 53±13 μs.

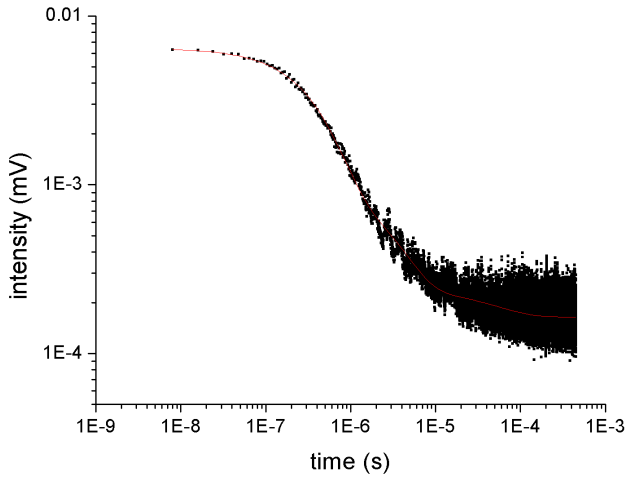

Figure 4.7: EL decay curve measured at 612 nm

The shortest lifetime of 0.52±0.11 μs was regarded as the fluorescence limited by the device current. Although fluorescence is a fast process usually having a lifetime of a few nanoseconds, it can be sustained as long as there is still current through the device. The longest component of 53±13 μs was considered as the triplet, which has been reported to have lifetimes in the order of a few tens of microseconds in other materials, such as the well known Alq_3 which has a triplet lifetime about 25±15 μs.[99] The component of 4.4±1.8 μs is much longer than singlet lifetime, but shorter than the component of 53±13 μs. Thus we consider it as a reduced lifetime for the triplets that are quenched by mechanisms such as triplet-polaron interaction, TTA, or dissociation.

Theoretically, the EL spectra measured should be a sum of all the three processes taking place in the device: fluorescence, phosphorescence and triplet-triplet-annihilation. At a specific wavelength, the contribution of each process can be calculated from the parameters of the fitted decay curve by multiplying the lifetime with its corresponding prefactor: $t_i \times A_i$, where t_i is the lifetime and A_i is its prefactor. If lifetime and prefactor data were obtained by recording decay curve across various wavelengths, then eventually we can plot the product $t_i \times A_i$ against wavelength to give the separate spectra for each process. Figure 4.8 shows the spectra of each processes obtained using the above method when the device was operated at 12 V.

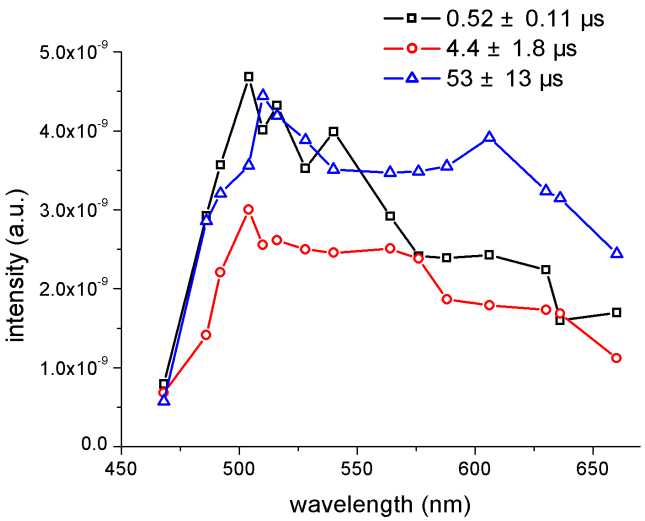

Figure 4.8: Contribution of different process to the EL spectra at 12V driving voltage

The fastest component 0.52±0.11 µs peaks at around 504 nm, and is dominated by high energy fluorescence. The longest component 53±13 µs shows the biggest contribution to the low energy emission at 606 nm, and exhibits another peak at 510 nm. The fact that there is a long lifetime emission at 510 nm could be due to reasons such as the mixing of triplets and singlets, or the TTA process. The medium component 4.4±1.8 µs has a peak at around 504 nm, and a relatively even distribution across the lower energy region.

4.2 Use of perfluorinated zinc complex 55 as host material for NIR emitter $Er(FTPIP)_3$

The development of NIR OLEDs has seen increasing interests due to their potential application in areas like optical communication, laser technology and bio-imaging.[100] Since the fabrication of the first NIR OLED in our group using Erq_3 (q= 8-hydroxyquinolate) as the emitting material,[101] exploitation of devices with higher performance has been ongoing.

Two important prerequisites for improved performance of lanthanide based OLED are the efficient coupling of triplet energy level with the excited energy level of metal ions,

and the minimum quenching of NIR emission by the organic environment. Perfluorinated chromophores, such as the $Zn(F\text{-}BTZ)_2$, could be ideal hosts to meet both requirements. Therefore, we fabricated the device ITO/ HMTPD (50 nm)/ $Zn(F\text{-}BTZ)_2$ (12 nm) + $Er(FTPIP)_3$ (8 nm)/ Alq_3 (50 nm)/ LiF (1 nm)/ Al (100 nm), where $Zn(F\text{-}BTZ)_2$ and $Er(FTPIP)_3$ are co-evaporated in the molar ratio of 4:1. The EL spectrum in the region of NIR is showed in Figure 4.9. The peak at 1534 nm corresponds to the typical $^4I_{13/2} - {}^4I_{15/2}$ transition, which has a lifetime of about τ=420 µs (Figure 4.10). This device is the first example of a NIR emitting OLED showing good sensitization and long electroluminescence lifetime.

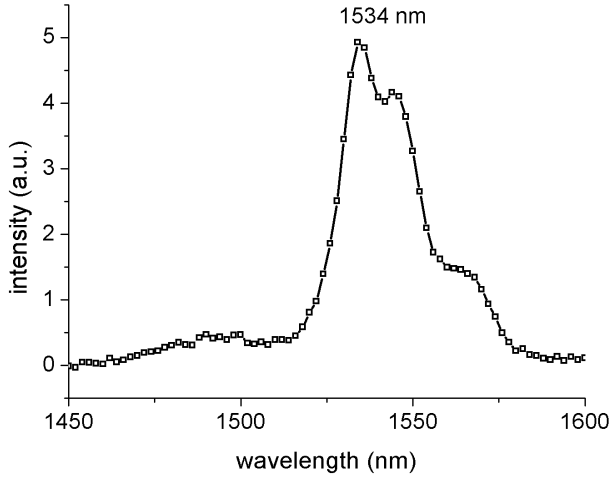

Figure 4.9: EL spectra of doped device showing Er^{3+} emission

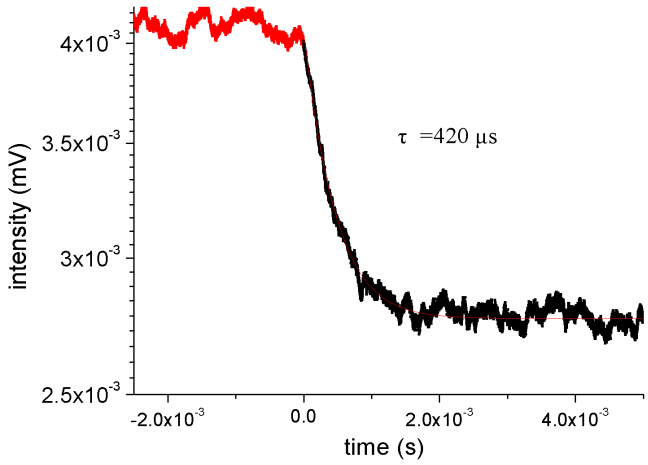

Figure 4.10: EL lifetime of device ITO/HMTPD/$Zn(F\text{-}BTZ)_2$+$Er(FTPIP)_3$/Alq_3/LiF/Al

4.3 Summary of Chapter 4

Organic light emitting diodes (OLEDs) were fabricated using the perfluorinated zinc complex of 2-(2-hydroxy-3,4,5,6-tetrafluorophenyl)-4,5,6,7-tetrafluorobenzothizole, $Zn(F\text{-}BTZ)_2$ (**55**), as an emission layer. The optimised device structure ITO/HMTPD/$Zn(F\text{-}BTZ)_2$/Alq_3/LiF/Al exhibited dual-emissive electroluminescence, with a long lifetime phosphorescence and a short lifetime fluorescence, indicating enhanced spin-obit coupling and increased spin mixing by substituting hydrogen atoms by fluorine atoms.

A long-lifetime erbium complex, $Er(FTPIP)_3$, was doped into the $Zn(F\text{-}BTZ)_2$ layer in the OLED structure ITO/HMTPD/$Zn(F\text{-}BTZ)_2$+$Er(FTPIP)_3$/Alq_3/LiF/Al at 20% molar percentage. Long-lifetime electroluminescence from erbium at the important telecommunication wavelength of 1.5 μm was observed.

Chapter 5 - Experimental part I: Synthesis and characterisation

5.1 General procedures

All the starting materials were used as bought without further purification. Solvents including DCM, diethyl ether, toluene, DMF, and THF are dried by a MBraun solvent purification system. Anhydrous methanol was produced by refluxing the solvent with Mg granules followed by distillation. Anhydrous DME was produced by refluxing the solvent with CaH_2 for 1 h followed by distillation. Anhydrous 1,4-dioxane was produced by refluxing the solvent with Na and benzophenone followed by distillation. All the acid chlorides, including compounds **3**, **8** and **12**, were prepared by refluxing the corresponding carboxylic acids in thionyl chloride followed by distillation. Flash chromatography was performed using Zeochem ZEOprep 60 silica gel (40–63 μm). NMR spectra were recorded with the Bruker AVIII 400 Spectrometer. IR spectra were obtained by attenuated total reflectance (ATR) on a Perkin Elmer Spectrum 65 FTIR spectrometer. Mass spectra were recorded by the EPSRC National Service Mass Spectrometry Service Centre at Swansea. Elemental analysis results were obtained by using the service from MEDAC Ltd (Surrey, GU24 8JB, UK).

X-ray quality crystals of zinc complexes were grown by vacuum sublimation in a sealed glass pipette (with a pressure below 10^{-6} mbar, temperature between 250 °C and 300 °C). The sublimation pipette was prepared according to the following procedure: the narrow tube end of the pipette was sealed by a blow-torch, and then a glass-fibre filter paper was pushed in to reside at the conical junction between the narrow tube and the wide tube. The sample to be sublimed was loaded into the wide tube and stopped from entering the narrow tube by the filter paper. The pipette was connected to a pump at the wide tube end. After the pipette was pumped down to a pressure below 10^{-6} mbar, its wide tube end was sealed by a blow-torch. During the sublimation, the wide tube part with the sample inside was seated in the tube-furnace, leaving the narrow tube part

exposed outside the furnace to condense the sublimated vapor to form crystal. Structures were solved and refined using the Bruker SHELXTL Software Package.

DFT Calculations were performed using the Spartan′10 software package, version 1.0.1, using the DFT RB3LYP method with the 6-31G(D) basis set. Geometry parameters were optimised by the calculation rather than using the crystallographic data.

The fitting of all the lifetime curves in this thesis has been done by using OriginPro 8 software and exponential functions. The fitting goodness was judged by the coefficient of determination (R^2). The higher value of R^2 ($R^2 \leq 1$), the better the fitting is. All the lifetime values given in the thesis were adopted when the fit was able to give a R^2 value above 0.9.

5.2 Preparation of *N*-(pentafluorophenyl)-3,4,5,6-tetrafluoro-2-methoxy-benzamide (4)

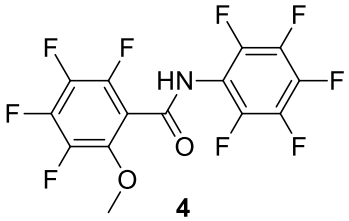

4

2-Methoxy-3,4,5,6-tetrafluorobenzoyl chloride (**3**) (2.79 g, 11.5 mmol) in dry DCM (70 mL) was added dropwise to a solution of pentafluoroaniline (4.39 g, 24 mmol) in dry DCM (35 mL) over 20 min under N_2. The mixture was stirred at room temperature under N_2 for 24 h, then the solvent was evaporated at reduced pressure. The resulting residue was recrystallised from $CHCl_3$–petrol to give amide **4** (3.48 g, 78%) as a white, fluffy solid, mp 114–115.5°C. ν_{max}/cm^{-1} 3225, 1686, 1488, 1320, 1239, 1150, 991, 641; δ_H (400 MHz, $CDCl_3$) 4.08 (3H, s, OMe), 7.78 (1H, br s, NH); δ_F (376 MHz, $CDCl_3$) –139.2 (1F, d, *J* 22 Hz), –144.2 (2F, d, *J* 22 Hz), –149.8 (1F, t, *J* 22 Hz), –154.7 (1F, dd, *J* 22, 11 Hz), –155.2 (2F, t, *J* 22 Hz), –160.4 (1F, t, *J* 22 Hz), –161.8 (1F, t, *J* 22 Hz); HRMS (CI) *m*/*z* found 390.0171; $C_{14}H_5F_9NO_2$ ($M+H^+$) requires 390.0169.

5.3 Preparation of 2-(3,4,5,6-tetrafluoro-2-methoxyphenyl)-4,5,6,7-tetrafluoro-benzothiazole (5)

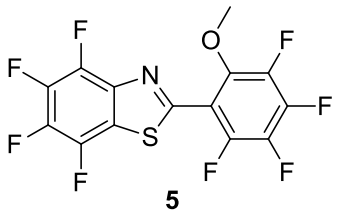

5

N-(Pentafluorophenyl)-3,4,5,6-tetrafluoro-2-methoxybenzamide (**4**) (3.03 g, 7.79 mmol) and P_2S_5 (865 mg, 3.89 mmol) were refluxed in dry dioxane (80 mL) under N_2 for 20 h. The solvent was evaporated and the residue was extracted with ether and washed with aqueous $NaHCO_3$. The organic phase was dried over Na_2SO_4, filtered and evaporated. The resulting pale yellow solid was subjected to flash chromatography (gradient from petroleum–DCM 6:1 to 4:1) to give **5** (2.14 g, 71%) as a white solid, mp 110–111 °C. ν_{max}/cm^{-1} 1637, 1490, 1467, 1346, 1088, 998, 885, 820, 747; δ_H (270 MHz, $CDCl_3$) 4.08 (s, OMe); δ_F (367 MHz, $CDCl_3$) –137.6 (1F, ddd, *J* 22, 9, 5 Hz), –139.3 (1F, dd, *J* 21, 16 Hz), –147.6 (1F, dd, *J* 19, 16 Hz), –150.8 (1F, td, *J* 21, 5 Hz), –156.3 (1F, dd, *J* 21, 9 Hz), –158.1 (1F, t, *J* 19 Hz), –158.4 (1F, t, *J* 19 Hz), –162.5 (1F, t, *J* 21 Hz); HRMS (EI) *m*/*z* found 384.9801; $C_{14}H_5F_9NO_2$ (M^+) requires 384.9802.

5.4 Preparation of 2-(3,4,5,6-tetrafluoro-2-hydroxyphenyl)-4,5,6,7-tetrafluoro-benzothiazole (6)

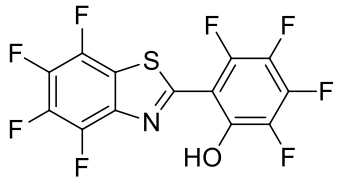

6

BBr_3 (4.0 mL, 42 mmol) was added to a solution of 2-(3,4,5,6-tetrafluoro-2-methoxyphenyl)-4,5,6,7-tetrafluorobenzothiazole (**5**) (1.00 g, 2.60 mmol) in dry DCM (16 mL) under N_2. The mixture was stirred at room temperature for 2 h and then poured onto ice (150 g). The resulting suspension was extracted with DCM twice and ether once. The combined organic phases were dried over Na_2SO_4 and evaporated to leave **6** as a yellowish-white solid (960 mg, 99%), mp 158–159 °C. ν_{max}/cm^{-1} 1668, 1542, 1489, 1437, 1406, 1353, 1270, 1144, 1100, 1050, 988, 750; δ_H (270 MHz, $CDCl_3$) 8.01 (br, OH); δ_F (367 MHz, $CDCl_3$) –138.8 (1F, dd, *J* 20, 15 Hz), –139.4 (1F, td, *J* 15, 8 Hz), –147.8 (1F, t, *J* 17 Hz), –149.2 (1F, td, *J* 15, 6 Hz), –156.0 (1F, t, *J* 20 Hz), –156.3 (1F, t, *J* 20 Hz), –161.4 (1F, ddd, *J* 20, 9, 4 Hz), –170.3 (1F, td, *J* 19, 4 Hz); HRMS (EI) *m*/*z* found 370.9650; $C_{14}HF_8NOS$ (M^+) requires 370.9646.

5.5 Preparation of *N*-(pentafluophenyl)-2-methoxybenzamide (9)

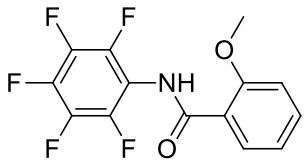

9

A solution of 2-methoxybenzoyl chloride (**8**) (0.85 g, 0.74 mL, 5.0 mmol) in dry DCM (12 mL) was added dropwise to a solution of pentafluoroaniline (1.83 g, 10.0 mmol) in dry DCM (12 mL). The mixture was stirred under N_2 at room temperature for 24 h, after which an additional portion of pentafluoroaniline (0.018 g, 0.1 mmol) was added to ensure complete consumption of the acyl chloride. After a further 5 h the solvent was evaporated and the resulting residue was recrystallized from chloroform to give *N*-pentafluorophenyl-2-methoxybenzamide (**9**) (1.53 g, 96%) as a white solid, mp 161.5–163 °C. ν_{max}/cm^{-1} (ATR) 3301 (NH), 1673 (C=O), 1655, 1602, 1519, 1458, 1290, 1231, 1186, 1096, 1048, 981, 759; δ_H (270 MHz, $CDCl_3$) 7.07 (1H, d, *J* 8.1 Hz), 7.14 (1H, td, *J* 8.1, 1.1 Hz), 7.55 (1H, ddd, *J* 8.1, 7.3, 1.9 Hz), 8.26 (1H, dd, *J* 7.8, 1.9 Hz), 9.38 (1H, s, NH); δ_F (376 MHz, $CDCl_3$) –145.5 (2F, m), –158.8 (1F, t, *J* 20 Hz), –163.9 (2F, m); HRMS (ESI) *m/z* found 318.0551; $C_{14}H_9F_5NO_2$ ($M+H^+$) requires 318.0548.

5.6 Preparation of 4,5,6,7-tetrafluoro-2-(2-methoxyphenyl)benzothiazole (10)

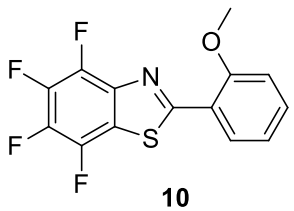

10

P_2S_5 (0.27 g, 1.2 mmol) and *N*-(pentafluorophenyl)-2-methoxybenzamide (**9**) (1.20 g, 3.80 mmol) were refluxed under N_2 in dry dioxane (10 mL) for 24 h. The solvent was evaporated and the residue was dissolved in chloroform and washed with aqueous $NaHCO_3$. The organic extract was dried ($MgSO_4$) and evaporated, leaving **10** (1.19 g, 100%) as a pale orange solid, mp 204–206 °C. ν_{max}/cm^{-1} (ATR) 2843, 1598, 1583, 1484, 1454, 1440, 1351, 1287, 1256, 1231, 1163; δ_H (270 MHz, $CDCl_3$) 4.11 (3H, s, OMe), 6.98–7.15 (2H, m), 7.36–7.50 (1H, m), 8.42 (1 H, dd, *J* 7.9, 1.5 Hz); δ_F (377 MHz, $CDCl_3$) –140.7 (1F, dd, *J* 20.5, 15.4 Hz), –150.1 (1F, dd, *J* 19.0, 15.6 Hz), –160.2 (1F, t, *J* 19.3 Hz), –161.0 (1F, t, *J* 20.1 Hz); HRMS (ESI) *m/z* found 314.0260; $C_{14}H_8F_4NOS$ ($M+H^+$) requires 314.0257.

5.7 Preparation of 4,5,6,7-tetrafluoro-2-(2-hydroxyphenyl)benzothiazole (11)

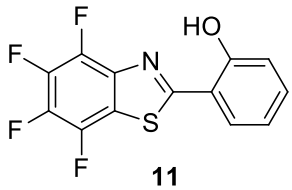

11

BBr_3 (3.0 mL, 32 mmol) was added to a solution of 4,5,6,7-tetrafluoro-2-(2-methoxyphenyl)benzothiazole (**10**) (1.00 g, 3.19 mmol) in dry DCM (16 mL). The mixture was stirred under N_2 at room temperature for 3 h and then poured onto ice. The resulting suspension was extracted with chloroform, which was dried (Na_2SO_4), then concentrated under vacuum to give **11** as a white solid (960 mg, 100%), mp 181–183 °C. Found: C, 52.26; H, 1.48; N, 4.51. $C_{13}H_5F_4NOS$ requires: C, 52.18; H, 1.68; N, 4.68. UV (MeCN) λ_{max} 288 (ε 18400), 335 (16800); ν_{max}/cm^{-1} (ATR) 2950 (OH), 1550, 1490, 1230, 1020; δ_H (270 MHz, $CDCl_3$) 7.00 (1H, dt, *J* 8.1, 1.4 Hz), 7.13 (1H, dd, *J* 8.1, 1.0 Hz), 7.46 (1H, dt, *J* 8.1, 1.4 Hz), 7.64 (1H, dd, *J* 8.1, 1.4 Hz), 11.62 (1H, s, OH); δ_F (376 MHz, $CDCl_3$) –139.2 (1F, dd, *J* 23, 15 Hz), –148.6 (1F, dd, *J* 21, 15 Hz), –157.8 (1F, t, *J* 21 Hz), –158.9 (1F, t, *J* 21 Hz); HRMS (APCI) *m/z* found 300.0101; $C_{13}H_6F_4NOS$ ($M+H^+$) requires 300.0101.

5.8 Preparation of 3-ethoxycarbonyl-2-methyl-5,6,7,8-tetrafluoro-4*H*-1,4-dihydrobenzopyran-4-one (13)

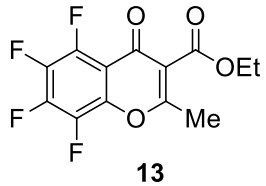

13

A mixture of Mg (0.782 g, 32.7 mmol), ethyl acetoacetate (4.24 g, 32.7 mmol) and dry toluene (12.0 mL) was refluxed under N_2 for an hour. Then pentafluorobenzoyl chloride (**12**) (7.52 g, 32.6 mmol) was added to the mixture and refluxed overnight. After cooling down, the mixture was extracted with ether and 2M HCl. The organic layer was separated and dried over Na_2SO_4. The solvent was evaporated to give a brown oily residue, which was subjected to flash chromatography (DCM–petrol 9:1) and then recrystallised from hexane to give **13** as a white solid (1.24 g, 12.5%), mp 90-92 °C (lit.[59] 91-92 °C).

5.9 Preparation of 2-(2-hydroxy-3,4,5,6-tetrafluorophenyl)benzothiazole (15)

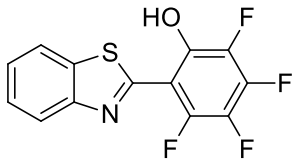

15

Method A: A mixture of 2-aminothiophenol (**14**) (1.35 g, 10.8 mmol) and 3-ethoxycarbonyl-2-methyl-5,6,7,8-tetrafluoro-4*H*-1,4-dihydrobenzopyran-4-one (**13**) (0.820 g, 2.70 mmol) in dry toluene (32 mL) was refluxed under N_2 overnight. After cooling, the yellow precipitate was filtered off and recrystallized from toluene to yield a bright yellow solid (0.115 g), which was indicated to be a mixture by ^{1}H NMR. Flash chromatography (petrol–DCM, 4:1) gave the title product **15** as a pale yellow solid (48 mg, 6%), mp 226–228 °C (lit.[59] 193–195 °C). Found: C, 52.09; H, 1.68; N, 4.56. $C_{13}H_5F_4NOS$ requires: C, 52.18; H, 1.68; N, 4.68. ν_{max}/cm^{-1} (ATR) 1644 (br), 1500, 1418, 986, 761. UV (MeCN) λ_{max} 292 (ε 18500), 325 (16700); δ_H (400 MHz, DMSO-d_6) 7.60 (1H, t, *J* 7.5 Hz), 7.67 (1H, t, *J* 7.5 Hz), 8.24 (1H, d, *J* 7.5 Hz), 8.29 (1H, d, *J* 7.5Hz), 13.51 (1H, s, OH); δ_F (376 MHz, DMSO-d_6) –139.9 (1F, m), –140.0 (1F, m), –152.9 (1F, m), –162.3 (1F, m); HRMS (APCI) *m*/*z* found: 300.0095; $C_{13}H_6F_4NOS$ ($M+H^+$) requires 300.0101.

Method B: 2-Methoxy-3,4,5,6-tetrafluorobenzoyl chloride (**3**) (0.50 g, 2.0 mmol) was added dropwise to a solution of 2-aminothiophenol (**14**) (0.26 g, 2.0 mmol) in dry *N*-methyl-2-pyrrolidone (2.0 mL). The mixture was stirred at 100 °C under N_2 for 24 h and then poured into water. The precipitate was filtered off and washed with water. After drying, it was recrystallised from chloroform, and subjected to chromatography on silica gel in a sintered funnel ($CHCl_3$/hexane 2:3, preheated before using). The early fraction was collected and evaporated to give the title product as a flaky, lemon-yellow solid (250 mg, 54%), with mp, IR, ^{1}H NMR and ^{19}F NMR data in agreement with those for **15** prepared by *Method A* above.

5.10 Preparation of 2-(2-Benzothiazol-2-yl-1-hydroxyvinyl)-3,4,5,6-tetrafluorophenol (16)

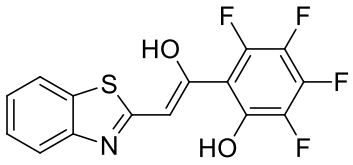

16

A mixture of 2-aminothiophenol (1.00 g, 8.02 mmol) and 3-ethoxycarbonyl-2-methyl-5,6,7,8-tetrafluoro-4*H*-1,4-dihydrobenzopyran-4-one (**13**) (1.22 g, 4.01 mmol) in dry toluene (32 mL) was refluxed under N_2 overnight. After cooling, the precipitate was filtered off and repeatedly recrystallised from toluene. 2-(2-Benzothiazol-2-yl-1-hydroxyvinyl)-3,4,5,6-tetrafluorophenol (**16**) (54 mg, 4%) was obtained as a bright yellow solid, mp>200 °C (decomp). ν_{max}/cm^{-1} (ATR) 3157, 1658, 1521, 1432, 1204, 1146, 987, 926, 749, 720, 686; δ_H (400 MHz, DMSO-d_6) 6.75 (1H, s), 7.34 (1H, t, *J* 8 Hz), 7.44–7.60 (2H, m), 7.96 (1H, d, *J* 8 Hz), 13.59 (1H, br, OH), 15.63 (1H, br, OH); δ_F (376 MHz, DMSO-d_6) –139.7 (1F, m), –154.0 (1F, m), –165.2 (1F, m), –173.2 (1F, m); HRMS (APCI) *m/z* found: 342.0203; $C_{15}H_8F_4NO_2S$ ($M+H^+$) requires 342.0206.

5.11 Preparation of pentafluorophenyl isothiocyanate (22)

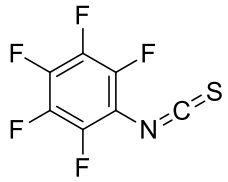

22

A solution of thiophosgene (6.5 g, 56 mmol) in dry toluene (30 mL) was added dropwise over 15 min to a mixture of pentafluoroaniline (7.05 g, 38 mmol), dry toluene (50 mL) and dry DMF (2.0 mL). The mixture was heated at 90 °C for 4 h. Then the mixture was cooled down and the upper orange layer was collected via a cannula under nitrogen. The majority of the solvent was distilled off and the rest solution was fractionally distilled under reduced pressure to give pentafluorophenyl isothiocyanate (5.03 g, 59%) as a colourless liquid, bp 60 °C/~3 mmHg (lit.[102] bp 68 °C/4.5 mmHg); ν_{max}/cm^{-1}(ATR) 2008, 1633, 1517, 1468, 1359, 1184, 1024, 992, 773; δ_F (376 MHz, $CDCl_3$) –146.9 (2F, d, *J* 16 Hz, F–2,6), –157.3 (1F, t, *J* 22 Hz, F–4), –162.7 (2F, t, *J* 20 Hz, F–3,5).

5.12 Preparation of *N*-(2,3,4,5,6-pentafluorophenyl)thiourea (23)

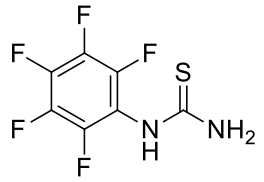

23

A mixture of pentafluorophenyl isothiocyanate (**22**) (4.40 g, 19.6 mmol) and conc. aqueous ammonia (7.82 mL, 118 mmol) was stirred in air at room temperature for 2 h. The water was evaporated off and the resulting solid was dried and recrystallised from toluene to give *N*-(2,3,4,5,6-pentafluorophenyl)thiourea (3.30 g, 69%) as a white solid, mp 153.5–154.8 °C (lit.[61] 154.8–155.2 °C). ν_{max}/cm^{-1}(ATR) 3353, 1625, 1535, 1510, 1400, 1003, 733; δ_F (376 MHz, DMSO-*d*6) –141.8 (2F, d, *J* 22 Hz, F–2,6), –153.7 (1F, t, *J* 24 Hz, F–4), –160.3 (2F, t, *J* 22 Hz, F–3,5).

5.13 Preparation of 2-amino-4,5,6,7-tetrafluorobenzothiazole (24)

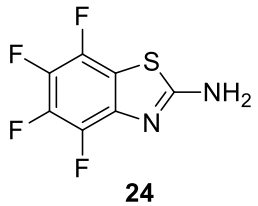

24

A solution of *N*-(2,3,4,5,6-pentafluorophenyl)thiourea (**23**) (1.78 g, 7.35 mmol) in dry toluene (11 mL) was refluxed for 4 h. Then the pale brown solution was allowed to cool down and the solvent was evaporated off under reduced pressure. The resulting solid was partitioned between brine and ether. The organic extract was dried over Na_2SO_4, filtered and evaporated. The resulting brown residue was recrystallised from toluene to give 2-amino-4,5,6,7-tetrafluorobenzothiazole (0.845 g, 52%) as a white solid, mp 198.5–202 °C (lit.[61] 202–203 °C). ν_{max}/cm^{-1}(ATR) 3493, 3090, 1635, 1553, 1478, 1321, 994, 874; δ_F (376 MHz, DMSO-d_6) –137.1 (1F, dd, *J* 24, 13 Hz, F–4), –150.8 (1F, dd, *J* 21, 13 Hz, F–7), –158.1 (1F, t, *J* 20 Hz, F–5), –164.3 (1F, t, *J* 20 Hz, F–6).

5.14 Attempted preparation of bis(perfluorobenzothiazol-2-yl)amine (18) in toluene

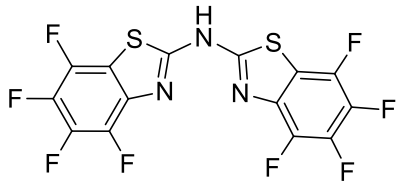

18

Pentafluorophenyl isothiocyanate (**22**) (0.20 g, 0.90 mmol) was added to a solution of 2-amino-4,5,6,7-tetrafluorobenzothiazole (**24**) (0.20 g, 0.90 mmol) in hot dry toluene (2.0 mL), the mixture was refluxed under N_2 overnight. A yellow precipitate was formed and collected by filtration, and then recrystallised from ethyl acetate and hexane to give a white solid (0.0741 g, 16.9%), mp 266–269 °C. δ_F (376 MHz, DMSO-d_6) –138.1 (2F, s, F–4), –149.1 (2F, s, F–7), 157.4 (2F, s, F–5), 160.6 (2F, s, F–6). On this basis it was judged to be identical to material that had been prepared by Ahmed Dellali using a similar procedure and which had been found by high resolution mass spectrometry to have the molecular formula $C_{15}H_2F_8N_4S_3$ (Ahmed Dellali, Msc Dissertation, Queen Mary, University of London, 2009). This solid was hydrolysed in a refluxing mixture of concentrated hydrochloric acid (37%, 1.5 mL) and trifluoroacetic acid (12 mL) for 3 h. Then the solvent was evaporated and the resulting solid was neutralised with excess amount of $NaHCO_3$ solution and extracted with EtOAc. The organic phase was dried over sodium sulfate, and concentrated to give a pale yellow solid. TLC (EtOAc) of this solid against compound **24** showed the same red fluorescence and R_f value, and IR spectrum was similar to that of **24**: ν_{max}/cm^{-1}(ATR) 3495, 3097, 1636, 1555, 1477, 1322, 996, 869.

5.15 Attempted preparation of bis(perfluorobenzothiazol-2-yl)amine (18) in DMF

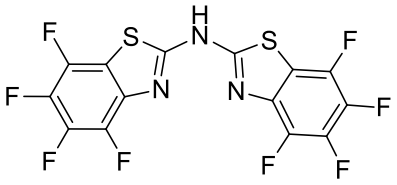

18 expected

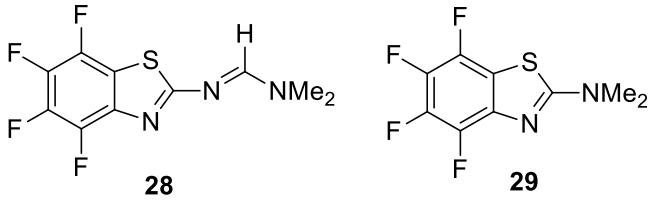

28 **29**

obtained products

Pentafluorophenyl isothiocyanate (**22**) (0.14 mL, 0.99 mmol) was added to a solution of 2-amino-4,5,6,7-tetrafluorobenzothiazole (**24**) (0.22 g, 0.99 mmol) in dry DMF (2 mL). The mixture was refluxed under N_2 for 113 hours, and the solvent was evaporated under reduced pressure. Diethyl ether was added to the residue and the suspension was filtered to remove insoluble dark brown solid. The filtrate was subjected to flash chromatography (ether/petroleum, gradient from 1:9 to 7:3) to obtain *N*,*N*-Dimethyl-*N*'-(4,5,6,7- tetrafluorobenzothiazol-2-yl)formamidine (**28**) (68 mg, 25%) as a white solid (last fractions), mp 128–130 °C. ν_{max}/cm^{-1}(ATR) 2935, 1717, 1618, 1459, 1329, 1194, 1082, 1001, 871, 784; δ_H (270 MHz, $CDCl_3$) 3.16 (3H, d, *J* 0.5 Hz, –Me), 3.20 (3H, s, –Me), 8.48 (1H, s, N=CH); δ_F (376 MHz, $CDCl_3$) –141.4 (1F, dd, *J* 21, 14 Hz, F–4), –152.7 (1F, dd, *J* 20, 14 Hz, F–7), –161.7 (1F, t, *J* 20 Hz, F–5), –165.4 (1F, t, *J* 21 Hz, F–6); HRMS (CI) *m/z* found: 278.0370, $C_{10}H_8F_4N_3S$ ($[M+H]^+$) requires 278.0370.

2-Dimethylamino-4,5,6,7-tetrafluorobenzothiazole (**29**) (7.3 mg, 3%) was also isolated as a minor component which eluted the column before **28** from, mp 79–83 °C. δ_H(270 MHz, $CDCl_3$) 3.24 (s); δ_F (376 MHz, $CDCl_3$) –141.5 (1F, dd, *J* 21, 13 Hz, F–4), –154.3 (1F, ddd, *J* 20, 13, 3 Hz, F–7), –161.2 (1F, t, *J* 20 Hz, F–5), –168.0 (1F, td, *J* 21, 3 Hz, F–6); HRMS (CI) *m/z* found: 251.0263, $C_9H_7F_4N_2S$ ($[M+H]^+$) requires 251.0266.

5.16 Preparation of bis(4,5,6,7-tetrafluorobenzothiazol-2-yl)amine (18)

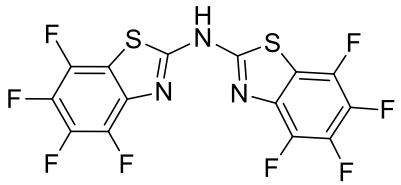

18

2-Amino-4,5,6,7-tetrafluorobenzothiazole (**24**) (262 mg, 1.18 mmol) was heated to 290 °C under N_2 for 3 h. After cooling down, the resulting dark solid was dissolved in a mixture of EtOAc/$CHCl_3$ (1:6) and immediately subjected to flash chromatography (EtOAc/$CHCl_3$ 1:8). The early fractions that showed purple fluorescence under UV were collected and concentrated to give a pale yellow solid (123 mg, 49%), mp 301.5–303.5°C. ν_{max}/cm^{-1}(ATR) 3247, 1650, 1547, 1482, 1277, 1088, 1000, 877, 798; δ_F(376 MHz, DMSO-d_6) –136.47 (2F, dd, *J* 23, 14 Hz, F–4,4'), –148.06 (2F, dd, *J* 20, 14 Hz, F–7,7'), –156.00 (2F, t, *J* 20 Hz, F–5,5'), –159.55 (2F, t, *J* 20 Hz, F–6,6'). HRMS (APCI) *m/z* found: 427.9557, $C_{14}H_2F_8N_3S_2$ ($[M+H]^+$) requires 427.9546.

5.17 Preparation of *N*-(benzothiazol-2-yl)-*N*'-phenylthiourea (32)

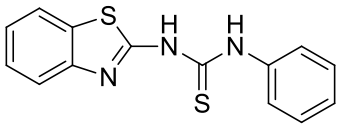

32

A solution of phenyl isothiocyanate (**31**) (3.6 mL, 30 mmol) in dry toluene (20 mL) was added to a solution of 2-aminobenzothiazole (**30**) (4.5 g, 30 mmol) in dry toluene (20 mL). The mixture was refluxed under N_2 for 24 h then allowed to cool down. The precipitate was filtered off, then washed with toluene followed petrol to give the product (**32**) as a yellow solid (4.5 g, 53%), mp 199-202 °C (lit.[103] 201–203 °C).

5.18 Preparation of bis(benzothiazolyl)amine (19) following literature[62]

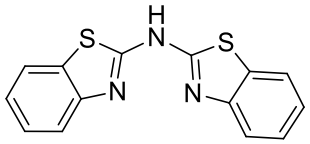

19

To a well stirred suspension of *N*-(benzothiazol-2-yl)-*N*'-phenylthiourea (**32**) (1.4 g, 5.0 mmol) in 98% H_2SO_4 (10 mL) in an ice bath, NBS (0.89 g, 5.0 mmol) in 98% H_2SO_4 (10 mL) was slowly added. The mixture was stirred in air for 10 min and then poured onto ice. The result suspension was neutralised with conc. ammonia. Then the precipitate was filtered, washed with water and dried to give a yellowish solid (0.99 g). A portion (0.50 g) of this crude product was subjected to recrystallisation in EtOH, and a pale yellow solid (0.27 g, 54%) was obtained as the title product (**19**), mp 247-249 °C (lit.[62] 256–258 °C).

5.19 Preparation of 2-iodobenzothiazole (34)

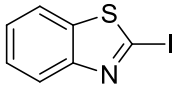

34

To a solution of *p*-TsOH (1.719 g, 9 mmol) in undried MeCN was added 2-aminobenzothiazole (0.451 g, 3.0 mmol). The resulting suspension of amine salt was cooled to 10–15 °C and to this suspension was gradually added a solution of $NaNO_2$ (0.414 g, 6.0 mmol) and KI (1.245 g, 7.5 mmol) in H_2O (1.8 mL). The reaction mixture was stirred for 10 min and then allowed to warm up to 20 °C and stirred for another 4 h in air. Then to the reaction mixture was added H_2O (50 mL), 1M $NaHCO_3$ (to pH 9–10) and 2M $Na_2S_2O_3$ (6 mL). The dark brown suspension was extracted with ether and purified by flash chromatography (first petrol–ether 97:3 and then petrol–ether 90:10) to give 2-iodobenzothiazole (175 mg, 22%) as a white solid, mp 76–78 °C (lit.[63] 79–80 °C).

5.20 Attempted preparation of bis(benzothiazol-2-yl)amine (19) by copper(I) catalysed coupling of 30 and 34 (*attempt I*)

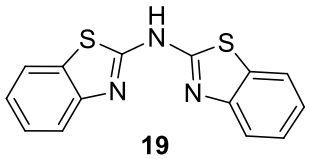

19

A suspension of K_2CO_3 (69 mg, 0.25 mmol), CuI (4.8 mg, 0.025 mmol) and proline (5.8 mg, 0.05 mmol) in dry DMSO (0.2 mL) was added to a mixture of 2-iodobenzothiazole (**34**) (65 mg, 0.25 mmol) and 2-aminobenzothiazole (**30**) (37.5 mg, 0.25 mmol). The reaction mixture was stirred at 80 °C under N_2. After 24 h the mixture was cooled to room temperature and quenched with excess dilute HCl, filtered and washed with H_2O. The precipitate was dissolved in boiling ethanol and the insoluble residue was filtered off. The filtrate was evaporated under reduced pressure and recrystallisation of the residue from ethanol was attempted. A very small amount of precipitate was obtained (3 mg). TLC (EtOAc/petrol 1:1) was used to compare the recrystallised product with starting materials and the authentic product **19** previously obtained via cyclisation of *N*-(benzothiazol-2-yl)-*N*'-phenylthiourea (**32**) with NBS. This TLC showed that the obtained product was a mixture of two components neither of which was starting material or the wanted product **19**.

5.21 Attempted preparation of bis(benzothiazol-2-yl)amine (19) by copper(I) catalysed coupling of 30 and 34 (*attempt II*)

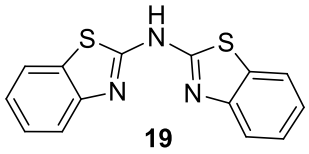

19

A suspension of CuI (7.6 mg, 0.040 mmol) and 2,2'-bipyridyl (6.2 mg, 0.040 mmol) in 5.5 ml dry toluene was added to a mixture of 2-iodobenzothiazole (**34**) (260 mg, 1.0 mmol) and 2-aminobenzothiazole (**30**) (150 mg, 1.0 mmol). Potassium *tert*-butoxide (224 mg, 2.0 mmol) was then added. The reaction mixture was refluxed under N_2 for 3.5 h and then allowed to cool to room temperature. The mixture was treated with excess 2M HCl and filtered to obtain a brown solid. Attempts were made to recrystallise the brown solid but only some very fine brown powder was obtained. TLC (EtOAc/DCM 1:1) was used to compare the recrystallisation mother liquor with starting materials and authentic product **19**. It showed that the obtained product was a mixture of four components which included small amounts of both starting materials and two other red spots, but none of these showed the same purple fluorescence and R_f value as the product **19** obtained through the cyclisation of *N*-(benzothiazol-2-yl)-*N*'-phenylthiourea (**32**) with NBS.

5.22 Preparation of 2-bromobenzothiazole (35)

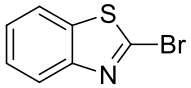

35

A hot solution of 2-aminobenzothiazole (0.975 g, 6.5 mmol) in glacial acetic acid (25 mL) was quickly cooled to 0 °C and added to sodium nitrite (0.5 g, 7.2 mmol) in ice-cold sulphuric acid (4 mL).

Copper(I) bromide was freshly prepared by mixing a solution of anhydrous copper(II) sulfate (1.2 g, 7.5 mmol) and potassium bromide (1.04 g, 8.7 mmol) in water (6 mL) with one of sodium metabisulphite (0.41 g, 2.2 mmol) and sodium hydroxide (0.27 g, 6.75 mmol) in water (3 mL). To this mixture was added the diazonium solution, followed immediately by 48% aqueous hydrobromic acid (0.5 mL).

After stirring under N_2 for 16 h the mixture was filtered. The filtrate was neutralised with saturated sodium hydrocarbonate solution, and extracted with DCM. The organic phase was dried over anhydrous sodium sulfate, filtered and evaporated. A dark brown oily crude product was obtained and subjected to flash chromatography (petrol–ethyl acetate 37:1) to give 2-bromobenzothiazole (**35**) (260 mg, 19%) as a brown oily liquid. δ_H (400 MHz, $CDCl_3$) 7.34 (1H, t, *J* 7.5 Hz, H–5) , 7.40 (1H, t, *J* 7.5 Hz, H–6) , 7.73 (1H, d, *J* 7.5 Hz, H–7), 7.92 (1H, d, *J* 7.5 Hz, H–4). This compound is known.[104]

5.23 Attempted preparation of bis(benzothiazol-2-yl)amine (19) by palladium catalysed coupling of 30 and 35

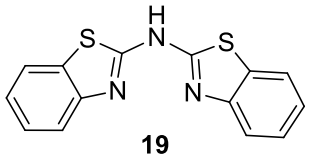

19

A mixture of 2-bromobenzothiazole (**35**) (0.107 g, 0.500 mmol), $Pd(OAc)_2$ (0.011 g, 0.05 mmol), 2,2'-bis(diphenylphosphino)-1,1'-binaphthyl (BINAP) (0.094 g, 0.15 mmol) and sodium *tert*-butoxide (0.144 g, 1.5 mmol) in dry toluene (3.3 mL) was stirred under N_2 for 5 min at room temperature. 2-Aminobenzothiazole (**30**) (0.075 g, 0.500 mmol) was added and the mixture was refluxed under N_2 for 2 h. Then the mixture was concentrated and acidified with 1M HCl (15 mL). The precipitate was filtered off and washed with water. An attempt to recrystallise it from EtOH did not yield any solid. TLC of the solution did not show the purple fluorescent spot that corresponds to the authentic product **19** obtained previously through the cyclisation of *N*-(benzothiazol-2-yl)-*N*'-phenylthiourea (**32**) with NBS.

5.24 Preparation of bis(benzothiazol-2-yl)amine (19)

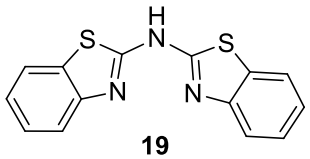

19

2-Aminobenzothiazole (0.3 g, 2 mmol) was heated to 270 °C under N_2 for 1h. After cooling down a brown solid was obtained, which was recrystallised from EtOH in the presence of charcoal to obtain bis(benzothiazol-2-yl)amine (**19**) as a white solid (0.123 g, 43%), mp 254–256.5 °C (lit.[62] 256–258 °C); ν_{max}/cm^{-1}(ATR) 2778 (br), 1606, 1546, 1490, 1437, 1278, 1173, 926, 748; δ_H (400 MHz, DMSO-d_6) 7.27 (2H, t, *J* 7.5 Hz, H–5,5') , 7.43 (2H, t, *J* 7.5 Hz, H–6,6') , 7.65 (2H, br, H–7,7') , 7.94 (2H, d, *J* 7.5 Hz, H–4,4'), 12.84 (1H, s, NH); δ_C (400 MHz, DMSO-d_6) 117.9 (2C, br), 121.9 (2C, s), 122.9 (2C, s), 126.3 (2C, s), 127.0 (2C, s), 130.2 (2C, br), 162.7 (2C, br).

5.25 Preparation of *N*-phenyl-*N*'-tetrafluorobenzothiazol-2-yl-thiourea (36)

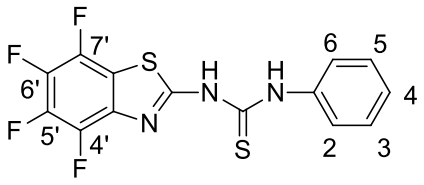

36

Phenyl isothiocyanate (**31**) (0.135 mL, 1.13 mmol) was added to a solution of 2-amino-4,5,6,7-tetrafluorobenzothiazole (**24**) (250 mg, 1.13 mmol) in dry toluene (1.5 mL). The mixture was refluxed for 72 h under N_2 and the precipitate was collected by filtration, washed with toluene and petrol, and recrystallised from acetonitrile to give *N*-phenyl-*N*'-(4,5,6,7-tetrafluorobenzothiazol-2-yl)thiourea (**36**) (210 mg, 52%) as a white solid, mp 232.5–233.5 °C. ν_{max}/cm^{-1}(ATR) 3149, 2981, 1541, 1484, 1360, 1256, 1214, 1168, 1097, 1007, 880; δ_H (270 MHz, DMSO-d_6) 7.25 (1H, t, *J* 8.1 Hz, H–4), 7.42 (2H, t, *J* 8.1 Hz, H–2,6), 7.58 (2H, d, *J* 8.1 Hz, H–3,5), 10.42 (1H, s, NH) 12.70 (1H, s, NH); δ_F (376 MHz, DMSO-d_6) –137.9 (1F, s, F–4'), –149.2(1F, s, F–7'), –156.3(1F, s, F–5'), –159.1(1F, s, F–6'); HRMS (APCI) *m/z* found: 358.0094, $C_{14}H_8F_4N_3S_2$ ($[M+H]^+$) requires 358.0090.

5.26 Preparation of benzothiazol-2-yl-(tetrafluorobenzothiazol-2-yl)amine (20) by cyclisation with NBS

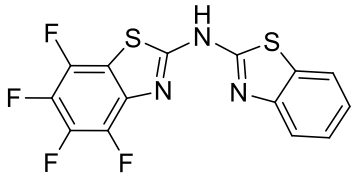

20

To a well stirred solution of *N*-phenyl-*N*'-(4,5,6,7-tetrafluorobenzothiazol-2-yl)thiourea (**36**) (190 mg, 0.532 mmol) in concentrated H_2SO_4 (1.5 mL) in an ice bath, NBS (95 mg, 0.53 mmol) in concentrated H_2SO_4 (1.5 mL) was slowly added. The mixture was stirred for 15 min in air and then poured into ice-cooled water (30 mL). The mixture was neutralised with concentrated ammonia and the precipitate was filtered off and washed with water. The wet solid was dried by adding methanol and evaporating off the solvent repeatedly. The dry solid was recrystallised from ethanol to give (benzothiazol-2-yl)-(4,5,6,7-tetrafluorobenzothiazol-2-yl)amine (**20**) (41.7 mg, 22.1%), mp 286–289 °C. ν_{max}/cm^{-1}(ATR) 3077, 2920, 1579, 1479, 1189, 1084, 998, 876, 749; δ_H(400 MHz, DMSO-d_6, 353 K) 7.40 (1H, t, *J* 7.5 Hz, H‑5) , 7.56 (1H, t, *J* 6.6 Hz, H‑6), 7.67 (1H, d, *J* 6.6 Hz, H–7), 7.93 (1H, d, *J* 7.5 Hz, H–4), 13.32 (1H, s, NH); δ_F (376 MHz, DMSO–d_6) –136.6 (1F, s, F–4'), –148.2 (1F, m, F–7'), –156.6 (1F, m, F–6'), –160.5 (1F, m, F–5'); MS (EI) *m/z* found 354.9, $C_{14}H_5F_4N_3S_2$ ($[M]^+$) requires 355.0. There was a pair of peaks with equal intensity observed at *m/z* 432.9 and 434.9 in the mass spectrum, indicating the existence of brominated by-product.

5.27 Attempted preparation of *N*-(2-iodophenyl)-*N*'-(4,5,6,7-fluorobenzothiazol- 2-yl)thiourea (39)

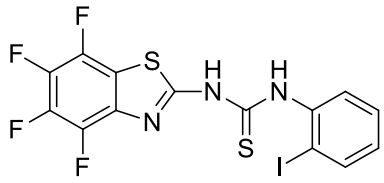

39

To a solution of 2-aminotetrafluorobenzothiazole (**24**) (55 mg, 0.25 mmol) and triethylamine (TEA) (0.25 mmol) in a mixture of dry DCM (3 mL) and dry ether (1.5 mL) was added 2-iodophenyl isothiocyanate (65 mg, 0.25 mmol). The mixture was stirred under N_2 for 24 h at room temperature. No reaction occurred as indicated by TLC and IR. Then the solvent was replaced with toluene and the mixture was refluxed for 96 h. But the starting materials still remained largely unreacted.

5.28 Attempted preparation of 1-(benzothiazol-2-yl)-3-(perfluorophenyl)-thiourea (40) using nonfluorinated amine as nucleophile

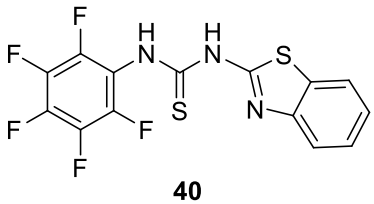

40

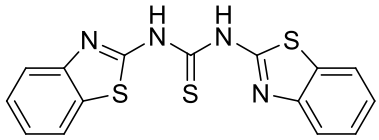

41

Pentafluorophenyl isothiocyanate (**22**) (0.10 mL, 160 mg, 0.71 mmol) was added to a solution of 2-aminobenzothiazole (**30**) (106 mg, 0.708 mmol) in dry toluene (5.0 mL). The mixture was refluxed under N_2 overnight and the precipitate was filtered and washed with toluene to give 1,3-bis(benzothiazol-2-yl)thiourea (**41**) (95.8 mg, 40%) as a yellow solid, mp 244.5–246 °C. ν_{max}/cm^{-1}(ATR) 3232, 3062, 2745, 1593, 1531, 1459, 1407, 1329, 1300, 1259, 891; δ_H (400 MHz, DMSO-d_6) 7.35 (2H, br, H–6,6'), 7.49 (2H, br, H–5,5'), 7.68 (2H, br, H–7,7'), 7.95 (2H, d, *J* 7.6 Hz, H–4,4'), 12.44 (1H, br, NH), 13.69 (1H, br, NH). HRMS (APCI) *m/z* found: 343.0134, $C_{15}H_{11}N_4S_3$ ($[M+H]^+$) requires 343.0140.

5.29 Preparation of 2-(isothiocyanato)benzothiazole (42)

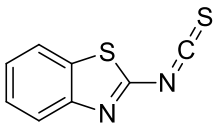

42

A solution of thiophosgene (0.61 mL, 8.0 mmol) in dry toluene (10 mL) was added dropwise to a hot solution of 2-aminobenzothiazole (**30**) (3.00 g, 20 mmol) in dry toluene (30 mL), and the mixture was stirred under N_2 for 2 h at 90 °C. After cooling, the suspension was filtered through celite. The filtrate was concentrated under vacuum and subjected to flash chromatography (DCM/petroleum 3:5) to give the title compound **42** as a yellow liquid (0.29 g, 23%). ν_{max}/cm^{-1}(ATR) 1995 (N=C=S), 1577, 1469, 1440, 1265, 938, 734. δ_H (400 MHz, $CDCl_3$) 7.33-7.45 (3H, m, H–5,6,7) 7.66 (1H, dd, *J* 7.8, 1.2 Hz, H–4). HRMS (APCI) *m/z* found: 192.9891, $C_{15}H_{11}N_4S_3$ ($[M+H]^+$) requires: 192.9889).

5.30 Preparation of *N*-(benzothiazol-2-yl)-*N*'-(pentafluorophenyl)thiourea (40) from 42 and pentafluoroaniline

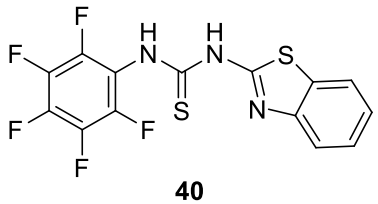

40

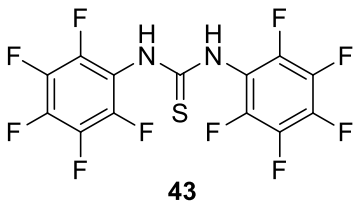

43

2-(Isothiocyanato)benzothiazole (**42**) (0.12 g, 0.62 mmol) was added to a solution of pentafluoroaniline (0.38 g, 2.077 mmol) in dry toluene (0.5 mL). The mixture was stirred under N_2 for 5 days at room temperature. Then the precipitate was filtered off, washed with toluene, and recrystallised from chloroform/petrol to give the title product **40** as a white, fluffy solid (4 mg, 2%), mp>230 °C; ν_{max}/cm^{-1}(ATR) 3307, 3158, 2996, 1660, 1574, 1498, 1312, 1221, 1144, 979, 735; δ_H (400 MHz, $CDCl_3$) 7.35 (1H, t, *J* 8 Hz, H–6), 7.47 (1H, t, *J* 8 Hz, H–5), 7.72 (1H, br, H–7), 7.75 (1H, d, *J* 8 Hz, H–4), 10.21 (1H, s, NH), 12.47 (1H, s, NH); δ_F (376 MHz, $CDCl_3$) –143.3 (m), –152.5 (m), –160.6 (m).

The filtrate was concentrated and subjected to flash chromatography (DCM/petrol 10:7) to give *N*,*N*'-bis(pentafluorophenyl)thiourea **43** as a white powder (50 mg, 20%), mp 206–208 °C; ν_{max}/cm^{-1}(ATR) 3307, 1720, 1660, 1495, 1310, 1248, 1144, 976, 736, 690; δ_H (400 MHz, $CDCl_3$) 7.13 (s, NH); δ_F (376 MHz, $CDCl_3$) –143.4 (t, *J* 16 Hz, F–4), –152.6 (m, F–2,6), –160.7 (m, F–3,5); HRMS (APCI) *m/z* found: 408.9843, $C_{13}H_3F_{10}N_2S$ ($[M+H]^+$) requires 408.9852.

5.31 Preparation of (benzothiazol-2-yl)-(4,5,6,7-tetrafluorobenzothiazol-2-yl)amine (20)

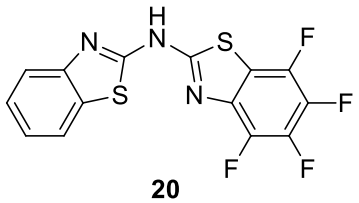

20

2-Aminobenzothiazole (150 mg, 1.0 mmol) and 2-amino-4,5,6,7-tetrafluorobenzothiazole (222 mg, 1.0 mmol) were mixed by dissolving in DCM followed by evaporation of the solvent. The resulting solid mixture was heated to 280 °C under N_2 for 2 h. After cooling, a dark solid was obtained. This crude product was dissolved in EtOAc/petrol (1:2) then subjected to flash chromatography (EtOAc/petrol, first 1:5 then 1:4). The first product-containing fractions were combined. After evaporating the solvent, the title product **20** was obtained as a white solid (150 mg, 42%), mp 294.5–296.5 °C. ν_{max}/cm^{-1} (ATR) 3041 (br), 1579, 1465, 1289, 1224, 1188, 1135, 1167, 995, 876, 748; δ_H (400 MHz, DMSO-d_6) 7.31 (1H, t, *J* 8 Hz, H–6), 7.46 (1H, t, *J* 8 Hz, H–5), 7.60 (1H, br, H–7), 7.96 (1H, d, *J* 8 Hz, H–4), 13.33 (1H, br, NH); δ_F (376 MHz, DMSO-d_6) –140.2 (1F, m, F–4), –151.8 (1F, m, F–7), –160.2 (1F, m, F–5), –164.2 (1F, m, F–6); HRMS (APCI) *m/z* found 355.9932, $C_{14}H_6F_4N_3S_2$ ($[M+H]^+$) requires 355.9934.

5.32 Preparation of *N*, *N*'-bis(pentafluorophenyl)malonamide (45)

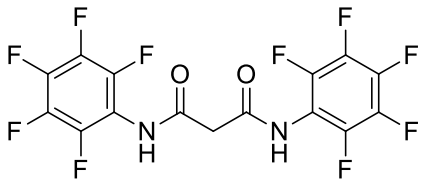

45

A solution of malonyl dichloride (0.88 mL, 9.0 mmol) in dry DCM (60 mL) was added dropwise to a suspension of pentafluoroaniline (6.6 g, 36 mmol) in dry DCM (30 mL) at 0 °C under N_2. Then the mixture was allowed to warm up to room temperature and stirred overnight. The solvent was evaporated under reduced pressure and the residue was extracted with 2M HCl and ethyl acetate. The organic phase was dried over Na_2SO_4, filtered and concentrated. The resulting yellow solid was washed with cold DCM (20 mL), then recrystallised from EtOH/H_2O to give *N*,*N*'-bis(pentafluorophenyl)-malonamide (**45**) as a white solid (3.7 g, 94%), mp 215–217 °C (lit. 215 °C, Ahmed Dellali, Msc Dissertation, Queen Mary, University of London, 2009).

5.33 Preparation of *N*, *N*'-bis(pentafluorophenyl)dithiomalonamide (46)

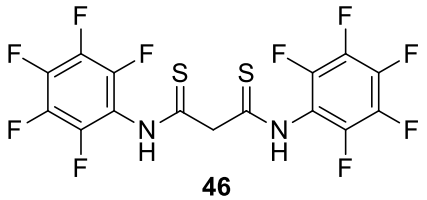

46

A suspension of *N*, *N*'-bis(perfluorophenyl)malonamide (**45**) (217 mg, 0.500 mmol) and Lawesson's reagent (202 mg, 0.500 mmol) in dry toluene (2 mL) was refluxed for 3.5 h under N_2. After cooling, the solvent was removed under reduced pressure, and the resulting residue was subjected to flash chromatography (DCM/petrol 5:1). The fractions for the major polar compound were collected and concentrated to give *N*,*N*'-bis(pentafluorophenyl)propanebis(thioamide) (**46**) as a yellow solid (130 mg, 52%), mp 46–49 °C; ν_{max}/cm^{-1}(ATR) 3199, 2977, 1655, 1519, 1364, 1124, 993, 751; δ_H(400 MHz, $CDCl_3$) 4.61 (2H, s, NH), 9.26 (2H, s, CH_2); δ_F (376 MHz, $CDCl_3$) –142.8 (4F, m), –152.5 (4F, m), –161.1 (4F, m); HRMS (ESI) *m/z* found: 464.9568, $C_{15}H_3F_{10}N_2S_2$ ($[M-H]^-$) requires 464.9572.

5.34 Preparation of bis(perfluorobenzothiazol-2-yl)methane (47)

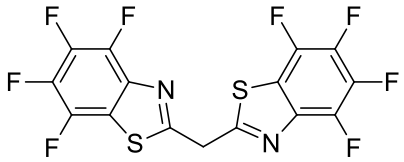

47

A solution of *N*, *N*'-bis(pentafluorophenyl)dithiomalonamide (**46**) (50 mg, 0.11 mmol) in dry toluene was refluxed for 72 h under N_2. Then the solvent was evaporated under reduced pressure and the resulting residue was subjected to flash chromatography (DCM/petrol 5:2) to give bis(4,5,6,7-tetrafluorobenzothiazol-2-yl)methane (**47**) as a yellow-brown solid (72 mg, 46%), mp 143–146 °C; ν_{max}/cm^{-1}(ATR) 2881, 1654, 1575, 1479, 1397, 1352, 1290, 1177, 1084, 995, 878; δ_H (400 MHz, $CDCl_3$) 4.98 (2H, s, CH_2); δ_F (376 MHz, $CDCl_3$) –137.8 (2F, m, F–4,4'), –146.8 (2F, m, F–7,7'), –156.9 (2F, m, F–5,5'), –157.4 (2F, m, F–6,6'); HRMS (APCI) *m/z* found 426.9594, $C_{15}H_3F_8N_2S_2$ ($[M+H]^+$) requires 426.9604.

5.35 Preparation of *N*-(benzothiazol-2-yl)methanesulfonamide (50)

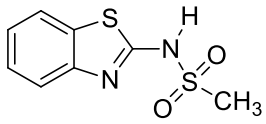

50

A solution of 2-aminobenzothiazole (1.50 g, 10 mmol), methanesulfonyl chloride (0.85 mL, 11 mmol) and dry pyridine (0.89 mL, 11 mmol) in dry DCM (50 mL) was stirred in an ice bath. The reaction was followed by TLC (EtOAc). After 4 h more pyridine (11 mmol) and methanesulphonyl chloride (11 mmol) were added to the mixture to make the reaction complete. After another 6 h the reaction mixture was quenched with 1M HCl and filtered. The precipitate was treated with excess 1M NaOH solution and the insoluble residue was filtered off. The filtrate was again treated with HCl to give a fluffy precipitate, which was collected by filtration and washed with distilled water to give *N*-(benzothiazol-2-yl)methanesulfonamide (**50**) (278 mg, 12%) as a white solid, mp 252–254.5 °C (lit.[105] 250–251 °C); ν_{max}/cm^{-1}(ATR) 3029, 1555, 1459, 1293, 1118, 982, 746; δ_H (270 MHz, $CDCl_3$) 3.00 (3H, s, CH_3), 7.21-7.42 (3H, m, H–5,6,7), 7.78 (1H, d, *J* 7.8 Hz, H–4), 12.97 (1H, s, NH).

5.36 Preparation of *N*-(benzothiazol-2-yl)trifluoromethanesulfonamide (51)

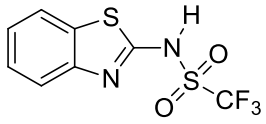

51

Under the protection of N_2, a solution of trifluoromethanesulfonic anhydride (1.85 mL, 11 mmol) in dry DCM (20 mL) was added dropwise to a solution of 2-aminobenzothiazole (1.50 g, 10 mmol) and dry pyridine (0.89 mL, 11 mmol) in dry DCM (20 mL). Then the mixture was stirred at room temperature for 10 h. Then the mixture was treated with excess 2M HCl and filtered. The DCM layer of the filtrate was washed with HCl and distilled water. The organic phase was dried over $MgSO_4$ and the solvent was evaporated to give an orange solid, which was treated with excess 1M NaOH and then filtered. The filtrate was acidified with excess 2M HCl and the precipitate that formed was collected, washed with distilled water and recrystallised from ethanol to give *N*-(benzothiazol-2-yl)trifluoromethanesulfonamide (**51**) (309 mg, 11%), mp 255.5–258.5 °C (lit.[106] 253.5–255.5 °C); ν_{max}/cm^{-1}(ATR) 3111, 1539, 1461, 1347, 1174, 1128, 972; δ_H (270 MHz, DMSO-d_6) 7.38-7.56 (3H, m, H–5,6,7), 7.97 (1H, d, *J* 8.1 Hz, H–4).

5.37 Preparation of *N*-(4,5,6,7-tetrafluorobenzothiazol-2-yl)trifluoromethanesulfonamide (52)

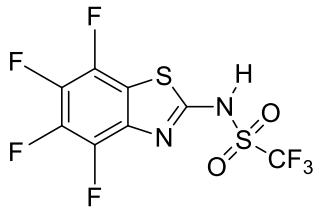

52

Under the protection of N_2, a solution of trifluoromethanesulfonic anhydride (0.092 mL, 0.55 mmol) in dry DCM (5 mL) was added dropwise to a solution of 2-amino-4,5,6,7-tetrafluorobenzothiazole (0.11 g, 0.50 mmol) and dry pyridine (0.045 mL, 0.55 mmol) in dry DCM (5 mL) at 0 °C. Then the mixture was allowed to warm to the room temperature and stirred for 10 h. The mixture was washed with 2M HCl twice and water once. The DCM layer was dried over $MgSO_4$ and the solvent was evaporated to give a bright yellow solid, which was subjected to flash chromatography (ethyl acetate-DCM 65:35) to obtain *N*-(4,5,6,7-tetrafluorobenzothiazol-2-yl)trifluoromethanesulfonamide (**52**) (45.7 mg, 26%), mp 257.5–260 °C. ν_{max}/cm^{-1}(ATR) 3648, 1466, 1318, 1200, 1126, 1011, 958, 880. δ_F (376 MHz, $CDCl_3$) –74.08 (3F, s, CF_3), –137.41 (1F, dd, *J* 23, 14 Hz, F–4), –149.26 (1F, ddd, *J* 21, 14, 3 Hz, F–7), –158.75 (1F, t, *J* 21 Hz, F–5), –162.75 (1F, t, *J* 22 Hz, F–6); HRMS (EI) *m*/*z* found 353.9361, $C_8H_1O_2N_2F_7S_2$ (M^+) requires 353.9362.

5.38 Preparation of the zinc complex of 2-(3,4,5,6-tetrafluoro-2-hydroxy-phenyl)benzothiazole (53)

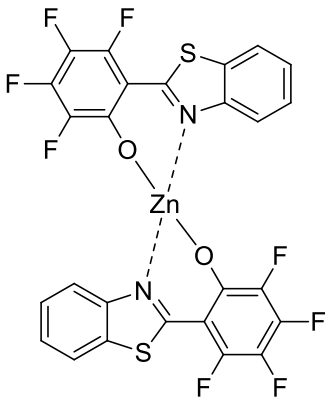

53

To a boiling solution of 2-(3,4,5,6-tetrafluoro-2-hydroxyphenyl)benzothiazole (**15**) (23.8 mg, 0.0796 mmol) in MeOH (50 mL) was added 0.1 M methanolic KOH (0.79 mL, 0.0796 mmol), followed by a solution of $Zn(OAc)_2{\cdot}2H_2O$ (8.72 mg, 0.0398 mmol) in MeOH (5 mL). A yellow precipitate gradually formed and the mixture was kept boiling and stirring for another 45 min, after which the precipitate was filtered off and washed with boiling MeOH to yield **53** as a bright yellow, fluffy solid (21.1 mg, 80%), mp > 400°C. Found: C, 47.25; H, 1.25; N, 4.18. $C_{26}H_8F_8N_2O_2S_2Zn$ requires: C, 47.18; H, 1.22; N, 4.23%. ν_{max}/cm^{-1} (ATR) 1656, 1481, 1404, 1259, 998, 750; λ_{max} (DMSO) 431 (ε 42500), 295 (23500); δ_H (400 MHz, DMSO-d_6) 8.34 (1H, d, *J* 8 Hz), 8.06 (1H, d, *J* 8 Hz), 7.40–7.49 (2H, m); δ_F (376 MHz, DMSO-d_6) –141.7 (m), –141.8 (m), –157.6 (m), –163.7 (m); HRMS (APCI) *m*/*z* found 660.9269; $C_{26}H_9F_8N_2O_2S_2Zn$ ($M+H^+$) requires 660.9264.

5.39 Preparation of the zinc complex of 4,5,6,7-tetrafluoro-2-(2-hydroxy-phenyl)benzothiazole (54)

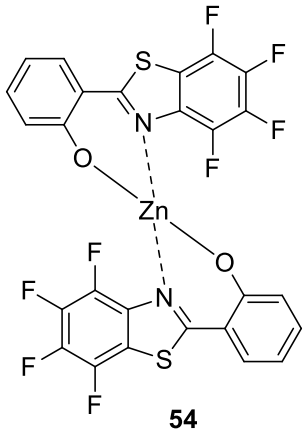

54

To a solution of 4,5,6,7-tetrafluoro-2-(2-hydroxyphenyl)benzothiazole (**11**) (0.30 g, 1 mmol) in chloroform (15 mL) was added 1 M KOH in MeOH (1.0 mL, 1.0 mmol). The resultant bright yellow precipitate was filtered off and washed with chloroform to give the potassium salt of the ligand (0.286 g, 85%). A portion of this potassium salt (68 mg, 0.2 mmol) was dissolved in MeOH (3 mL) and mixed with a solution of $Zn(OAc)_2 \cdot 2H_2O$ (11 mg, 0.1 mmol) in MeOH (0.5 mL). The mixture was refluxed for 12 min and the resultant yellow precipitate was filtered off, washed with MeOH and dried. The filtrate was concentrated under vacuum to give a second crop of precipitate, which was combined with the first crop to give the zinc complex **54** (50.7 mg, 77%), mp > 400 °C. Found: C, 47.29; H, 1.61; N, 4.02. $C_{26}H_8F_8N_2O_2S_2Zn$ requires: C, 47.18; H, 1.22; N, 4.23 %. ν_{max}/cm^{-1}(ATR) 1480, 1417, 1198, 1013, 883; λ_{max} (DMSO) 398 (ε 40200), 281 (24000); δ_H (400 MHz, DMSO-d_6) 8.22 (1H, d, *J* 8 Hz), 7.23 (1H, t, *J* 8 Hz), 7.09 (1H, d, *J* 8 Hz), 6.67 (1H, t, *J* 8 Hz); δ_F (376 MHz, DMSO-d_6) –140.5 (m), –151.3 (m), –161.0 (m), –163.2 (m) HRMS (APCI) *m*/*z* found 660.9265; $C_{26}H_9F_8N_2O_2S_2Zn$ ($M+H^+$) requires 660.9264.

5.40 Preparation of the zinc complex of 2-(3,4,5,6-tetrafluoro-2-hydroxy-phenyl)-4,5,6,7-tetrafluorobenzothiazole (55)

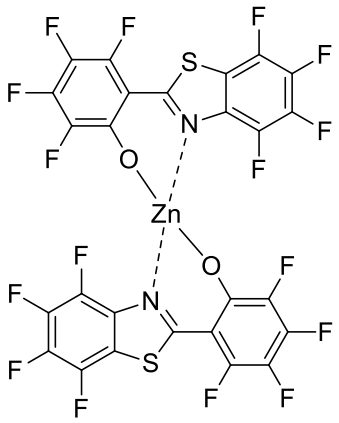

55

To a boiling solution of 2-(3,4,5,6-tetrafluoro-2-hydroxyphenyl)-4,5,6,7-tetrafluorobenzothiazole (**6**) (649 mg, 1.75 mmol) in 1:1 Et_2O-MeOH was added 1 M KOH in MeOH (1.80 mL, 1.80 mmol); the colour changed from pale yellow to bright yellow at once. After 5 min the solvent was evaporated and the bright yellow residue was dissolved in boiling water. To the resultant solution was added aqueous $Zn(OAc)_2 \cdot 2H_2O$ (287 mg, 1.31 mmol). A bright yellow precipitate formed immediately. After 30 min the mixture was filtered whilst hot; the precipitate was washed with boiling water and dried to give zinc complex **55** (645 mg, 92%), mp 338-340 °C. Found: C, 38.61; H, <0.10; N, 3.64. $C_{26}F_{16}N_2O_2S_2Zn$ requires C, 38.76; H, 0.00; N, 3.47 %. λ_{max} (DMSO) 404 (ε 31900), 282 (23100); δ_F (376 MHz, CD_3OD) –141.4 (m), –142.7 (m), –149.3 (m), –157.7 (m), –161.8 (m), –162.5 (m), –166.3 (m), –181.6 (m); HRMS (APCI) *m*/*z* found 826.8329; $C_{26}F_{16}N_2NaO_2S_2Zn$ ($M+Na^+$) requires 826.8329.

5.41 Preparation of the zinc complex of bis(benzothiazol-2-yl)amine (56)

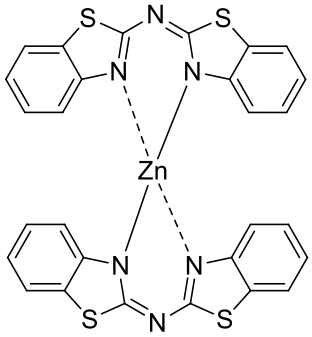

56

To a boiling solution of bis(benzothiazol-2-yl)amine (**19**) (1000 mg, 3.53 mmol) in EtOH was added a solution of zinc acetate dihydrate (582 mg, 2.65 mmol) in EtOH. A white precipitate gradually formed and the suspension was refluxed for 1 h. Then the mixture was subjected to a hot filtration. The resulting precipitate was washed by boiling EtOH a few times and dried under vacuum to give the title zinc complex **56** as a white solid, (890 mg, 80%). Found: C, 53.19; H, 2.82; N, 13.36. $C_{28}H_{16}N_6S_4Zn$ requires C, 53.37; H, 2.56; N, 13.33 %; ν_{max}/cm^{-1} (ATR) 3063, 2901, 1536, 1435, 1257, 1195, 1020, 914, 744, 686; λ_{max} (DMSO) 379 (ε 124000), 362 (111000); δ_H (600 MHz, DMSO-d_6) 7.02 (2H, d, *J* 7.8 Hz, H-4,4'); 7.17 (2H, t, *J* 7.8 Hz, H-6,6'), 7.22 (2H, t, *J* 7.8 Hz, H-5,5'), 7.85 (2H, d, *J* 7.8 Hz, H-7,7'); HRMS (APCI) *m/z* found: 627.9594, $C_{28}H_{16}N_6S_4Zn$ (M^+) requires 627.9605.

5.42 Preparation of the zinc complex of benzothiazol-2-yl-(tetrafluorobenzothiazol-2-yl)amine (57)

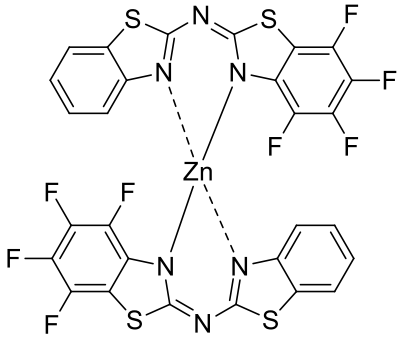

57

To a boiling solution of (benzothiazol-2-yl)-(4,5,6,7-tetrafluorobenzothiazol-2-yl)amine (**20**) (120 mg, 0.34 mmol) in EtOH was added a solution of zinc acetate dihydrate (56 mg, 0.25 mmol) in EtOH. The mixture was refluxed for 10 min and then one drop of water was added to initiate precipitation. The resulting suspension was refluxed for another 1 h and then allowed to cool down. The precipitate was too fine to filter immediately, so it was aged for 48 h to enable a hot filtration. The obtained precipitate was washed a few times with boiling EtOH and dried under vacuum to give the title zinc complex **57** as a pale yellow powder. (65 mg, 49%). ν_{max}/cm^{-1} (ATR) 3405, 1467, 1445, 1286, 1198, 1096, 1006, 881, 749, 699; λ_{max} (DMSO) 375 (ε 99500), 360 (88700); δ_H (600 MHz, DMSO-d_6, 90 °C) 7.19 (1H, t, *J* 7.8 Hz, H–6), 7.27 (1H, t, *J* 7.8 Hz, H–5), 7.33 (1H, *J* 7.8 Hz, H–7), 7.81 (1H, d, *J* 7.8 Hz, H–4); δ_F (376 MHz, DMSO-d_6) –140.9 (1F, m, F–4), –153.8 (1F, m, F–7), –160.6 (1F, m, F–5), –165.8 (1F, m, F–6); HRMS (APCI) *m/z* found: 771.8843, $C_{28}H_8F_8N_6S_4Zn$ (M^+) requires 771.8852.

5.43 Preparation of the zinc complex of bis(4,5,6,7-tetrafluorobenzothiazol-2-yl)amine (58)

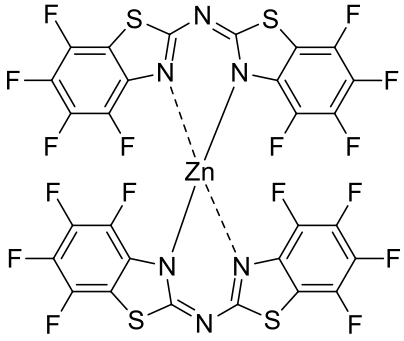

58

To a boiling solution of bis(4,5,6,7-tetrafluorobenzothiazol-2-yl)amine (**18**) (176 mg, 0.41 mmol) in EtOH was added a solution of zinc acetate dihydrate (136 mg, 0.62 mmol) in EtOH. A white precipitate gradually formed after 10 min and the suspension was refluxed for another 1 h. Then the mixture was filtered while hot. The resulting precipitate was washed by boiling EtOH a few times and dried under vacuum to give the title zinc complex **58** as a white solid, (149 mg, 79%). Found: C, 36.56; H, <0.10; N, 9.20. $C_{28}F_{16}N_6S_4Zn$ requires C, 36.64; H, 0.00; N, 9.15 %. ν_{max}/cm^{-1} (ATR) 1536, 1449, 1285, 1209, 1172, 1096, 1011, 884, 860, 695; λ_{max} (DMSO) 373 (ε 112000), 357 (97900); δ_F (376 MHz, DMSO-d_6) –141.2 (2F, dd, *J* 23, 12 Hz, F–4, 4'), –154.0 (2F, m, F–7, 7'), –163.0 (2F, t, *J* 23 Hz, F–5, 5'), –168.8 (2F, t, *J* 23 Hz, F–6, 6'); HRMS (EI) *m/z* found: 915.8103, $C_{28}F_{16}N_6S_4Zn$ (M^+) requires 915.8098.

5.44 Attempted preparation of the zinc complex of *N*-(Benzothiazol-2-yl)methanesulfonamide (59)

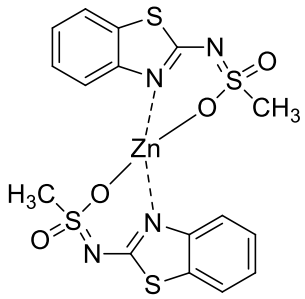

59

A solution of zinc acetate dihydrate (55mg, 0.25mmol) in boiling MeOH was added to a solution of *N*-(benzothiazol-2-yl)methanesulfonamide (**50**) (114 mg, 0.5 mmol) in boiling MeOH. The mixture was kept boiling and stirred for 0.5 h. The solution stayed clear and no precipitate was formed. Then the mixture was cooled to room temperature and the solvent was evaporated off. A white powder was obtained and recrystalised from MeOH to give white crystals (38.5 mg) that had almost identical melting point and IR spectra as the starting material **50**, mp=248.5–251 °C; ν_{max}/cm^{-1}(ATR) 3034, 1550, 1465, 1315, 1122, 965, 751.

5.45 Attempted preparation of zinc complex of *N*-(benzothiazol-2-yl)trifluoromethanesulfonamide (60)

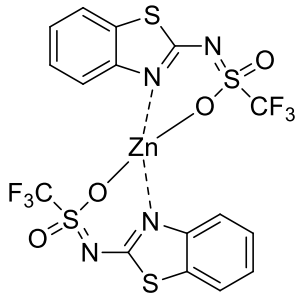

60

A solution of zinc acetate dihydrate (31mg, 0.14mmol) in boiling MeOH was added to a solution of *N*-(benzothiazol-2-yl)trifluoromethanesulfonamide (**51**) (100mg, 0.282 mmol) in boiling MeOH. The mixture was kept boiling and stirred for 0.5 h. The solution stayed clear and no precipitate was formed. Then the mixture was cooled to room temperature and the solvent was evaporated off to get a white powder (111.2 mg) with almost identical melting point and IR spectra as the ligand **51**, mp 243.5–247 °C; ν_{max}/cm^{-1}(ATR) 3110, 1542, 1461, 1347, 1173, 1129, 977.

5.46 Attempted preparation of tris(2-(benzothiazol-2-yl)phenoxy)erbium (65)

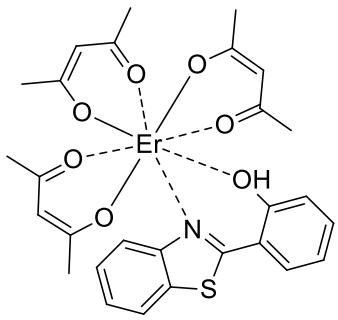

63

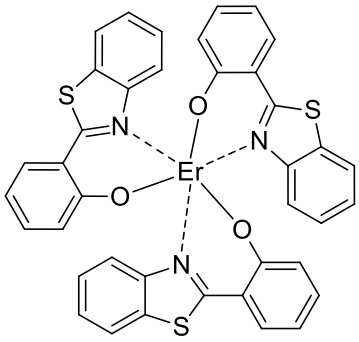

65

A hot solution of $Er(acac)_3$ (160 mg, 0.34 mmol) in MeCN (10 mL) was added to a hot solution of 2-(2-hydroxyphenyl)benzothiazole (227 mg, 1.0 mmol) in MeCN (15 mL). The mixture was refluxed for 2 h and a precipitate was formed, which was then filtered off and washed with MeCN a few times to give **63** as a pale pink solid (138 mg, 60%), mp 291-293.5 °C; δ_H (400 MHz, $CDCl_3$) 2.07-2.28 (m, -Me), 3.63 ($-CH_2-$), 5.50 (-CH=), 6.96 (1H, t, *J* 8 Hz), 7.10 (1H, d, *J* 8 Hz), 7.36-7.44 (2H, m), 7.51 (1H, t, *J* 8 Hz), 7.70 (1H, d, *J* 8 Hz), 7.91 (1H, d, *J* 8 Hz), 7.99 (1H, d, *J* 8 Hz), 12.49 (1H, s). This pink solid was subjected to sublimation under high vacuum ($<3\times10^{-6}$ mbar) between 350 °C and 370 °C to obtain **65** as a yellow solid (18.2 mg, 11%), decomp.>400 °C; HRMS (APCI) *m/z* found: 844.0281, $C_{39}H_{24}N_3O_3S_3Er$ (M^+) requires 844.0277; species corresponding to $Er(BTZ)_2(acac)$ and $Er(BTZ)(acac)_2$ were also observed in the mass spectrum.

5.47 Preparation of caesium tetrakis(2,3,4,5-tetrafluoro-6-(perfluorobenzo-thiazol-2-yl)phenoxy)erbate(III) (70)

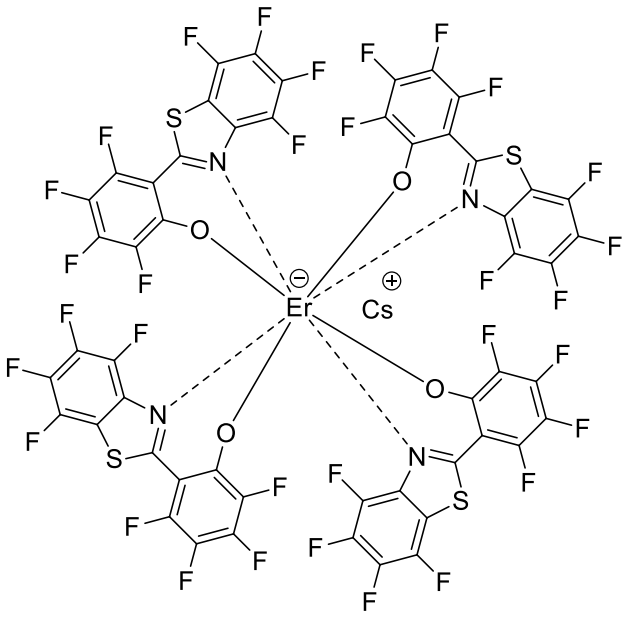

70

A solution of Cs_2CO_3 (65.2 mg, 0.200 mmol) in MeOH (15 mL) was added into a solution of 2-(2-hydroxy-3,4,5,6-tetrafluoro-phenyl)-4,5,6,7-tetrafluorobenzothiazole (**6**) (148 mg, 0.400 mmol) in DCM (20 mL). After stirring for 5 min the solvent was evaporated and the resulting solid was washed with DCM, and redissolved in MeCN. To this solution was added $ErCl_3 \cdot 6H_2O$ (38.2 mg, 0.100 mmol) in MeOH (3 mL). After refluxing for 10 min the solvent was evaporated. The resulting bright yellow solid was extracted with cold MeCN and filtered. The filtrate was concentrated under reduced pressure to give **70** as a uniform orange film (175.1 mg, 98%) on the inner surface of the round bottom flask. MS (MALDI) *m/z* found: 1645.8, $C_{52}F_{32}N_4O_4S_4Er$ ($[M\text{-}Cs^+]^-$) requires 1645.8. Attempted recrystallisation of this material did not give the desired erbium complex; only the Cs salt of the ligand was obtained as identified by single crystal X-ray diffraction.

Chapter 6 - Experimental part II: Physics experiments

6.1 Device structure and preparation

6.1.1 Device structure

A typical multilayer organic light emitting diode (OLED) has the device structure as shown in Figure 7.1. The substrate is a transparent glass slide, on top of which a transparent layer of indium tin oxide (ITO) is used as the conducting anode. All the other layers were grown layer by layer through thermal evaporation.

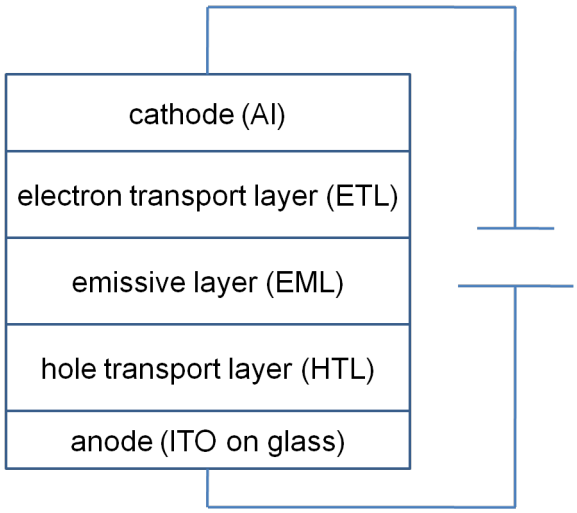

Figure 7.1: Structure of a multilayer OLED

The working mechanism of an OLED is presented in Figure 7.2. The electrons are injected from the cathode, and then transported into the emissive layer (EML) through the electron transport layer (ETL). Similarly, holes are injected from the anode, and also transported into the EML from the hole transport layer (HTL). The electrons and holes in the EML are able to form bound excited states called excitons, which then can de-excite through radiative process (light emission) or radiationless process to the ground state.

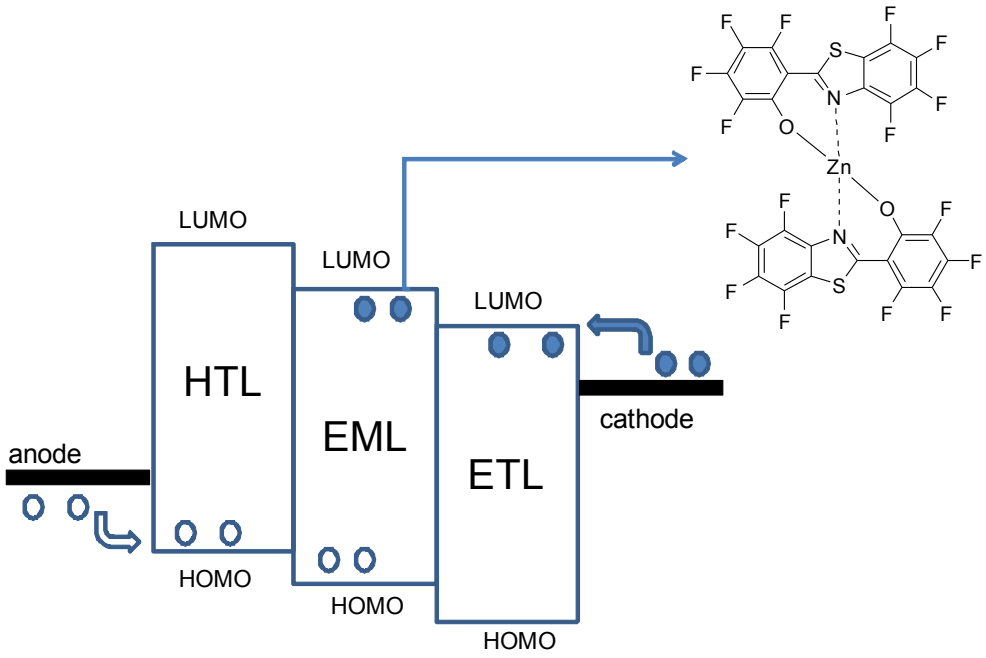

Figure 7.2: Mechanism of a working OLED

In this research, we investigated the performance of perfluorinated phenolate zinc complex **55** as the emissive material. According to the DFT calculation results introduced in Chapter 3, the perfluorinated material has relative low HOMO (–6.1 eV) and LUMO (–2.7 eV) energy levels. In order to achieve good emission efficiency from the device, the HTL and ETL materials have to be carefully chosen to match the fluorinated EML material.

In our experiment, the electron transport material used was the well known Alq_3 which has a LUMO about -3.1 eV. HMTPD was selected as the HTL material instead of the widely used material TPD because HMTPD has a lower HOMO (–5.9 eV) than TPD (–5.5 eV), thus a smaller barrier for holes at the HTL/EML interface.[95] In summary, the composition of device and the thickness of layers can be presented as ITO/ HMTPD (50 nm)/ zinc complex (20 nm)/ Alq_3 (50 nm)/ LiF (1 nm)/ Al (100 nm).

6.1.2 Device preparation

1. Substrate preparation

The quality of substrate can directly affect the performance of devices. We have developed a standard procedure for the preparation of patterned ITO substrate. The first step is a thorough cleaning of the substrate surface, which is crucial for the following step of patterning.

Step 1: Cleaning ITO substrate

1) The ITO substrate was thoroughly clean with detergent.
2) Ultrasonicated in pure water with detergent for 15 minutes.
3) The substrate was wash with pure water, then ultrasonicated in pure water twice, 5 minutes each time.
4) Ultrasonicated in acetone twice, 5 minutes each time.
5) Ultrasonicated in chloroform twice, 5 minutes each time.

The purchased substrate has a uniform layer of ITO covering the whole surface glass. In order to achieve the desired pattern of ITO as the anode, the substrate has to go through the photolithography process to transfer the desired image from a mask to the ITO layer, and the unwanted part of ITO has to be removed by etching. This process is done with the assist of a photo sensitive material called photo resist, which only becomes soluble in developer solution after exposured to UV light.

Step 2: Patterning ITO substrate by photolithography

1) Photoresist was spin coated on top of ITO substrate.
2) Thermally cured the sample in an oven at 90 °C for 15 minutes.
3) Cooled down the substrate, and then covered the substrate with the mask, which is a transparent plastic sheet with opaque pattern.
4) Exposed the substrate with mask on top to UV light for 1 minute, so the photo resist under the transparent part got exposure, while the area under the opaque pattern was protected.

5) The exposed photo resist was washed away with the developer solution (*Microposit 351 developer*) for 45 seconds, and the substrate was rinsed with distilled water, while the unexposed photo resist still stays on top of ITO and protect the patterned part of ITO from etching.
6) The substrate was soaked in the etching solution made of HCl (48%), HNO_3 (2%) and distilled water (50%) at 48-50 °C for 1.5 min and then rinsed with distilled water, so the ITO layer was removed except the patterned area.
7) Ultrasonicated the substrate in acetone and chloroform twice to remove the unexposed photo resist. The finished ITO substrate should have the pattern illustrated in figure 7.3.

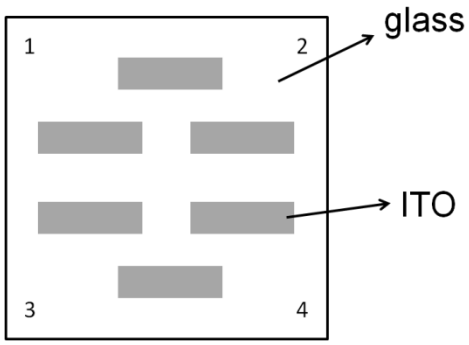

Figure 7.3: Patterned ITO substrate

After patterning, the ITO substrate was treated with oxygen plasma before growing organic layers on it. The purpose was to increase the ITO's work function, lowering the barrier for injecting holes at the ITO/HTL interface.

Step 3: Plasma treatment of ITO substrate

1) The substrate was put in the chamber of plasma system and the chamber was pumped down.
2) The chamber was filled with oxygen and then pumped down again, repeat 3 to 5 times.
3) Purged out the residue air with 1.5~4 mbar oxygen flow for 5 mins.

4) The oxygen pressure was adjusted to 0.3~0.4 mbar, then the plasma was ignited with 30% generator power and kept for 5 mins.

After plasma treatment, the ITO substrate was transferred to the evaporation system immediately, and kept in vacuum for the following deposition. If exposed to the air for too long, the plasma treated ITO substrate will lose its improvement of work function.

2. Device growth

All the layers on the ITO substrate were grown in the Kurt J. Lesker evaporation system. The structure of this is illustrated in figure 7.4.

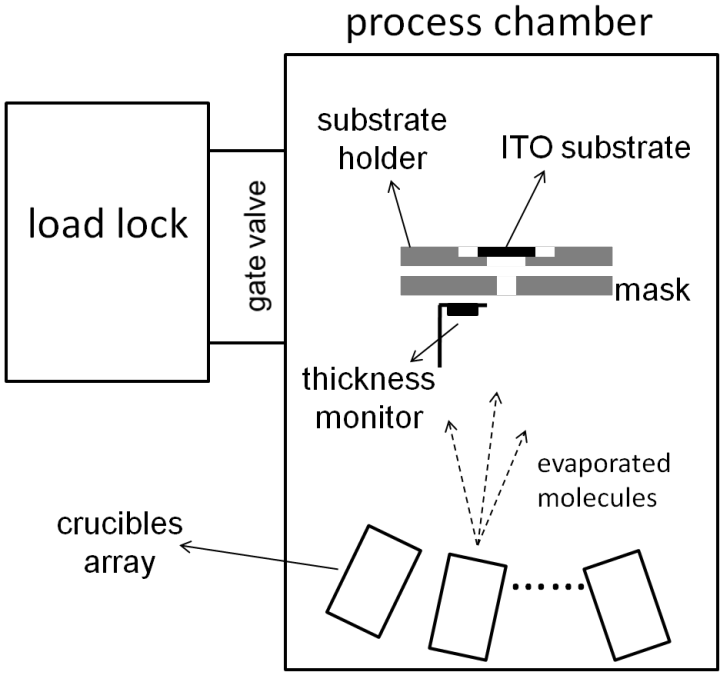

Figure 7.4: Kurt J. Lesker evaporation system

The evaporating system is composed of two chambers: the load lock (LL) and the processing chamber (PC). The LL is used as a transitional chamber for transporting the substrate between the atmosphere and the PC. It has a smaller volume than the PC so can be pumped down or vented faster. The PC is where all the evaporation processes take place, and is always kept under high vacuum with pressure around 10^{-7} mbar or lower. All the materials are heated in their respective crucibles at the bottom of PC, so

the molecules are thermally evaporated and diffuse upwards to eventually condense on the ITO substrate. The shape of the condensing area on the substrate is controlled by a mask below the substrate. We use a square shaped mask for organic layers and LiF, and a rectangular shaped mask for aluminum. As a result of the control by masks, the device was fabricated with a structure as shown in figure 7.5, and can be presented as glass/ ITO/ HMTPD (50 nm)/ zinc complex (20 nm)/ Alq_3 (50 nm)/ LiF (1 nm)/ Al (100 nm) from the bottom to the top. There are four diodes that can work separately on a substrate. The working area of a diode is defined by the overlapping area of the anode (ITO) and the cathode (Al).

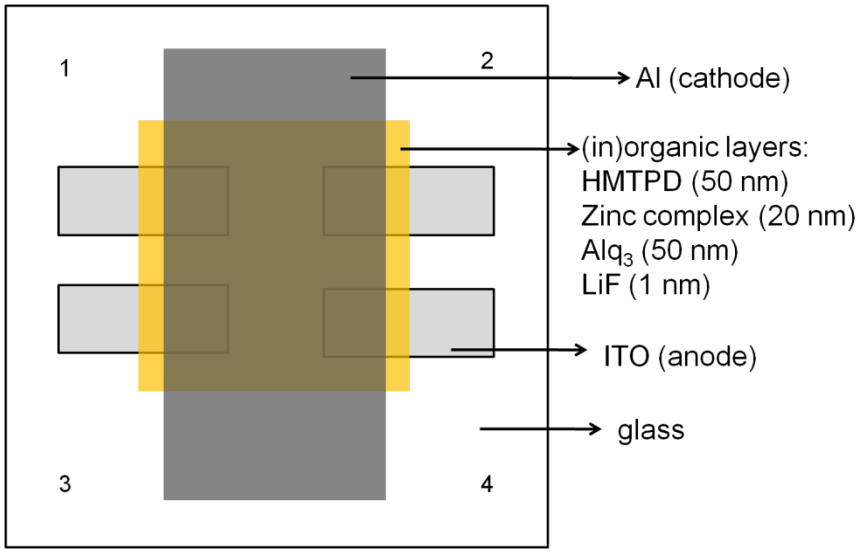

Figure 7.5: Structure of a fabricated device with four diodes on a substrate

Materials are usually evaporated one after another, each as a separate layer. But sometimes two materials need to be co-evaporated together to make a doped layer, with one material being the host and the other being the dopant. The co-evaporated layer can be controlled to have a specific molar ratio of the two materials, which depends on the ratios of material density, evaporating rate and molar mass. It can be calculated from the following equation:

$$\frac{moles\ of\ Er(FTPIP)_3}{moles\ of\ Zn(FBTZ)_2} = \frac{\rho_{Er(FTPIP)_3}}{\rho_{Zn(FBTZ)_2}} \cdot \frac{rate_{Er(FTPIP)_3}}{rate_{Zn(FBTZ)_2}} \cdot \frac{molar\ mass_{Zn(FBTZ)_2}}{molar\ mass_{Er(FTPIP)_3}}$$

The density of $Er(FTPIP)_3$ is 2.016 g/cm^3, and that of $Zn(FBTZ)_2$ is 2.167 g/cm^3. The molar mass of $Er(FTPIP)_3$ is 2495.8 g/mol, and that of $Zn(FBTZ)_2$ is 805.8 g/mol.[46,88] If a layer with the molar ratio of 20% $Er(FTPIP)_3$/ 80% $Zn(FBTZ)_2$ is demanded, the evaporating ratio of the two materials needs to be controlled as about 2:3.

3. Thickness calibration

The thickness of materials deposited on the substrate can be measured by a quartz crystal monitor. The reading value from the monitor can be affected by the densities of different materials and the height differences between the substrate and the monitor. But as long as the material type and the position of the monitor are fixed, the reading value will be proportional to the real thickness by a coefficient. The evaporation system needs to be informed of this coefficient, which can be reflected in the 'tooling factor' (TF) in the controlling software, to give the corrected thickness of deposited film.

Once the real thickness for a deposited film is measured by a DekTak profilometer, the tooling factor can be calculated:

$$TF = TF_{initial} \times \frac{T_m}{T_r}$$

Where TF is the new tooling factor, $TF_{initial}$ is the pre-set tooling factor in the software, T_m is the measured thickness, T_r is the read value from the monitor.

6.2 Experimental methods

6.2.1 IVL characterisation

The current-voltage-light (IVL) measurement is usually the first characterisation to be done on a fabricated device. This measurement provides direct information of the performance of a device, for example, its turn-on voltage and power efficiency. In the measuring process, a series of steady voltage steps were applied on the diode, at the same time the current and light output were recorded. A Keithley 236 voltage/current source measure unit was used to provide the voltage and to measure the current. The absolute luminescence intensity was measured using a Newport 1830C optical power meter, which contains an integrating sphere to capture all the emitted light and a

calibrated Newport 818 Series silicon photo-diode detector to convert the light signal to an electric signal.

6.2.2 Transient measurements of electroluminescence and device current

To understand all the dynamics happening during the emission, it is necessary to measure the emission spectra as well as the lifetimes of different radiative decay. The set up for the transient EL measurement is illustrated in figure 7.6. A Thurlby Thandar Instruments 40MHz TGA 1241 Arbitrary Waveform Generator was used to supply a square-wave driving voltage to the OLED and to provide a sync pulse to the oscilloscope as the reference. The emission from the OLED was focused by a pair of focal lenses and directed to a TRIAX 550 Spectrometer, then detected by a Thorn EMI 9202B S-20 photomultiplier tube (or Hamamatsu R5509-72 photomultiplier tube for infra-red) (PMT).

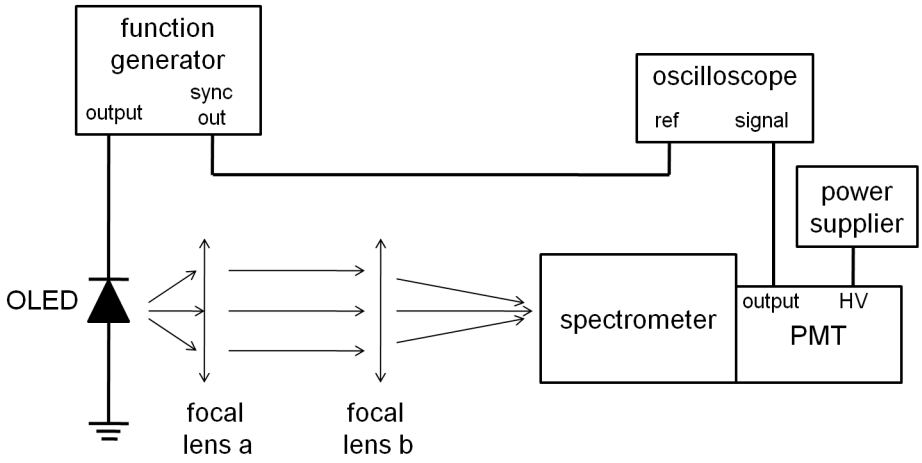

Figure 7.6: The set up for the measurement of EL spectra and lifetime

When measuring decay processes that with lifetimes on the scale of microseconds, attention needs to be paid to the resistance choice in the measuring circuit. Larger resistance can increase the signal intensity, but on the other hand would produce big RC decay that may match or exceed the real signal decay. The oscilloscope has two built-in resistances to choose from, 50 Ω and 1MΩ. Given that the signal intensity is big enough to be seen, the signal decay needs to be measured over the 50 Ω resistor, which gives a RC decay less than 5 ns.

If the emission from the device was not strong enough to be seen with the 50 Ω resistance, an ancillary resistance was used to magnify the signal. In this case, the value of the ancillary resistor was carefully chosen to give sufficient signal amplification but without yielding too large RC decay. When an ancillary resistor was used, the built-in resistance of oscilloscope was set to 1M Ω to act as a voltmeter (Figure 7.7).

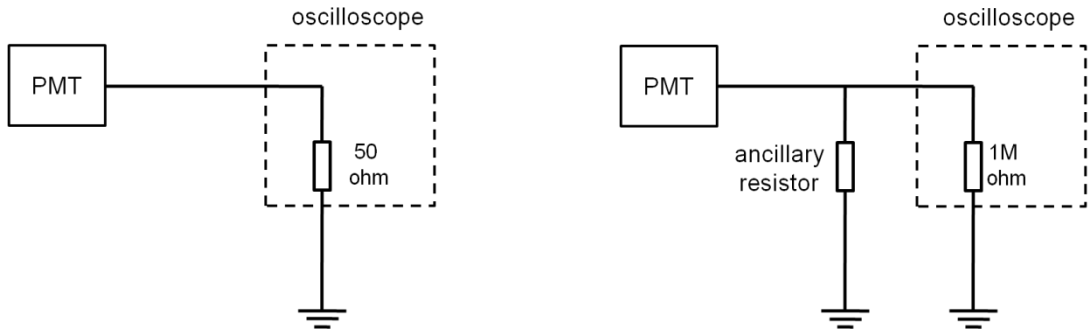

Figure 7.7: Resistance selection in case of strong signal intensity (left), and weak signal intensity (right)

The current through the device also has a lifetime, which is a consequence of the intrinsic capacitance and resistance of an OLED. Thus the current decay in the device was monitored and compared with the light decay. The set up for the transient current measurement is depicted in figure 7.8.

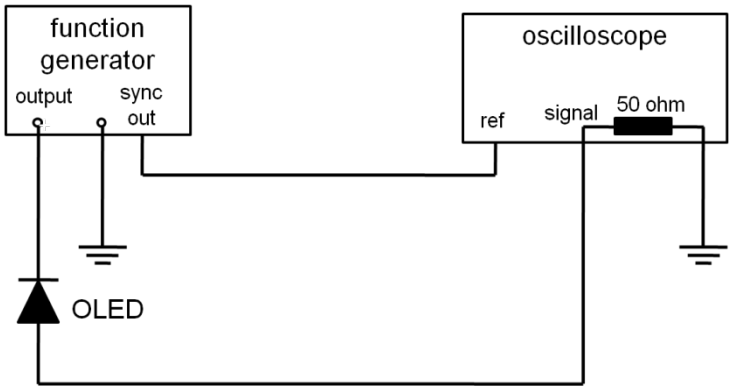

Figure 7.8: Set up for the measurement of transient current decay

Chapter 7 Conclusions and future work

7.1 Conclusions

1. Several new compounds of fully fluorinated and half fluorinated ligands based on benzothiazole derivatives have been successfully prepared, including 2-(2-hydroxy-3,4,5,6-tetrafluorophenyl)-4,5,6,7-tetrafluorobenzothiazole (**6**), 2-(2-hydroxyphenyl)-4,5,6,7-tetrafluorobenzothiazole (**11**), 2-(2-hydroxy-3,4,5,6-tetra fluorophenyl)benzothiazole (**15**), bis(4,5,6,7-tetrafluorobenzothiazol-2-yl)amine (**18**), *N*-(benzothiazol-2-yl)-4,5,6,7-tetrafluorobenzothiazol-2-amine (**20**), bis(per fluorobenzothiazol-2-yl)methane (**47**), *N*-(benzothiazol-2-yl)trifluoromethane sulfonamide (**51**) and *N*-(perfluorobenzothiazol-2-yl)trifluoromethanesulfonamide (**52**).

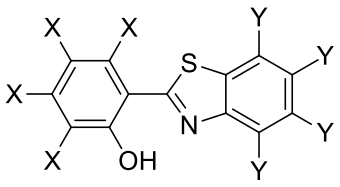

6 (X=Y=F)
11 (X=H, Y=F)
15 (X=F, Y=H)

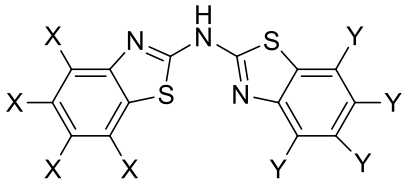

18 (X=Y=F)
20 (X=H, Y=F)

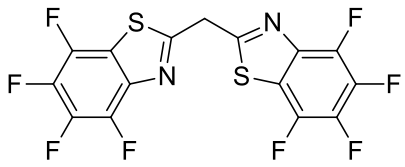

47

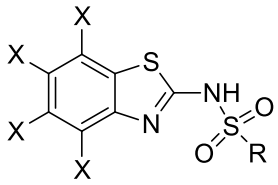

51: X=H, R=CF_3
52: X=F, R=CF_3

2. Two series of new compounds of the zinc complexes of fluorinated 2-(2-hydroxyphenyl)benzothiazoles (**53**-**55**) and fluorinated bis(benzothiazol-2-yl) amines (**57**-**58**) have been successfully prepared.

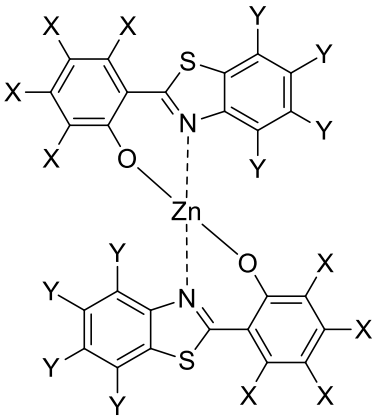

53 (X=F, Y=H)
54 (X=H, Y=F)
55 (X=Y=F)

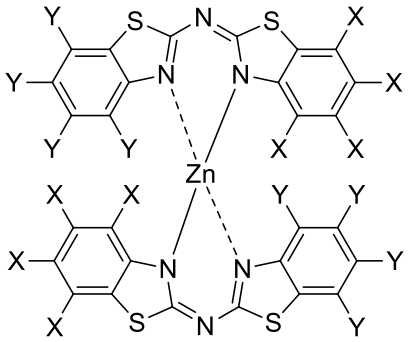

57 (X=H; Y=F)
58 (X=Y=F)

3. Single crystals of all the fluorinated zinc complexes have been grown by sublimation and characterised by XRD. These fluorinated zinc complexes are all monomeric, in contrast with the dimeric structure of $Zn(BTZ)_2$. Vairous π-π stacking modes, including π_H-π_H, π_H-π_F and π_F-π_F stacking, were observed in the crystals. In the crystals of those half fluorinated, three-dimensional complexes **54**, **55** and **57**, the π_H-π_F interaction is no longer the dominating driving force for molecular packing, which is widely observed in those partially fluorinated, or 1:1 mixtures of perfluorinated and nonfluorinated planar molecules. We consider that the dipole-dipole interaction between enantiomers and steric effects combine to guide the molecular packing here.

4. As found in many cases of organic semiconductor materials, fluorination decreases HOMO and LUMO simultaneously, but to different extent depending on the distribution of HOMO and LUMO on the framework of molecules. The subtle differences in decreasing HOMO and LUMO can explain the shift of photoluminescence spectra of these fluorinated molecules relative to the nonfluorinated parent molecules. An inverse relation between the spectra broadness and the dihedral angle of neighbouring aromatic rings in a conjugated system has been found. Decreasing dihedral angles lead to increasing broadening of emission

spectra.

5. The perfluorinated zinc complex of 2-(2-hydroxy-3,4,5,6-tetrafluorophenyl)-4,5,6,7-tetrafluorobenzothizole, $Zn(F\text{-}BTZ)_2$, has been applied as an active emission layer in organic light emitting diode (OLEDs). The electroluminescence of $Zn(F\text{-}BTZ)_2$ has shown remarkable phosphorescence in the red region apart from the green fluorescence, indicating enhanced spin mixing and intersystem crossing introduced by the substitution of the hydrogen atoms by fluorine atoms.

6. The ability of $Zn(F\text{-}BTZ)_2$ providing large population of triplets, together with the lack of CH or OH oscillators in the molecule, eventually allowed us to use it as an efficient chromophore to sensitise the erbium ions in a long-lifetime erbium complex, $Er(FTPIP)_3$. By doping $Er(FTPIP)_3$ into $Zn(F\text{-}BTZ)_2$ in the OLED, we achieved significant and long-lifetime emission from erbium at the important telecommunication wavelength of 1.5 μm.

7.2 Future work

1. The power efficiency of the phosphorescent OLED needs to be further improved to reach a higher practical level. Different combinations of other materials, especially for the hole injection and transport layer, can be tried to increase the population of holes in the device. And carriers blocking layers could be applied to confine carriers in the emissive layer.

2. The synthesis of compound **47** was successful and it could be used as a ligand to combine with several transition metals as its nonfluorinated counterpart.[66] However, if the erbium complex were made from the monovalent anion, there is still one proton left on the central carbon that will still act as a quenching source to reduce the lifetime. Thus it is desirable to replace that proton with a carbonyl or an oxime group, and compounds **48** and **49** would be two ideal synthesis targets.

3. A few luminescent zinc complexes with moderately high quantum yield have been made. Only the perfluorinated zinc complex of 2-(2-hydroxy-3,4,5,6-tetrafluoro-phenyl)-4,5,6,7-tetrafluorobenzothiazole (**55**) has been used to fabricate devices. The half fluorinated zinc complex of 2-(2-hydroxyphenyl)-4,5,6,7-tetrafluoro-benzothiazole (**54**) and the nonfluorinated zinc complex of bis(benzothiazol-2-yl)amine (**56**) also have the potential to be used as emissive materials to give green and blue emission respectively.

4. The crystal growth and XRD characterisation of the erbium complexes of 2-(2-hydroxy-3,4,5,6-tetrafluoro-phenyl)-4,5,6,7-tetrafluorobenzothiazole (**70** and **72**) would be desirable to obtain the structural and to further understand the physical properties. The preparation of erbium complexes from the perfluorinated ligand bis(4,5,6,7-tetrafluorobenzothiazol-2-yl)amine (**18**) needs to be carried out. The synthesis of the mercury complex from the nonfluorinated ligand (**19**) has been

reported[68], and considering the fact that the Er^{3+} ion has a smaller size that Hg^{2+}, therefore it would be possible to prepare the erbium complex from ligand **18**.

APPENDIX

A. Publications

Parts of the work described in this thesis have been published or submitted for publications:

1. Li, Z. *et al.* Luminescent Zinc(II) Complexes of Fluorinated Benzothiazol-2-yl Substituted Phenoxide and Enolate Ligands. *Inorg Chem* **52**, 1379-1387, doi:10.1021/ic302063u (2013).
2. Ye, H., Li, Z., Peng Y., Zheng Y., Sapelkin A., Adamopoulos G., Hernandez I., Wyatt P.B., Gillin W.P. High gain at low power-an efficient organo-erbium optical amplifier operating at telecommunications wavelengths. Submitted to *Nature.*
3. Li, Z. *et al*. Controlling electronic states and crystal packing of a novel blue luminescent zinc complex by fluorination, *Inorg Chem*, in preparation.
4. Li, Z. *et al*. Electrophosphorescence in a non-heave-metal zinc complex with perfluorinated ligand, *Adv. Mater*, in preparation.

B. Crystallographic parameters

1. Zinc complex **53**

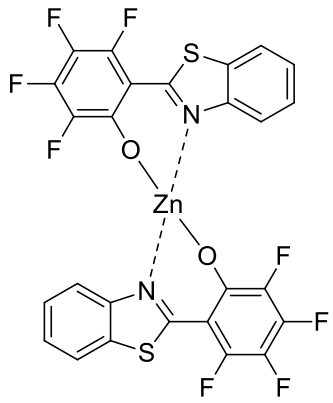

53

Chemical formula	$C_{26}H_8F_8N_2O_2S_2Zn$	
Formula weight	661.83	
Temperature	100(2) K	
Wavelength	1.54178 Å	
Crystal size	0.08 x 0.10 x 0.20 mm^3	
Crystal system	monoclinic	
Space group	P 1 21/c 1	
Unit cell dimensions	a = 12.6004(4) Å	α = 90°
	b = 24.1084(8) Å	β = 97.393(2)°
	c = 7.5640(3) Å	γ = 90°
Volume	2278.66(14) $Å^3$	
Z	4	
Density (calculated)	1.929 Mg/cm^3	
Absorption coefficient	4.127 mm^{-1}	
F(000)	1312	

Theta range for data collection	3.54 to 67.29°
Index ranges	-14<=h<=14, -27<=k<=28, -7<=l<=9
Reflections collected	36422
Independent reflections	4003 [R(int) = 0.0439]
Max. and min. transmission	0.7337 and 0.4924

Structure solution technique	direct methods	
Structure solution program	SHELXS-97 (Sheldrick, 2008)	
Refinement method	Full-matrix least-squares on F^2	
Refinement program	SHELXL-97 (Sheldrick, 2008)	
Function minimized	$\Sigma\, w(F_o^2 - F_c^2)^2$	
Data / restraints / parameters	4003 / 0 / 370	
Goodness-of-fit on F^2	1.045	
Δ/σ_{max}	0.001	
Final R indices	3713 data; $I>2\sigma(I)$	R1 = 0.0284, wR2 = 0.0775
	all data	R1 = 0.0308, wR2 = 0.0791
Weighting scheme	$w=1/[\sigma^2(F_o^2)+(0.0454P)^2+1.6208P]$ where $P=(F_o^2+2F_c^2)/3$	
Largest diff. peak and hole	0.482 and -0.379 eÅ^{-3}	
R.M.S. deviation from mean	0.062 eÅ^{-3}	

2. Zinc complex **54**

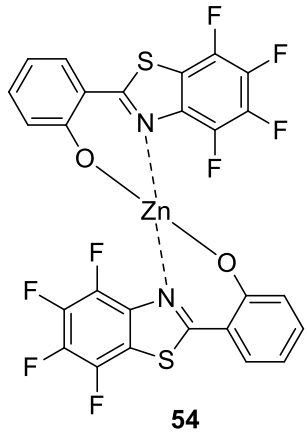

54

Empirical formula	$C_{26}H_8F_8N_2O_2S_2Zn$
Formula weight	661.83
Temperature	100(2) K
Wavelength	0.71073 Å
Crystal size	0.10 x 0.12 x 0.16 mm^3
Crystal system	Monoclinic
Space group	P 1 21/n 1
Unit cell dimensions	a = 7.350(5) Å b = 25.035(5) Å c = 12.638(5) Å
Volume	2284.8(19) $Å^3$
Z	4
Density (calculated)	1.924 Mg/cm^3
Absorption coefficient	1.356 mm^{-1}
F(000)	1312

Theta range for data collection	1.63 to 24.48°
Index ranges	-8<=h<=8, -29<=k<=29, -14<=l<=14
Reflections collected	39792
Independent reflections	3778 [R(int) = 0.0306]
Structure solution technique	direct methods
Structure solution program	SHELXS-97 (Sheldrick, 2008)

Refinement method	Full-matrix least-squares on F^2	
Refinement program	SHELXL-97 (Sheldrick, 2008)	
Function minimized	$\Sigma w(F_o^2 - F_c^2)^2$	
Data / restraints / parameters	3778 / 0 / 370	
Goodness-of-fit on F^2	0.878	
Final R indices	3464 data; $I>2\sigma(I)$	R1 = 0.0397, wR2 = 0.1034
	all data	R1 = 0.0441, wR2 = 0.1071
Weighting scheme	$w=1/[\sigma^2(F_o^2)+(0.0683P)^2+9.0745P]$ where $P=(F_o^2+2F_c^2)/3$	
Largest diff. peak and hole	2.148 and -0.505 $eÅ^{-3}$	
R.M.S. deviation from mean	0.082 $eÅ^{-3}$	

3. Zinc complex of **55**

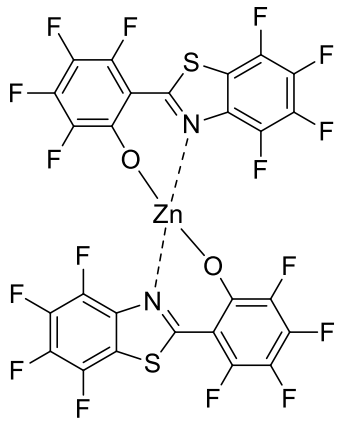

55

Chemical formula	$C_{26}F_{16}N_2O_2S_2Zn$
Formula weight	805.77
Temperature	100(2) K
Wavelength	0.71073 Å
Crystal size	0.12 x 0.14 x 0.24 mm^3
Crystal system	triclinic
Space group	P -1
Unit cell dimensions	a = 7.7232(2) Å α = 92.4460(10)°
	b = 11.8735(3) Å β = 103.5580(10)°
	c = 13.9100(4) Å γ = 93.9180(10)°
Volume	1234.85(6) $Å^3$
Z	2
Density (calculated)	2.167 Mg/cm^3
Absorption coefficient	1.320 mm^{-1}
F(000)	784

Theta range for data collection	1.72 to 26.37°
Index ranges	-9<=h<=9, -14<=k<=14, -17<=l<=17
Reflections collected	22725
Independent reflections	5027 [R(int) = 0.0142]
Coverage of independent reflections	99.3%
Absorption correction	multi-scan

Max. and min. transmission	0.8577 and 0.7423	
Structure solution technique	direct methods	
Structure solution program	SHELXS-97 (Sheldrick, 2008)	
Refinement method	Full-matrix least-squares on F^2	
Refinement program	SHELXL-97 (Sheldrick, 2008)	
Function minimized	$\Sigma\, w(F_o^2 - F_c^2)^2$	
Data / restraints / parameters	5027 / 0 / 442	
Goodness-of-fit on F^2	1.174	
Δ/σ_{max}	0.001	
Final R indices	4713 data; $I>2\sigma(I)$	R1 = 0.0485, wR2 = 0.1500
	all data	R1 = 0.0511, wR2 = 0.1546
Weighting scheme	$w=1/[\sigma^2(F_o^2)+(0.1090P)^2+1.2311P]$ where $P=(F_o^2+2F_c^2)/3$	
Largest diff. peak and hole	4.425 and -0.515 eÅ^{-3}	
R.M.S. deviation from mean	0.118 eÅ^{-3}	

4. Zinc complex of **56**

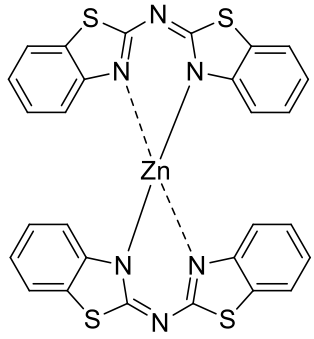

56

Chemical formula	$C_{28}H_{16}N_6S_4Zn$
Formula weight	630.08
Temperature	100(2) K
Wavelength	0.71073 Å
Crystal size	0.080 x 0.150 x 0.300 mm^3
Crystal habit	translucent pale yellow Block
Crystal system	triclinic
Space group	P -1
Unit cell dimensions	a = 12.0981(7) Å α = 69.4080(10)° b = 14.9995(8) Å β = 84.5710(10)° c = 15.6485(9) Å γ = 80.5810(10)°
Volume	2620.3(3) $Å^3$
Z	4
Density (calculated)	1.597 Mg/cm^3
Absorption coefficient	1.288 mm^{-1}
F(000)	1280

Theta range for data collection	1.39 to 28.31°
Index ranges	-16<=h<=9, -20<=k<=19, -20<=l<=20
Reflections collected	45236
Independent reflections	12734 [R(int) = 0.0185]
Coverage of independent reflections	97.6%
Absorption correction	multi-scan
Max. and min. transmission	0.9040 and 0.6986

Structure solution technique	direct methods	
Structure solution program	SHELXS-97 (Sheldrick, 2008)	
Refinement method	Full-matrix least-squares on F^2	
Refinement program	SHELXL-97 (Sheldrick, 2008)	
Function minimized	$\Sigma\, w(F_o^2 - F_c^2)^2$	
Data / restraints / parameters	12734 / 0 / 703	
Goodness-of-fit on F^2	1.056	
Δ/σ_{max}	0.001	
Final R indices	11068 data; $I>2\sigma(I)$	R1 = 0.0346, wR2 = 0.0972
	all data	R1 = 0.0429, wR2 = 0.1039
Weighting scheme	$w=1/[\sigma^2(F_o^2)+(0.0543P)^2+3.7817P]$ where $P=(F_o^2+2F_c^2)/3$	
Largest diff. peak and hole	1.243 and -0.366 eÅ^{-3}	
R.M.S. deviation from mean	0.096 eÅ^{-3}	

5. Zinc complex of **57**

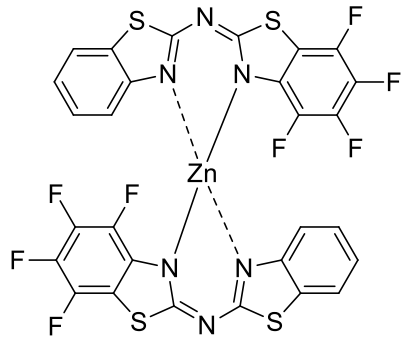

57

Chemical formula	$C_{28}H_8F_8N_6S_4Zn$
Formula weight	774.01
Temperature	100(2) K
Wavelength	0.71075 Å
Crystal size	0.06 x 0.04 x 0.03 mm^3
Crystal system	Monoclinic
Space group	P 21/n
Unit cell dimensions	a = 12.7529(6) Å α = 90°
	b = 14.8871(6) Å β = 90.040(6)°
	c = 14.7137(10) Å γ = 90°
Volume	2793.4(3) $Å^3$
Z	4
Density (calculated)	1.840 Mg/cm^3
Absorption coefficient	1.266 mm^{-1}
F(000)	1536

Theta range for data collection	3.07 to 27.49°
Index ranges	-15<=h<=16, -19<=k<=19, -19<=l<=16
Reflections collected	19428
Independent reflections	6319 [R(int) = 0.0400]
Completeness to theta = 27.49°	98.7%
Max. and min. transmission	0.9630 and 0.9279
Refinement method	Full-matrix least-squares on F^2

Data / restraints / parameters	6319 / 115 / 449	
Goodness-of-fit on F^2	1.034	
Final R indices	$I>2\sigma(I)$	R1 = 0.0550, wR2 = 0.1373
	all data	R1 = 0.0711, wR2 = 0.1469
Largest diff. peak and hole	1.296 and -0.721 $eÅ^{-3}$	

6. Zinc complex **58**

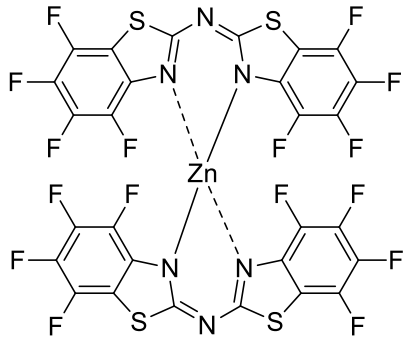

58

Chemical formula	$C_{28}F_{16}N_6S_4Zn$	
Formula weight	917.95	
Temperature	100(2) K	
Wavelength	1.54178 Å	
Crystal size	0.10 x 0.20 x 0.30 mm^3	
Crystal system	triclinic	
Space group	P -1	
Unit cell dimensions	a = 10.281(5) Å	α = 79.798(5)°
	b = 10.321(5) Å	β = 88.735(5)°
	c = 14.776(5) Å	γ = 89.951(5)°
Volume	1542.7(12) $Å^3$	
Z	2	
Density (calculated)	1.976 Mg/cm^3	
Absorption coefficient	4.887 mm^{-1}	
F(000)	896	

Theta range for data collection	3.04 to 67.21°
Index ranges	-11<=h<=12, -12<=k<=10, -17<=l<=16
Reflections collected	14955
Independent reflections	5201 [R(int) = 0.0282]
Max. and min. transmission	0.6407 and 0.3219
Structure solution technique	direct methods

Structure solution program	SHELXS-97 (Sheldrick, 2008)	
Refinement method	Full-matrix least-squares on F^2	
Refinement program	SHELXL-97 (Sheldrick, 2008)	
Function minimized	$\Sigma\ w(F_o^2 - F_c^2)^2$	
Data / restraints / parameters	5201 / 0 / 496	
Goodness-of-fit on F^2	1.058	
Δ/σ_{max}	0.001	
Final R indices	5137 data; $I>2\sigma(I)$	R1 = 0.0266, wR2 = 0.0687
	all data	R1 = 0.0269, wR2 = 0.0690
Weighting scheme	$w=1/[\sigma^2(F_o^2)+(0.0353P)^2+1.0032P]$ where $P=(F_o^2+2F_c^2)/3$	
Largest diff. peak and hole	0.349 and -0.379 eÅ^{-3}	
R.M.S. deviation from mean	0.069 eÅ^{-3}	

References:

(1) Tang, M. L.; Bao, Z. *Chemistry of Materials* **2010**, *23*, 446.

(2) Cho, D. M.; Parkin, S. R.; Watson, M. D. *Organic Letters* **2005**, *7*, 1067.

(3) Crouch, D. J.; Skabara, P. J.; Heeney, M.; McCulloch, I.; Coles, S. J.; Hursthouse, M. B. *Chemical Communications* **2005**, 1465.

(4) Sakamoto, Y.; Suzuki, T.; Kobayashi, M.; Gao, Y.; Fukai, Y.; Inoue, Y.; Sato, F.; Tokito, S. *J Am Chem Soc* **2004**, *126*, 8138.

(5) Shirakawa, H.; Louis, E. J.; Macdiarmid, A. G.; Chiang, C. K.; Heeger, A. J. *J Chem Soc Chem Comm* **1977**, 578.

(6) Letheby, H. *Proceedings of the Royal Society of London* **1862**, *12*, 550.

(7) Akamatu, H.; Inokuchi, H.; Matsunaga, Y. *Nature* **1954**, *173*, 168.

(8) Tang, C. W.; Vanslyke, S. A. *Appl Phys Lett* **1987**, *51*, 913.

(9) Baldo, M. A.; O'Brien, D. F.; Thompson, M. E.; Forrest, S. R. *Phys Rev B* **1999**, *60*, 14422.

(10) Zhang, S.; Song, J.; Kreouzis, T.; Gillin, W. P. *Journal of Applied Physics* **2009**, *106*, 043511.

(11) You, Y.; Park, S. Y. *Dalton Transactions* **2009**, *0*, 1267.

(12) Chou, P.-T.; Chi, Y. *European Journal of Inorganic Chemistry* **2006**, *2006*, 3319.

(13) Zhou, J.; Liang, Q.; Dong, J. *Carbon* **2010**, *48*, 1405.

(14) Zhang, X.-F.; Xu, H.-J. *Journal of the Chemical Society, Faraday Transactions* **1993**, *89*, 3347.

(15) Babudri, F.; Farinola, G. M.; Naso, F.; Ragni, R. *Chem. Commun.* **2007**, 1003.

(16) Shi, Y.-W.; Shi, M.-M.; Huang, J.-C.; Chen, H.-Z.; Wang, M.; Liu, X.-D.; Ma, Y.-G.; Xu, H.; Yang, B. *Chemical Communications* **2006**, *0*, 1941.

(17) Reichenbacher, K.; Suss, H. I.; Hulliger, J. *Chemical Society Reviews* **2005**, *34*, 22.

(18) Patrick, C. R.; Prosser, G. S. *Nature* **1960**, *187*, 1021.

(19) Bacchi, S.; Benaglia, M.; Cozzi, F.; Demartin, F.; Filippini, G.; Gavezzotti, A.

Chemistry – A European Journal **2006**, *12*, 3538.

(20) Desiraju, G. R. *Accounts of Chemical Research* **2002**, *35*, 565.

(21) Schwarzer, A.; Weber, E. *Crystal Growth & Design* **2008**, *8*, 2862.

(22) Plenio, H. *ChemBioChem* **2004**, *5*, 650.

(23) Takemura, H.; Iwanaga, T.; Shinmyozu, T. *Tetrahedron Letters* **2006**, *47*, 8989.

(24) Takemura, H.; Nakashima, S.; Kon, N.; Yasutake, M.; Shinmyozu, T.; Inazu, T. *J Am Chem Soc* **2001**, *123*, 9293.

(25) Kang, I.-N.; Shim, H.-K.; Zyung, T. *Chemistry of Materials* **1997**, *9*, 746.

(26) Gurge, R. M.; Sarker, A. M.; Lahti, P. M.; Hu, B.; Karasz, F. E. *Macromolecules* **1997**, *30*, 8286.

(27) Babudri, F.; Cardone, A.; Chiavarone, L.; Ciccarella, G.; Farinola, G. M.; Naso, F.; Scamarcio, G. *Chemical Communications* **2001**, *0*, 1940.

(28) Facchetti, A.; Deng, Y.; Wang, A.; Koide, Y.; Sirringhaus, H.; Marks, T. J.; Friend, R. H. *Angewandte Chemie International Edition* **2000**, *39*, 4547.

(29) Facchetti, A.; Mushrush, M.; Yoon, M.-H.; Hutchison, G. R.; Ratner, M. A.; Marks, T. J. *J Am Chem Soc* **2004**, *126*, 13859.

(30) Sakamoto, Y.; Komatsu, S.; Suzuki, T. *J Am Chem Soc* **2001**, *123*, 4643.

(31) Sakamoto, Y.; Komatsu, S.; Suzuki, T. *Synthetic Metals* **2003**, *133–134*, 361.

(32) Heidenhain, S. B.; Sakamoto, Y.; Suzuki, T.; Miura, A.; Fujikawa, H.; Mori, T.; Tokito, S.; Taga, Y. *J Am Chem Soc* **2000**, *122*, 10240.

(33) Sakamoto, Y.; Suzuki, T.; Miura, A.; Fujikawa, H.; Tokito, S.; Taga, Y. *J Am Chem Soc* **2000**, *122*, 1832.

(34) Komatsu, S.; Sakamoto, Y.; Suzuki, T.; Tokito, S. *Journal of Solid State Chemistry* **2002**, *168*, 470.

(35) Swartz, C. R.; Parkin, S. R.; Bullock, J. E.; Anthony, J. E.; Mayer, A. C.; Malliaras, G. G. *Organic Letters* **2005**, *7*, 3163.

(36) Katz, H. E.; Lovinger, A. J.; Johnson, J.; Kloc, C.; Siegrist, T.; Li, W.; Lin, Y. Y.; Dodabalapur, A. *Nature* **2000**, *404*, 478.

(37) Ragni, R.; Plummer, E. A.; Brunner, K.; Hofstraat, J. W.; Babudri, F.; Farinola,

G. M.; Naso, F.; De Cola, L. *J. Mater. Chem.* **2006**, *16*, 1161.

(38) Mears, R. J.; Reekie, L.; Jauncey, I. M.; Payne, D. N. *Electronics Letters* **1987**, *23*, 1026.

(39) Hasegawa, Y.; Ohkubo, T.; Sogabe, K.; Kawamura, Y.; Wada, Y.; Nakashima, N.; Yanagida, S. *Angew Chem Int Edit* **2000**, *39*, 357.

(40) Mancino, G.; Ferguson, A. J.; Beeby, A.; Long, N. J.; Jones, T. S. *J Am Chem Soc* **2006**, *128*, 17153.

(41) Zheng, Y.; Pearson, J.; Tan, R. H. C.; Gillin, W. P.; Wyatt, P. B. *J Mater Sci-Mater El* **2009**, *20*, 788.

(42) Bunzli, J.-C. G.; Piguet, C. *Chemical Society Reviews* **2005**, *34*, 1048.

(43) Dexter, D. L. *The Journal of Chemical Physics* **1953**, *21*, 836.

(44) Forster, T. *Discussions of the Faraday Society* **1959**, *27*, 7.

(45) Chen, B. L.; Yang, Y.; Zapata, F.; Qian, G. D.; Luo, Y. S.; Zhang, J. H.; Lobkovsky, E. B. *Inorg Chem* **2006**, *45*, 8882.

(46) Glover, P. B.; Bassett, A. P.; Nockemann, P.; Kariuki, B. M.; Van Deun, R.; Pikramenou, Z. *Chem-Eur J* **2007**, *13*, 6308.

(47) Tan, R. H. C.; Pearson, J. M.; Zheng, Y.; Wyatt, P. B.; Gillin, W. P. *Appl Phys Lett* **2008**, *92*.

(48) Zheng, Y. X.; Motevalli, M.; Tan, R. H. C.; Abrahams, I.; Gillin, W. P.; Wyatt, P. B. *Polyhedron* **2008**, *27*, 1503.

(49) de Oteyza, D. G.; Barrena, E.; Ossó, J. O.; Sellner, S.; Dosch, H. *J Am Chem Soc* **2006**, *128*, 15052.

(50) Peisert, H.; Knupfer, M.; Schwieger, T.; Fuentes, G. G.; Olligs, D.; Fink, J.; Schmidt, T. *Journal of Applied Physics* **2003**, *93*, 9683.

(51) Katz, H. E.; Bao, Z.; Gilat, S. L. *Accounts of Chemical Research* **2001**, *34*, 359.

(52) Ugarova, N. N.; Brovko, L. Y. *Luminescence* **2002**, *17*, 321.

(53) Yu, G.; Yin, S. W.; Liu, Y. Q.; Shuai, Z. G.; Zhu, D. B. *J Am Chem Soc* **2003**, *125*, 14816.

(54) Xu, X. J.; Liao, Y.; Yu, G.; You, H.; Di, C. G.; Su, Z. M.; Ma, D. G.; Wang, Q.; Li, S. Y.; Wang, S. Q.; Ye, J. P.; Liu, Y. Q. *Chem Mater* **2007**, *19*, 1740.

(55) Bingshe, X.; Huixia, X.; Liuqing, C.; Xiaohong, F.; Xuguang, L.; Hua, W. *Organic Electronics* **2008**, *9*, 267.

(56) Roh, S. G.; Kim, Y. H.; Seo, K. D.; Lee, D. H.; Kim, H. K.; Park, Y. I.; Park, J. W.; Lee, J. H. *Adv Funct Mater* **2009**, *19*, 1663.

(57) Katkova, M. A.; Pushkarev, A. P.; Balashova, T. V.; Konev, A. N.; Fukin, G. K.; Ketkov, S. Y.; Bochkarev, M. N. *J Mater Chem* **2011**, *21*, 16611.

(58) Bazyl, I. T.; Kisil, S. P.; Burgart, Y. V.; Saloutin, V. I.; Chupakhin, O. N. *Journal of Fluorine Chemistry* **1999**, *94*, 11.

(59) Bazyl', I. T.; Kisil', S. P.; Burgart, Y. V.; Saloutin, V. I. *Journal of Fluorine Chemistry* **2000**, *103*, 3.

(60) Brembilla, A.; Roizard, D.; Lochon, P. *Synthetic Communications* **1990**, *20*, 3379.

(61) Herkes, F. E. *Journal of Fluorine Chemistry* **1979**, *13*, 1.

(62) Ganín, J.; Meléndez, E.; Merchán, F. L.; Merino, P.; Orduna, J.; Tejero, T. *Synthetic Communications* **1990**, *20*, 2327.

(63) Krasnokutskaya, E. A.; Semenischeva, N. I.; Filimonov, V. D.; Knochel, P. *Synthesis* **2007**, *2007*, 81.

(64) Wagner-Jauregg, T.; Helmert, E. *Berichte der deutschen chemischen Gesellschaft (A and B Series)* **1942**, *75*, 935.

(65) Karshtedt, D.; Bell, A. T.; Tilley, T. D. *J Am Chem Soc* **2005**, *127*, 12640.

(66) Abbotto, A.; Bruni, S.; Cariati, F.; Pagani, G. A. *Spectrochimica Acta Part A: Molecular and Biomolecular Spectroscopy* **2000**, *56*, 1543.

(67) Ambrosetti, R.; Bellucci, G.; Bianchini, R.; Bigoli, F.; Deplano, P.; Pellinghelli, M. A.; Trogu, E. F. *Journal of the Chemical Society, Perkin Transactions 2* **1991**, *0*, 339.

(68) Téllez, F.; Peña-Hueso, A.; Barba-Behrens, N.; Contreras, R.; Flores-Parra, A. *Polyhedron* **2006**, *25*, 2363.

(69) Tan, R. H. C.; Motevalli, M.; Abrahams, I.; Wyatt, P. B.; Gillin, W. P. *J Phys Chem B* **2006**, *110*, 24476.

(70) Melman, J. H.; Rohde, C.; Emge, T. J.; Brennan, J. G. *Inorganic Chemistry*

2001, *41*, 28.

(71) Buzzeo, M. C.; Iqbal, A. H.; Long, C. M.; Millar, D.; Patel, S.; Pellow, M. A.; Saddoughi, S. A.; Smenton, A. L.; Turner, J. F. C.; Wadhawan, J. D.; Compton, R. G.; Golen, J. A.; Rheingold, A. L.; Doerrer, L. H. *Inorganic Chemistry* **2004**, *43*, 7709.

(72) Collings, J. C.; Smith, P. S.; Yufit, D. S.; Batsanov, A. S.; Howard, J. A. K.; Marder, T. B. *CrystEngComm* **2004**, *6*, 25.

(73) Cozzi, F.; Bacchi, S.; Filippini, G.; Pilati, T.; Gavezzotti, A. *Chemistry – A European Journal* **2007**, *13*, 7177.

(74) Berger, R.; Resnati, G.; Metrangolo, P.; Weber, E.; Hulliger, J. *Chemical Society Reviews* **2011**, *40*, 3496.

(75) Williams, J. H.; Cockcroft, J. K.; Fitch, A. N. *Angewandte Chemie International Edition in English* **1992**, *31*, 1655.

(76) Cozzi, F.; Bacchi, S.; Filippini, G.; Pilati, T.; Gavezzotti, A. *CrystEngComm* **2009**, *11*, 1122.

(77) Sapochak, L. S.; Padmaperuma, A.; Washton, N.; Endrino, F.; Schmett, G. T.; Marshall, J.; Fogarty, D.; Burrows, P. E.; Forrest, S. R. *Journal of the American Chemical Society* **2001**, *123*, 6300.

(78) Tang, M. L.; Bao, Z. A. *Chem. Mat.* **2011**, *23*, 446.

(79) Watt, S. W.; Dai, C.; Scott, A. J.; Burke, J. M.; Thomas, R. L.; Collings, J. C.; Viney, C.; Clegg, W.; Marder, T. B. *Angewandte Chemie International Edition* **2004**, *43*, 3061.

(80) Sakamoto, Y.; Suzuki, T.; Kobayashi, M.; Gao, Y.; Fukai, Y.; Inoue, Y.; Sato, F.; Tokito, S. *Journal of the American Chemical Society* **2004**, *126*, 8138.

(81) Collings, J. C.; Smith, P. S.; Yufit, D. S.; Batsanov, A. S.; Howard, J. A. K.; Marder, T. B. *Crystengcomm* **2004**, *6*, 25.

(82) Cozzi, F.; Bacchi, S.; Filippini, G.; Pilati, T.; Gavezzotti, A. *Chem-Eur J* **2007**, *13*, 7177.

(83) Sakamoto, Y.; Komatsu, S.; Suzuki, T. *Journal of the American Chemical Society* **2001**, *123*, 4643.

(84) Cho, D. M.; Parkin, S. R.; Watson, M. D. *Org Lett* **2005**, *7*, 1067.

(85)Xia, Y.; Viel, S.; Wang, Y.; Ziarelli, F.; Laurini, E.; Posocco, P.; Fermeglia, M.; Qu, F.; Pricl, S.; Peng, L. *Chemical Communications* **2012**, *48*, 4284.

(86)Yu, G.; Yin, S.; Liu, Y.; Shuai, Z.; Zhu, D. *Journal of the American Chemical Society* **2003**, *125*, 14816.

(87)Pawelka, Z. *Journal of the Chemical Society, Faraday Transactions 2: Molecular and Chemical Physics* **1988**, *84*, 1683.

(88)Li, Z.; Dellali, A.; Malik, J.; Motevalli, M.; Nix, R. M.; Olukoya, T.; Peng, Y.; Ye, H.; Gillin, W. P.; Hernández, I.; Wyatt, P. B. *Inorg Chem* **2013**, *52*, 1379.

(89)Crosby, G. A.; Demas, J. N. *The Journal of Physical Chemistry* **1971**, *75*, 991.

(90)Williams, A. T. R.; Winfield, S. A.; Miller, J. N. *Analyst* **1983**, *108*, 1067.

(91)Eliseeva, S. V.; Bunzli, J. C. G. *Chem. Soc. Rev.* **2010**, *39*, 189.

(92)Magennis, S. W.; Ferguson, A. J.; Bryden, T.; Jones, T. S.; Beeby, A.; Samuel, I. D. W. *Synthetic Metals* **2003**, *138*, 463.

(93)Tan, R. H. C.; Motevalli, M.; Abrahams, I.; Wyatt, P. B.; Gillin, W. P. *The Journal of Physical Chemistry B* **2006**, *110*, 24476.

(94)Chkoda, L.; Heske, C.; Sokolowski, M.; Umbach, E. *Applied Physics Letters* **2000**, *77*, 1093.

(95)Adachi, C.; Baldo, M. A.; Forrest, S. R.; Thompson, M. E. *Appl. Phys. Lett.* **2000**, *77*, 904.

(96)Ern, V.; Merrifield, R. E. *Physical Review Letters* **1968**, *21*, 609.

(97)Baldo, M. A.; Adachi, C.; Forrest, S. R. *Physical Review B* **2000**, *62*, 10967.

(98)Reineke, S.; Walzer, K.; Leo, K. *Physical Review B* **2007**, *75*, 125328.

(99)Baldo, M. A.; Forrest, S. R. *Physical Review B* **2000**, *62*, 10958.

(100) Eliseeva, S. V.; Bunzli, J.-C. G. *Chem. Soc. Rev.* **2010**, *39*, 189.

(101) Curry, R. J.; Gillin, W. P. *Applied Physics Letters* **1999**, *75*, 1380.

(102) Barton, D. H. R.; Fontana, G.; Yang, Y. *Tetrahedron* **1996**, *52*, 2705.

(103) Kumbhare, R. M.; Dadmal, T.; Kosurkar, U.; Vijay Kumar, K. *Journal of Heterocyclic Chemistry* **2012**, *49*, 342.

(104) Do, H.-Q.; Daugulis, O. *Organic Letters* **2008**, *11*, 421.

(105) Neidlein, R.; Krüll, H. *Archiv der Pharmazie* **1971**, *304*, 763.

(106) Trepka, R. D.; Harrington, J. K.; McConville, J. W.; McGurran, K. T.; Mendel, A.; Pauly, D. R.; Robertson, J. E.; Waddington, J. T. *Journal of Agricultural and Food Chemistry* **1974**, *22*, 1111.